ABSTRACT

CONTINUOUS MEDIUM ANALYSIS OF ELASTIC, PLASTIC AND VISCOELASTIC BEHAVIOR OF A MODEL SALT CAVITY

by Abdallah G. Dahir

The main objective of this investigation was to study creep motion and the distribution of stress and strain in the medium around a cylindrical cavity.

Rock behaves as a brittle material when differentially stressed under a low confining pressure. It was observed in nature that underground rocks show a tendency to flow under a triaxial state of stress. Accordingly, the possibility of using the information derivable from laboratory triaxial tests to predict the behavior of natural underground formations was investigated.

Theoretical analysis was made of stress, strain and boundary motion of a cylindrical salt model containing a coaxial cylindrical cavity. This analysis was based on the mathematical theories of elasticity, plasticity and viscoelasticity of a continuous medium. The constitutive equations assumed to describe the behavior of the rock salt were derived from a mechanical model consisting of elastic, viscoelastic and viscoplastic elements.

The elastic, viscoelastic and viscoplastic coefficients of rock salt were determined from experimental results of a triaxial

transition test simulating underground stress field in situ. The behavior of a model cylindrical salt cavity was studied in the laboratory by using a high pressure vessel, employing a liquid confining medium.

The material constants obtained from the triaxial tests were used to calculate the theoretical cavity closure of the model salt cavity. The experimental results were in close agreement with the theoretical predictions, indicating the validity of both the mechanical model and the theories of stress, strain and creep motion. The agreement between the theory and experimental creep results suggests that this study may be extended to underground rock formations.

CONTINUOUS MEDIUM ANALYSIS OF ELASTIC, PLASTIC AND VISCOELASTIC BEHAVIOR OF A MODEL SALT CAVITY

By

Abdallah George Dahir

A THESIS

Submitted to
Michigan State University
in partial fulfillment of the requirements
for the degree of

DOCTOR OF PHILOSOPHY

in
Mechanics

Department of Metallurgy, Mechanics and Material Science

1964

ACKNOWLEDGEMENTS

The author would like to express his sincere thanks to Dr. S. Serata, Thesis Advisor and Project Director, for his guidance in this study and careful checking of the manuscript.

The author is especially indebted to Dr. L. Malvern, Professor of Mechanics and Major Professor, for his valuable suggestions, help and encouragement for the theoretical development. Gratitude is also extended to Dr. G. Mase, Professor of Mechanics, for his interest and help whenever requested, Dr. G. Martin, Professor of Mechanical Engineering, for serving in his graduate committee, and to the National Science Foundation for their support of this project.

The author wishes to thank Mr. S. Sukurai for his valuable suggestions in the development of the mechanical model of rock salt.

Appreciation is also extended to Messrs. O. Abu-Gheida and E. Fiskers for providing laboratory help whenever requested, and to my wife Nancy for her encouragement and editing of this manuscript.

TABLE OF CONTENTS

LIST OF TABLES

LIST OF FIGURES

NOTATION

$\sigma_1, \sigma_2, \sigma_3$	principal stresses
σ_r	radial stress
σ_θ	tangential stress
σ_z	axial stress
$\sigma_x, \sigma_y, \sigma_z$	stresses in rectangular coordinates
$\sigma_x = \sigma_y = \sigma_L$	lateral stress
$\bar{\sigma}$	generalized or effective stress
$\sigma_r' = \sigma_r - \frac{\sigma_r + \sigma_\theta + \sigma_z}{3}$ $\sigma_\theta' = \sigma_\theta - \frac{\sigma_r + \sigma_\theta + \sigma_z}{3}$ $\sigma_z' = \sigma_z - \frac{\sigma_r + \sigma_\theta + \sigma_z}{3}$	deviatoric stresses
τ_o	octahedral shear stress
τ_f	octahedral shear stress at $t = \infty$
τ_i	octahedral shear stress at $t = 0$
K_o	octahedral shear strength
$\epsilon_x, \epsilon_y, \epsilon_z$	principal strain in rectangular coordinates
$\epsilon_x = \epsilon_y = \epsilon_z$	lateral strain
ϵ_r	radial strain
ϵ_θ	tangential strain
$\epsilon_r^e, \epsilon_\theta^e, \epsilon_z^e$	total elastic strains in 3 principal directions
$\epsilon_r^P, \epsilon_\theta^P, \epsilon_z^P$	total plastic strains in 3 principal directions

$\bar{\epsilon}_r^P$, $\bar{\epsilon}_\theta^P$, $\bar{\epsilon}_z^P$	effective plastic strains in 3 principal directions
$\frac{d\epsilon_r}{dt}$, $\frac{d\epsilon_\theta}{dt}$, $\frac{d\epsilon_z}{dt} = \dot{\epsilon}_r$, $\dot{\epsilon}_\theta$, $\dot{\epsilon}_z = d_r$, d_θ, d_z	principal strain rates in 3 directions
H'	slope of the equivalent stress/plastic strain curve
$d\lambda$	scalar or proportionality factor
a_o, b_o	inner and outer initial radii of a model cylindrical salt cavity, respectively
a	reduced cavity radius
r	radial coordinate
ρ	radius of the elastic-plastic boundary
r, θ	cylindrical coordinates
P_i	internal pressure of cavity
P_o	external pressure of cavity
P_ρ	pressure at the elastic plastic boundary
E	Young's modulus
μ	Poisson's ratio
G_1	octahedral shear modulus
G_2	retarded shear modulus
η_1	viscosity coefficient in viscoplastic region
η_2	viscosity coefficient in viscoelastic region
P	material constant
t	time

CHAPTER I

INTRODUCTION

1.1 General Remarks

Rock is a heterogeneous mixture of grains of polycrystalline materials which are randomly oriented and held together by bonding forces. It generally exhibits isotropic and homogeneous qualities under different kinds of loading. Geophysical explorations have demonstrated that rocks change their character and property and flow in varying degrees depending on the environmental conditions. Under uniaxial stress, they behave like brittle material. However, under a triaxial stress condition, which is normally the stress in an underground formation, it exhibits many of the characteristics of plastic material. Adams,[1] Bridgman,[9] Griggs[27] and others have employed pressures that varied from 3000 to 75,000 psi and produced plastic flow in marble, rocks and limestone. This phenomenon can be explained by solid state mechanics since molecular (or ionic) displacement in solids takes place whenever the shearing stress exceeds a definite limit of the intermolecular attraction.

Rock salt has been chosen as a model in the present study. It is encountered in large quantities as rock salt formations in many parts of the world. It flows more readily than other rocks as demonstrated by many natural salt domes. It is sufficiently homogeneous and

isotropic for theoretical studies and easy to machine any desired form of testing specimens. Recently, a great attention has been given to the triaxial behavior of rock salts because underground cavities can be used for radioactive waste disposal in quantity when the nuclear energy becomes necessity in the near future.

To date, the study of failure of rock salt has been restricted to conventional uniaxial compression tests or limited triaxial tests which cannot be used to distinguish the deformation mechanism of an underground rock salt. Because of these limitations, a transition test technique and a hollow cylinder technique were used to create testing conditions similar to that of underground formation.

Numerous observations have been made on stress and strain and creep motion in underground formations. However no basic principles describing this behavior or the mechanical properties have been formulated and verified. Some of the basic reasons are listed by Serata[70] as follows:

1. An underground formation is always subjected to triaxial stress, under which the behavior of the materials is quite different from the uniaxial compression.

2. The laboratory study of triaxial compression exceeds a certain value which is specific to the individual materials of the formation.

3. The laboratory study of triaxial compression requires

extreme high pressure testing instruments which make the study rather difficult.

4. In addition to the static overburden pressure, the ground formulations may be subjected to tectonic pressures.

5. Usually, an underground medium consists of a variety of formations, whose structural properties are different from each other.

6. Strain confinement in the underground formation, different from the conventional triaxial test.

1.2 Objectives

The main objectives of this investigation were to:

1. Establish basic mathematical relations describing the distribution of stress, strain and creep motion in the medium of a thick walled cylinder.

2. Verify that the mechanical model, consisting of elastic, viscoelastic and viscoplastic elements, describes the overall behavior of rock salt as a function of stress and time.

3. Determine the mechanical constants of the material such as, Young's modulus, Poisson's ratio, octahedral shear strength, retarded shear modulus and viscosity coefficients.

4. Verify from laboratory data the basic mathematical equations of stress, strain and strain rate distribution around a cylindrical cavity and the mechanical model of rock salt.

1.3 Experimental Techniques

By the very nature of the restraint offered by the massiveness of rock salt, underground openings are normally in a triaxial stress state. A thorough understanding of the distribution of stress, strain and creep motion in the medium around such openings requires a study of their behavior under multiaxial stress conditions. Elastic, viscoelastic, elastic-plastic, completely plastic and other stress conditions might prevail in underground formations.

Laboratory study of these stress states necessitated the development of two basically different testing techniques. First, a triaxial transition test was used to verify the applicability of the proposed mechanical model and to determine the elastic, viscoelastic and viscoplastic constants. These constants were used to calculate the theoretical cavity closure of the model salt cavity. Second, a high pressure, automatically controlled, vessel was developed to simulate underground cavity. Three different stress states of elastic, elastic-plastic and completely plastic states were obtained from this testing technique. The data obtained was used to verify the various mathematical equations describing the distribution of stress, strain and creep motion of the medium around a cylindrical salt cavity.

PART ONE: THEORETICAL ANALYSIS

CHAPTER II

PRINCIPLES OF STRESS AND STRAIN FIELDS AROUND A CYLINDRICAL CAVITY

2.1 Summary of Previous Work Done on Rock Salt

Rock salt tested in different laboratories indicates isotropic and homogeneous qualities under static and dynamic loading; while at the same time, it exhibits elastic, plastic, elasto-plastic and brittle properties within a practical range of testing pressures. Most rocks are exceedingly brittle when deformed under ordinary atmospheric pressure conditions. However, they in general exhibit a plastic nature in varying degrees with the increase of triaxial compression. This increase in ductility depends on environmental conditions such as high confining pressure, high temperature, differential stress and exposure to liquid. The confining pressure plays an important role in bringing about the transition from brittle to ductile flow as demonstrated by many investigators.[1, 9, 27, 30] Accordingly, it is desirable to review the properties of rock salt under uniaxial, biaxial and triaxial stress states.

2.1a Uniaxial stress tests

The uniaxial test is a common method extensively used to determine structural behavior of rocks under stress. The behavior of a

rock, with a consistent structural property, varies depending upon the testing method employed. The structural properties are usually defined by certain coefficients such as Young's modulus, Poisson's ratio and yielding stress. The value of the coefficients showed a wide variation depending on the investigator and method employed. The maximum strength of salt varies between 2300 psi and 5000 psi, while Young's modulus varies between 0.1×10^6 psi to 1.0×10^6 psi. Serata[70] attributed this wide variation to several factors, some of which are as follows:

1. Friction developed upon the loading surface.
2. Strain measuring devices, dial gages or strain gages.
3. Dimension of test specimen.

The friction developed on the loading surfaces of the salt increases the ultimate strength and modulus of elasticity by the formation of a triaxial stress zone in the central region of the specimen.

The strain measured by a dial gage is quite different from the same strain measured simultaneously by SR-4 strain gages.

The size of specimen has an important influence upon the stress-strain curves, which can be eliminated by use of the friction reducer and proper proportion of height-to-width ratio.

After these effects had been eliminated Serata [70] found the following mechanical properties:

1. The maximum strength of salt is 2300 psi with a standard

deviation of 200 psi.

2. The yield strength of salt is found to be in the range of 1800 psi to 2200 psi.

3. Mean value of Young's modulus was 0.14×10^6 psi with a standard deviation of 0.03×10^6 psi.

4. Poisson's ratio of value 1 has been found in granular aggregate, which is much higher than the theoretical limit of 0.5. The Poisson's ratio taken on a single crystal grain in the same aggregate reveals a value which is not greater than 0.5.

Chowdiah,[11] following the same procedure developed by Serata, reached the following conclusions:

1. The stress strain curve of rock salt does not exhibit linearity at any stage.

2. The approximate value of chord modulus of elasticity E is:

Stress range	Average E (SR-4 gages)	Average E (dial gages)
0 to 100	1.408×10^6 psi	0.4559×10^6 psi
1000 to 1000	0.1913×10^6 psi	0.1757×10^6 psi

3. The value of the Poisson's ratio obtained from SR-4 gages was greater than 0.5, whereas with dial gages the value increased linearly from 0 to 0.5 in the stress range 0 to 1500 psi and was larger than 0.5 beyond the stress 1500 psi.

4. The average failure strength of the material is 3,800 psi.

2.1b Biaxial stress tests

The failure of the material in a biaxial state of stress is different from that of uniaxial state. The load is applied in two directions and the material flows from the unconfined side. Chowdiah,[11] using dial gages, strain gages and photo-stress techniques, reached the following conclusions:

1. The material has the tendency to flow by yielding at equal horizontal and vertical loads of 4000 psi (corresponding to an octahedral shear stress value of 1885 psi).
2. Under equal biaxial compressive stresses of 4000 psi the circular opening tended to flow without collapsing, while an oval opening collapsed by undergoing large deformation under the same biaxial loads.
3. Photo-stress results justified the assumption of statistical homogeneity and isotropy of rock salt material.

2.1c Triaxial stress tests

Some of the earlier triaxial tests on rock salt were done by Adams[2] and his collaborators[1,4] on the increase in ductility and ultimate strength of rock salt under confining pressure.

Von Karman[78] performed triaxial tests under hydrostatic pressure. Samples of white marble and red sandstone were subjected to compressive external liquid pressures. The results show that the

stress-strain curves were similar to those of ductile metals which show work hardening and permanent deformations.

Griggs[27] continued the work started by Adams to study the relation of the triaxial characteristics of ultimate strength to the confining pressure and time under load. A liquid kerosene medium with a confining pressure of 13,000 atmospheres was applied to small solid cylinders of limestone, marble and quartz. Some of the main results obtained are:

1. A gradual change between brittle and ductile state is attained as confining pressure increases, and no sharp transition was noticed.
2. Continuous flow was not obtained in any of the materials used.
3. The ultimate strength of rocks decreases asymptotically to a certain value of strength at infinite time under load.
4. The rate of plastic deformation varied in proportion to the applied force.
5. The rate of plastic deformation at constant high loads decreases rapidly with time.

Bridgman[9] made some extension tests under hydrostatic pressures on rock salt crystals at an extension pressure of 420,000 psi. He obtained a reduction of 20% in sample area in rock salt, while on solenhofen limestone under hydrostatic pressure of 400,000 psi, he obtained an area reduction of 53%.

Handin[30] studied the triaxial behavior of cylindrical salt specimens (1" x 1/2") under a confining pressure of 5200 atmospheres. He indicated that salt has a remarkable ductility in comparison. At 1200 atmospheres a specimen was shortened 75 per cent before fracture. He also indicated that the increase of strength and ductility with confining pressure, so striking with many rocks, is much less pronounced in salt, and much of the effect is observed in the first few hundred atmospheres.

Handin's[30] work on the triaxial strength of salt was utilized by Serata[70] to construct Mohr's envelopes. The envelopes at low confining pressures gave smaller ultimate shear strengths than the envelopes at higher confining pressures. The minimum required mean principal stress for the creation of a plastic state was found to be 5500 psi. Beyond this value, the Mohr's envelope became horizontal.

Serata[70] created a large mean stress by subjecting cylindrical salt specimen (6" O.D., 2" I.D., 2" h), confined in a steel jacket, to an axial load of 16,000 psi. The important conclusion of his study is that the yield condition based on octahedral shear theory is applicable to rock salt whenever the mean stresses exceed 5500 psi.

Serata[70] and his collaborators[55, 65] developed a laboratory method by which the octahedral shear strength was determined and the transition region from elastic to plastic in continuous medium was illustrated. In their laboratory experiments, a cylindrical salt

specimen was closely fitted in a thick steel cylinder. The lateral pressure is developed on the specimen through restraint by the surrounding steel as the specimen is compressed axially. The lateral stress was calculated from the strain on the outer surface of the steel cylinder, measured by SR-4 strain gages.

The stress condition of the test specimen may be illustrated in the diagram of axial stress vs. lateral stress as in Fig. 2.1. The elastic state of stress is given as a straight line from the origin at the angle α defined by $\tan \alpha = \frac{\mu}{1 - \mu}$, where μ is Poisson's ratio, since $\frac{\sigma_L}{\sigma_z} = \frac{\mu}{1 - \mu}$ by Hooke's law under the condition of zero lateral strain. This elastic region extends between the two elastic lines OE and FG. The plastic state of stress is represented by another straight line, EF or HG, with the angle of tangent, $B = 45^{\circ}$ and expressed by

$$\sigma_z = \sigma_L \pm \frac{3}{\sqrt{2}} K_0$$

The elastic and plastic lines can be interpreted as follows: the stress condition of the specimen remains elastic until the overburden pressure, σ_z, reaches the yield point. When this point of transition is exceeded, the stress condition becomes plastic, and remains plastic regardless of the initial overburden load. (The elastic line FG and the plastic line HG represents the unloading stress state.)

Young's modulus and Poisson's ratio of the triaxially stressed medium can be obtained from measurement of the stress and strain

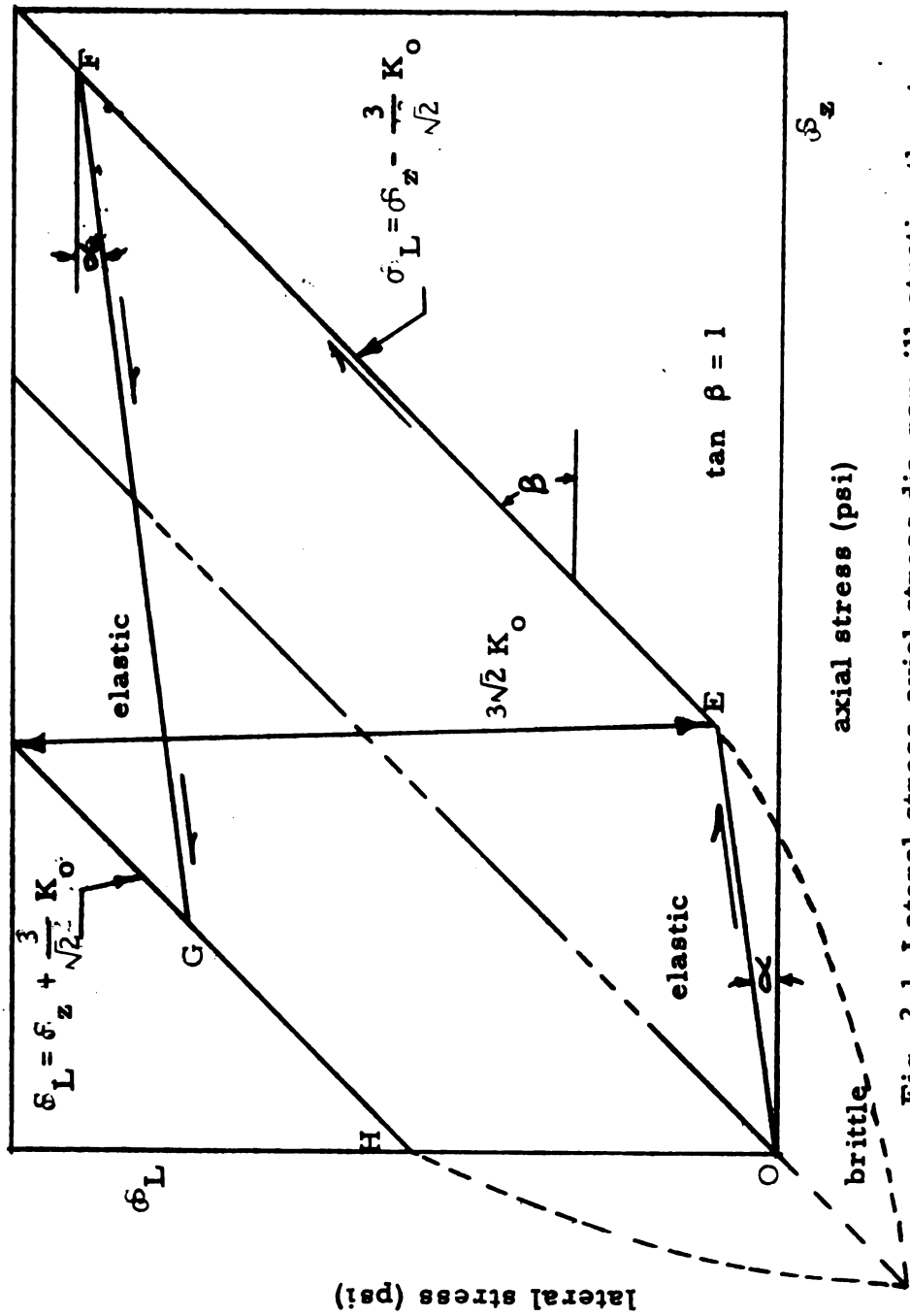

Fig. 2.1 Lateral stress-axial stress diagram illustrating the stress relations in a specimen restrained from lateral expansion

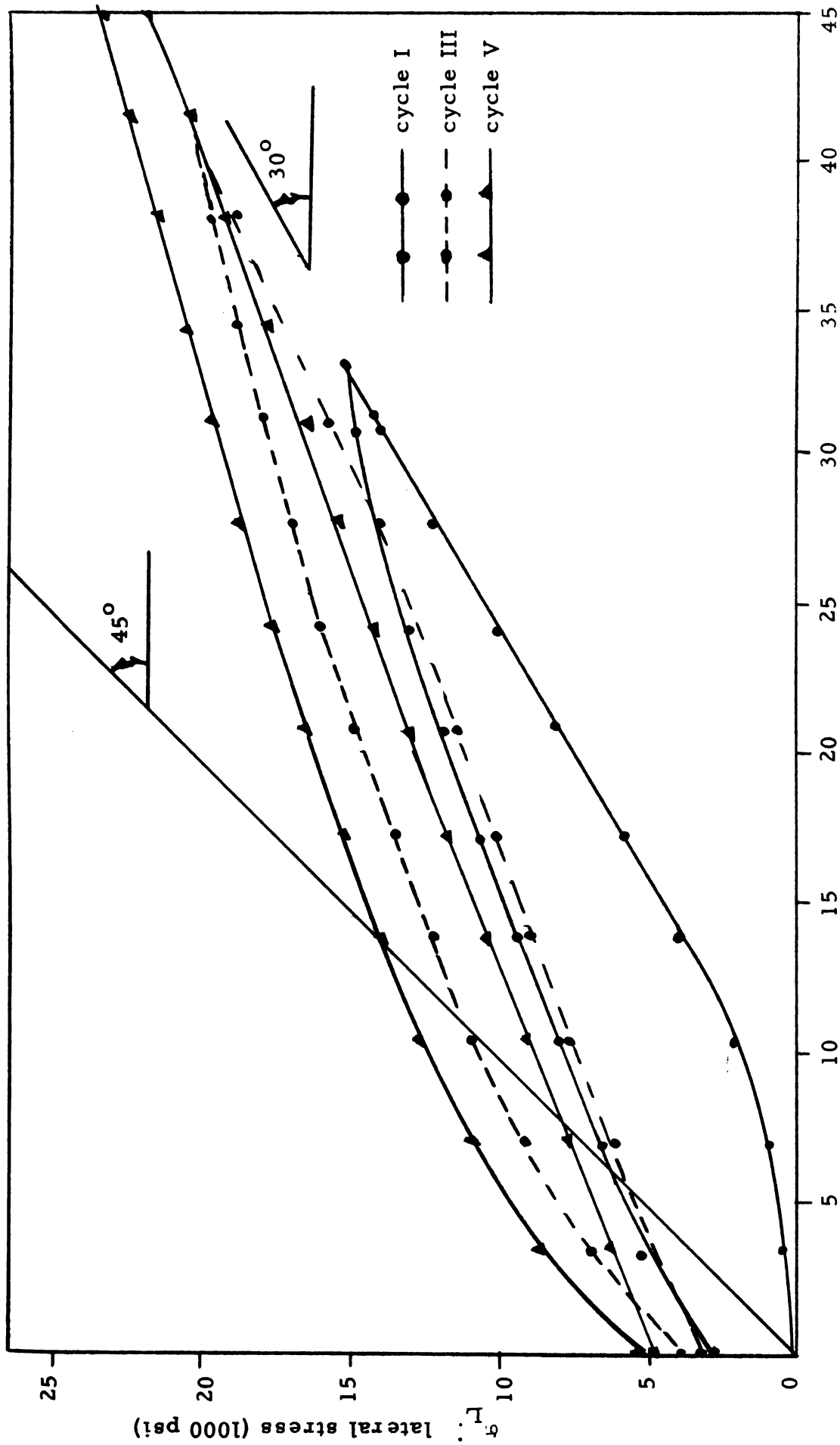

Fig. 2.2 Lateral stress-axial stress diagram showing loading cycles I, III, and V on limestone

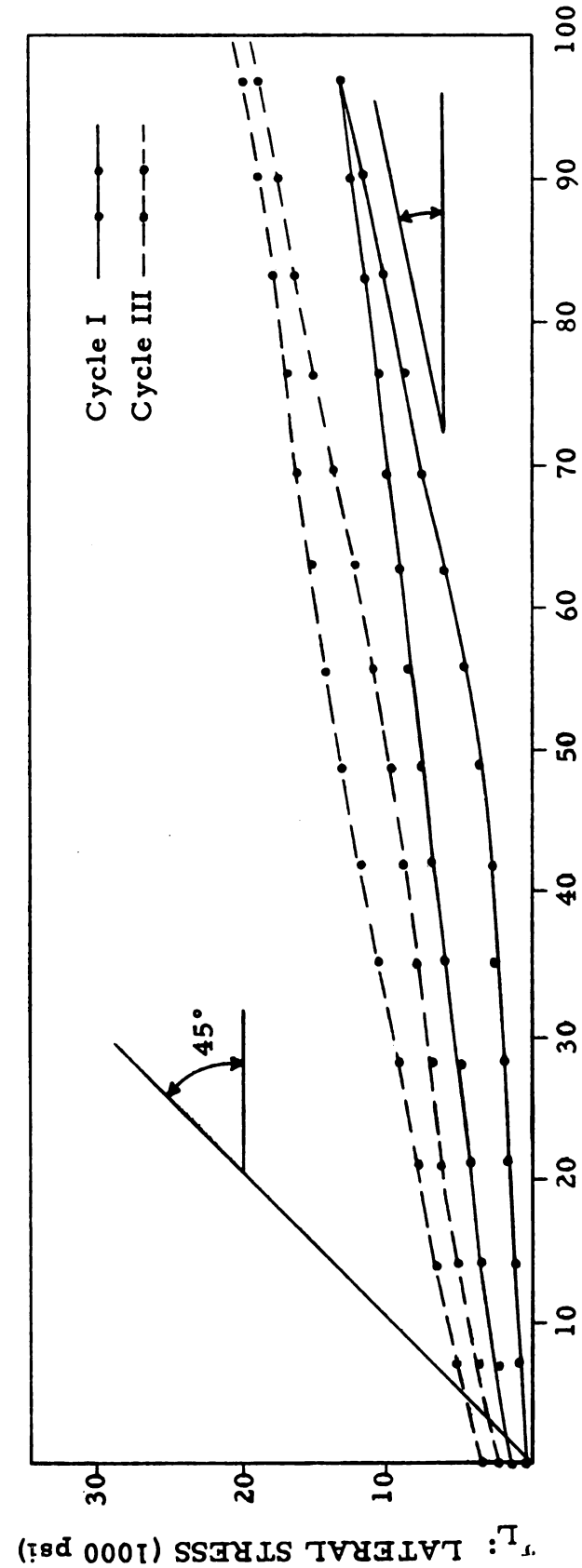

Fig. 2.3 Lateral stress - axial stress diagram showing loading cycles I and III on granite.

relationship in the elastic state OE by using the following equations:

$$\mu = \frac{1 - \Gamma A}{2A - \Gamma(A+1)} \qquad (2.1\text{-}1)$$

Where:

$$A = \tan \alpha = \frac{\sigma_L}{\sigma_z}$$

$$\Gamma = \tan \gamma = \frac{\epsilon_z}{\epsilon_L}$$

μ = Poisson's ratio

and the modulus of elasticity, E, is

$$E = \frac{\frac{\sigma_z}{2\sigma_L} - \frac{\sigma_L}{(\sigma_L + \sigma_z)}}{\frac{\epsilon_z}{2\sigma_L} - \frac{\epsilon_L}{(\sigma_L + \sigma_z)}} \qquad (2.1\text{-}2)$$

Experimental analysis of different rock salt samples showed a general agreement between theory and experimental results. However, Raman's[65] results on limestone and granite, Figs. 2.2 and 2.3 respectively, showed an unexpected behavior that is explained in the analysis to follow.

2.2 Elastic Analysis of Stress and Strain Distribution Around a Cylindrical Opening

An exact solution to the stress strain relation around a cavity opening using Hooke's law requires a simple geometrical form of the

cavity such as a circle, sphere or an ellipse. In an ideal form of cavity a theoretical solution to the problem can be obtained, which may provide a close approximation to a real cavity. Most of the underground openings do not have ideal geometrical forms and their exact solution is difficult to obtain. However, for practical purposes, the results of the analysis of idealized forms approximates that for the real forms. Thus the theory of elasticity can be applied to the stress and strain analysis provided the maximum shear stress around these geometrical openings never exceeds its critical value.

According to the mathematical theory of elasticity, when radially symmetrical stress is applied around a cylindrical cavity in plane strain the maximum shear stress always occurs on the boundary. By increasing the applied stress, the maximum shear stress at the boundary reaches a certain critical value. The magnitude of these critical stresses depends upon the forms of the cavity and the initial stress conditions. When these critical stresses exceed the maximum shear strength of the material, it causes failure at the boundary. The high stress concentration is then relieved by the development of the plastic zone in the highly concentrated stress area. In this area, the salt undergoes plastic flow, which causes a gradual reduction in the stress until an equlibrium condition is reached.

This theoretical analysis considers only a cavity in an ideally elastic and plastic medium. The cavity is assumed as a thick walled

tube loaded with a uniform external pressure P_0 and a small internal pressure P_i subjected to plane strain conditions and axial symmetry. From this imposed condition the cylindrical coordinate directions, r, θ, and z are the principal axis and the stresses σ_r, σ_θ and σ_z are the principal stresses.

2.2a Stress and strain analysis in completely elastic cylinder in plane strain

The general stress solution can be obtained from equilibrium equations and is generally represented for the case of radially symmetric plane strain with a superposed uniform axial strain ϵ_z as follows:[77]

$$\sigma_r = \frac{A}{r^2} + 2c$$

$$\sigma_\theta = -\frac{A}{r^2} + 2c \qquad (2.2\text{-}1)$$

$$\sigma_z = E\epsilon_z + 4\mu c$$

where A and C are constants.

When a_0 and b_0 are the inner and outer radii of the cylindrical cavity and P_i and P_0 the uniform internal and external pressures respectively, the two constants are determined by the given boundary conditions, and the equations become

$$\sigma_r = (P_0 - P_i) \cdot \frac{1}{r^2} \frac{a_0^2}{1 - \frac{a_0^2}{b_0^2}} + \frac{(P_i - P_0 \frac{b_0^2}{a_0^2}) \frac{a_0^2}{b_0^2}}{1 - \frac{a_0^2}{b_0^2}}$$

$$\sigma_\theta = -(P_0 - P_i) \cdot \frac{1}{r^2} \frac{a_0^2}{1 - \frac{a_0^2}{b_0^2}} + \frac{(P_i - P_0 \frac{b_0^2}{a_0^2}) \frac{a_0^2}{b_0^2}}{1 - \frac{a_0^2}{b_0^2}} \qquad (2.2\text{-}2)$$

$$\sigma_z = E \epsilon_z + 2\mu \frac{(P_i - P_0 \frac{b_0^2}{a_0^2}) \frac{a_0^2}{b_0^2}}{1 - (a_0^2/b_0^2)}$$

Thus:

$$A = (P_0 - P_i) \frac{a_0^2}{1 - (a_0^2/b_0^2)}$$

and

$$2c = \frac{(P_i - P_0 \frac{b_0^2}{a_0^2}) \frac{a_0^2}{b_0^2}}{1 - (a_0^2/b_0^2)} \qquad (2.2\text{-}3)$$

Substituting σ_r, σ_θ and σ_z of Eq. 2.2-2 in the following Hooke's law

$$\epsilon_r = \frac{1}{E} [\sigma_r - \mu (\sigma_\theta + \sigma_z)]$$

$$\epsilon_\theta = \frac{1}{E} [\sigma_\theta - \mu (\sigma_r + \sigma_z)] \qquad (2.2\text{-}4)$$

$$\epsilon_z = \frac{1}{E} [\sigma_z - \mu (\sigma_r + \sigma_\theta)]$$

the relations between strain and applied pressure are obtained, such that (for plane strain)

$$\epsilon_r = \frac{1}{E\left(1 - \frac{a_0^2}{b_0^2}\right)} \left[\frac{a_0^2}{r^2}(1+\mu)(P_0 - P_i) + (1 - \mu - 2\mu^2)\left(P_i \frac{a_0^2}{b_0^2} - P_0\right)\right]$$

(2.2-5)

$$\epsilon_\theta = \frac{1}{E\left(1 - \frac{a_0^2}{b_0^2}\right)} \left[-\frac{a_0^2}{r^2}(1+\mu)(P_0 - P_i) + (1 - \mu - 2\mu^2)\left(P_i \frac{a_0^2}{b_0^2} - P_0\right)\right]$$

$$\epsilon_z = \frac{1}{E}\sigma_z - \mu \frac{\left(P_i - P_0 \frac{b_0^2}{a_0^2}\right)\frac{a_0^2}{b_0^2}}{1 - \frac{a_0^2}{b_0^2}} = 0.$$

The principal strains are related to the displacement by

$$\epsilon_r = \frac{du_r}{du}$$

$$\epsilon_\theta = \frac{u_r}{r} \qquad (2.2\text{-}6)$$

$$\epsilon_z = \frac{du_z}{dz} = 0 \qquad \text{in plane strain,}$$

where $u_r = f(r)$; $u_\theta = u_z = 0$

The radial displacement is then expressed as

$$u_r = -\frac{1}{E\left(1 - \frac{a_0^2}{b_0^2}\right)} \left[\frac{a_0^2}{r}(1+\mu)(P_0 - P_i) - r(1 - \mu - 2\mu^2)\left(P_i \frac{a_0^2}{b_0^2} - P_0\right)\right]$$

(2.2-7)

For $P_i = 0$:

$$u_r = -\frac{(1+\mu)\,P_0}{E\left(1 - \frac{a_0^2}{b_0^2}\right)} \left[\frac{a_0^2}{r} + (1 - 2\mu)\,r\right] \qquad (2.2\text{-}8)$$

which is a linear relation between the external load and the radial displacement.

From Eq. 2.2-8, the modulus of elasticity may be expressed as,

$$E = - \frac{(1+\mu)}{\frac{\Delta u_0}{\Delta P_0}\left(1 - \frac{a_0^2}{b_0^2}\right)} \cdot 2a_0(1-\mu) \qquad (2.2\text{-}9)$$

where $\mu_0 = \mu(a_0)$.

By assuming a value of the Poisson's ratio and small strains where $a \cong a_0$ the modulus of elasticity may be determined from laboratory measurement of $\Delta u_0/\Delta P_0$ by using specimens of thick walled cylinder. If plane strain is assumed and internal pressure is set equal to zero, the stress distribution of Eq. 2.2-2 reduces to

$$\sigma_r = \frac{P_0}{\left(1 - \frac{a_0^2}{b_0^2}\right)}\left(\frac{a_0^2}{r^2} - 1\right)$$

$$\sigma_\theta = - \frac{P_0}{\left(1 - \frac{a_0^2}{b_0^2}\right)}\left(\frac{a_0^2}{r^2} + 1\right) \qquad (2.2\text{-}10)$$

$$\sigma_z = - \frac{2\mu P_0}{\left(1 - \frac{a_0^2}{b_0^2}\right)}$$

It is important to notice that in case of plane strain and external pressure only, the axial stress is not always the intermediate principal stress. The necessary conditions for σ_z not to be intermediate

are $\sigma_z \geq \sigma_r$ or $\sigma_z \leq \sigma_\theta$. From Eq. 2.2-10 this leads to

$$-2\mu \leq -\left(\frac{a_0^2}{r^2} + 1\right)$$

$$2\mu \geq \frac{a_0^2}{r^2} + 1$$

$$\frac{a_0^2}{r^2} \leq 2\mu - 1$$

This proves that σ_z is always the intermediate principal stress so long as $r \geq a_0$ and $\mu \neq 1/2$.

2.3 Elastic-Plastic Analysis of a Hollow Cylinder in Plane Strain

2.3a Theoretical consideration of yield criteria

Strength theories of a solid are usually described in terms of state of stress, strain and energy of distortion. Some of the theories that describe the yielding behavior of the material and relevant to this study are briefly summarized here.

1. Mohr's theory of rupture

The state of stress at any point may be represented graphically by a plot known as the Mohr diagram. The Mohr theory of rupture may be expressed by the statement that for a material there exists a boundary called Mohr envelope such that a Mohr circle within the envelope represents a stable condition, whereas a circle tangent to the envelope represents failure on the plane denoted by the point of

tangency. The hypothesis formulated by Mohr may be presented as follows:

1. The line of rupture is independent of the means by which it is obtained.
2. The line of rupture is independent of the intermediate principal stress.
3. The angle of rupture in the material is equal to the angle of the line connecting the points of the minimum stress and the tangent in the Mohr's circle.

In this theory the failure occurs when the maximum shear at a point reaches a critical value. The maximum shear stress, $\tau_{max} = \frac{\sigma_1 - \sigma_3}{2} = k$ where k is a function of $\frac{\sigma_1 + \sigma_3}{2}$, the abscissa of the center of Mohr circle. Triaxial study of rock salt[70] showed that the Mohr's envelope theory is applicable only when the temperature surpasses 500° F or the mean principal stress exceeds 5,500 psi. At this temperature and pressure the material becomes extremely ductile.

2. Coulomb's yield criteria

In principal stress space, the yield surface is a right hexagonal pyramid equally inclined to the deviatoric stress axes (σ_1', σ_2', σ_3'), with its apex on the line $\sigma_1' = \sigma_2' = \sigma_3'$. The hexagonal pyramid is irregular since the yield stress in tension differs from that in compression.[72] The stress equation on any failure plane is given by:

$$\sigma_{max} - N_\phi \sigma_{min} = 2C\sqrt{N_\phi}$$

where

$N_\phi = \tan^2 (45^o + \phi/2)$

C = is the cohesion

ϕ = is the angle of internal friction.

It can be seen from this equation that when $\phi = 0$, $N_\phi = 1$ and Coulomb's criterion becomes equivalent to the maximum shear theory, which is then a special case of Coulomb's criterion.

3. Maximum shear theory (Tresca yield condition)

This criterion is usually stated as "yielding occurs when the greatest absolute value of any one of the three principal shear stresses in the material reaches a certain value."[37] If σ_1 and σ_3 are the maximum and minimum principal stresses, and k is a constant for the material, then

$$\tau_{max} = \frac{\sigma_1 - \sigma_3}{2} = k$$

where k is the yield stress in pure shear.

In case of uniaxial condition $\sigma_1 = Y$, $\sigma_2 = \sigma_3 = 0$ then $\frac{Y}{2} = k$; hence the yield criterion can be stated as

$$\sigma_1 - \sigma_3 = Y$$

This theory may be considered as a special version of Mohr's theory. Both theories are independent of the intermediate principal stress and

consider only the maximum and minimum principal stresses to influence failure. In Mohr's theory the critical value, k, is a function of $\frac{\sigma_1 + \sigma_3}{2}$, the abscissa of the center of Mohr's circle, while in the maximum shear theory, k is a constant radius to any Mohr's circle representing yield conditions.

4. Energy of distortion theory (Mises yield condition)

This takes into account the intermediate principal stress, while the maximum shear stress theory and Mohr's theory assume yield independent of the intermediate principal stress. According to this theory,[33] "yielding begins when the (recoverable) elastic energy of distortion reaches a critical value. Thus a hydrostatic pressure does not cause yielding since it produces only elastic energy of compression in an isotropic solid." This criterion can be written in alternative form as

$$2 J_2' = \sigma_{ij}' \sigma_{ij}' = \sigma_1'^2 + \sigma_2'^2 + \sigma_3'^2 = 2 k^2$$

$$(\sigma_x - \sigma_y)^2 + (\sigma_y + \sigma_z)^2 + (\sigma_z - \sigma_x)^2 + 6 (\tau_{yz}^2 + \tau_{zx}^2 + \tau_{xy}^2) = 6 k^2$$

where k is a parameter depending on the amount of prestrain. The yield locus of this criterion is a circle of radius $\sqrt{2}\ k$ as indicated from the above equation.

The significant difference between Mises and Tresca's yield criteria is that "Mises criterion predicts that the maximum shear

stress in pure torsion is greater by a factor of 1.155 than in pure tension. Tresca's criterion, on the other hand, predicts that they are equal. However, both imply the same yield stress in uniaxial tension and compression, and both are independent of mean stress, $\sigma_m = 1/3\,(\sigma_1 + \sigma_2 + \sigma_3)$.

2.3b Stress analysis in elastic-plastic domain

Plasticity is an important factor for structural stability of salt cavities. The creation of a cavity results in large concentration of stresses that will be reduced to certain tolerable values by the plastic deformation of salt around the cavity. This deformation starts when the differential pressure acting around a cavity reaches a certain critical value. If this value is exceeded, the cavity deforms plastically and never fracture in brittle fashion under increasing pressure but merely widens the plastic zone surrounding the cavity.

When the external pressure is gradually increased from zero, the yield limit will be first reached at the inner surface. On further increase of the outside pressure the plastic domain extends outward into the elastic domain. If the cavity is considered as a thick walled tube, then the plastic domain may extend until the entire tube becomes plastic. The radius at the boundary between elastic and plastic domains is denoted by a "plastic radius," ρ.

For a symmetrical thick-walled cylinder where the external load is always larger than internal load, the main axis may be

considered as principal axis and $\sigma_r \geq \sigma_z \geq \sigma_\theta$. The general stress in the elastic region is governed by Eq. 2.2-1. From maximum shear theory

$$\sigma_\theta - \sigma_r = Y > 0 \qquad (2.3\text{-}1)$$

The stresses from Eq. 2.2-1 become

$$\sigma_\theta - \sigma_r = -\frac{2A}{r^2} \qquad (2.3\text{-}2)$$

From Eq. 2.2-2, it is seen that Eq. 2.3-1 can be satisfied only when P_i is larger than P_o. This contradicts the earlier assumption that P_o is always greater than P_i, and hence the maximum yield theory may be written as

$$\sigma_r - \sigma_\theta = \text{constant} = \frac{3}{2\sqrt{2}} K_o \qquad (2.3\text{-}3)$$

where K_o is the octahedral shearing strength of rock salt determined from the octahedral shear stress theory of failure.

$\tau_o = K_o = \frac{2}{3}(\sigma_1 - \sigma_3)$ for the condition $\sigma_2 = \sigma_3$. Since $\tau_{max} = \frac{\sigma_1 - \sigma_3}{2}$, therefore $\tau_{max} = \frac{3}{2\sqrt{2}} K_o$.

From Eqs. 2.2-1 and 2.2-3

$$\sigma_r - \sigma_\theta = \frac{2A}{r^2}$$

at first yield, $r = a_o$

$$A = \frac{3}{2\sqrt{2}} a_o^2 K_o \qquad (2.3\text{-}4)$$

Substituting this value into Eq. 2.2-2 gives the value of the pressure at first yield

$$(P_0 - P_i) \text{ at first yield} = \frac{3}{2\sqrt{2}} K_0 \left(1 - \frac{a_0^2}{b_0^2}\right) \qquad (2.3\text{-}5)$$

At the elastic-plastic boundary ($r = \rho$) the internal radial pressure is defined by P_ρ and $A = \frac{3}{2\sqrt{2}} \rho^2 K_0$

The pressure necessary to cause yielding at $r = \rho$ is then defined as

$$P_0 - P_\rho = \frac{3}{2\sqrt{2}} K_0 \left(1 - \frac{\rho^2}{b_0^2}\right) \qquad (2.3\text{-}6)$$

From this equation the unknown value of the radial pressure, P_ρ, at $r = \rho$ is given by

$$P_\rho = P_0 - \frac{3}{2\sqrt{2}} K_0 \left(1 - \frac{\rho^2}{b_0^2}\right) \qquad (2.3\text{-}7)$$

and from Eq. 2.2-3 at $r = \rho$

$$2c = \frac{\left(P_\rho - P_0 \frac{b_0^2}{\rho^2}\right) \frac{\rho^2}{b_0^2}}{\left[1 - (\rho^2/b_0^2)\right]} \qquad (2.3\text{-}8)$$

Substituting the value of P_ρ into above equation yields,

$$2c = -P_0 - \frac{3}{2\sqrt{2}} K_0 \frac{\rho^2}{b_0^2} \qquad (2.3\text{-}9)$$

The general stress distribution in the elastic region under the condition $\sigma_r \geq \sigma_z \geq \sigma_\theta$, is then defined as a function of plastic radius ρ by substituting the value of A and 2c into Eq. 2.2-1 such that

$$\sigma_r = \frac{1}{2} \frac{3}{2\sqrt{2}} K_0 \left(\frac{\rho^2}{r^2} - \frac{\rho^2}{b_0^2}\right) - P_0$$

$$\sigma_\theta = -\frac{1}{2} \frac{3}{2\sqrt{2}} K_0 \left(\frac{\rho^2}{r^2} + \frac{\rho^2}{b_0^2}\right) - P_0 \qquad (2.3\text{-}10)$$

$$\sigma_z = -\mu\left(\frac{3}{2\sqrt{2}} K_0 \frac{\rho^2}{b_0^2} + 2P_0\right)$$

this stress distribution equation holds in the elastic region prescribed by $\rho \leq r \leq b_0$.

The stress distribution equations in the plastic region prescribed by $a \leq r \leq \rho$ can be determined by using the equilibrium equation written in total derivative form since there is no variation with respect to z or θ.

$$\frac{d\sigma_r}{dr} + \frac{\sigma_r - \sigma_\theta}{r} = 0 \qquad (2.3\text{-}11)$$

The rest of the equilibrium equations vanish because of axial symmetry. Assuming ideal plasticity with no strain hardening, the yield condition is satisfied throughout the plastic region with the same constant K_0.

From maximum shear theory of yield

$$\sigma_r - \sigma_\theta = \frac{3}{2\sqrt{2}} K_0$$

therefore

$$\frac{d\sigma_r}{dr} = \frac{3}{2\sqrt{2}} \frac{K_0}{r}$$

or

$$\sigma_r = -\frac{3}{2\sqrt{2}} K_0 \ln r + c_1 \qquad (2.3\text{-}12)$$

The constant of integration is determined from the continuity condition at the elastic plastic boundary.

At $r = \rho$

$$\sigma_r]_{\text{elastic}} = \sigma_r]_{\text{plastic}}$$

Equating Eq. 2.3-10 and Eq. 2.3-12, the constant of integration is

$$c_1 = \frac{1}{2}\frac{3}{2\sqrt{2}}K_o\left(1 - \frac{\rho^2}{b_o^2}\right) + \frac{3}{2\sqrt{2}}K_o \ln \rho - P_o \qquad (2.3\text{-}13)$$

Substitute the value of c_1 back into Eq. 2.3-12 and use the maximum shear theory to obtain the following stress distribution.

$$\sigma_r = \frac{3}{2\sqrt{2}}K_o \ln\left(\frac{\rho}{r}\right) + \frac{1}{2}\frac{3}{2\sqrt{2}}K_o\left(1 - \frac{\rho^2}{b_o^2}\right) - P_o$$

$$\sigma_\theta = \frac{3}{2\sqrt{2}}K_o \ln\left(\frac{\rho}{r}\right) - \frac{1}{2}\frac{3}{2\sqrt{2}}K_o\left(1 + \frac{\rho^2}{b_o^2}\right) - P_o \qquad (2.3\text{-}14)$$

For plane strain, $\epsilon_z = 0$ and $\sigma_z = \mu(\sigma_r + \sigma_\theta)$, therefore:

$$\sigma_z = 2\mu\left[\frac{3}{2\sqrt{2}}K_o \ln\left(\frac{\rho}{r}\right) - \frac{3}{2\sqrt{2}}K_o \frac{\rho^2}{b_o^2} - P_o\right]$$

These equations describe the stress distribution in plastic region ($a \leq r \leq \rho$). The radius to the front of the plastic zone can be obtained as a function of the loading conditions of the cavity. By substituting the condition at the inner boundary ($r = a$), $P_i = -\sigma_r$, into Eq. 2.3-14 it may be expressed as:

$$\rho = a \exp. \left[\frac{1}{\frac{3}{2\sqrt{2}} K_c} (P_0 - P_i) - \frac{1}{2} \left(1 - \frac{\rho^2}{b_o^2}\right)\right] \qquad (2.3\text{-}15)$$

If the ratio, ρ/b_0 is sufficiently smaller than unity, Eq. 2.3-15 becomes with good approximation

$$\rho = a \exp. \left[\frac{1}{\frac{3}{2\sqrt{2}} K_o} (P_0 - P_i) - \frac{1}{2}\right] \qquad (2.3\text{-}16)$$

which exhibits a linear relation between ρ and $P_0 - P_i$ on semi-log diagram. These two equations (2.3-15 and 2.3-16) determine the advance of the plastic radius into the elastic region, if it is assumed that the change in internal radius is so small with respect to the mean radius that "a_0" instead of "a" can be used in the calculations. However, if the change in "a" is significant compared with the "a_0" value, this cannot be neglected and an expression for "a" in terms of ρ is to be solved simultaneously. It is interesting to note that the plastic radius is independent of the axial strain, ϵ_z, so long as $\sigma_r > \sigma_z > \sigma_\theta$.

2.3c Stress strain relation in combined elastic plastic domain.

When a specimen reaches the yield point at the inner boundary, a permanent plastic deformation will occur. Then the total deformation becomes a sum of a recoverable elastic deformation and a permanent plastic deformation. As the load increases the plastic region spreads outward until the whole cylinder becomes completely plastic, reaching an equilibrium with the outside loads. Whenever a

plastic condition is present, the general strain increment equation can be written as

$$d\epsilon_{ij} = d\epsilon_{ij}^{e} + de_{ij}^{P} \qquad (2.3\text{-}17)$$

Where the superscripts e and P denote the elastic and plastic components respectively. The elastic strain increments are given by Hooke's law as:

$$d\epsilon_{r}^{e} = \frac{1}{E}\left[d\sigma_{r} - \mu d\left(\sigma_{\theta} + \sigma_{z}\right)\right]$$

$$d\epsilon_{\theta}^{e} = \frac{1}{E}\left[d\sigma_{\theta} - \mu d\left(\sigma_{r} + \sigma_{z}\right)\right]$$

$$d\epsilon_{z}^{e} = \frac{1}{E}\left[d\sigma_{z} - \mu d\left(\sigma_{r} + \sigma_{\theta}\right)\right]$$

by knowing the changes in stresses, the elastic strain rate can be determined. If the plastic potential theory is used, the plastic strain increment may be determined as follows:

The strain increment vector has to be normal to the yield surface in stress space such that

$$d\epsilon_{ij}^{P} \propto \frac{\delta f}{\delta \sigma_{ij}} \qquad (2.3\text{-}19)$$

If the Mises yield condition is assumed, then

$$f = \frac{1}{6}\left[\left(\sigma_{x} - \sigma_{y}\right)^{2} + \left(\sigma_{y} - \sigma_{z}\right)^{2} + \left(\sigma_{z} - \sigma_{x}\right)^{2}\right] + \frac{1}{2}\left[\tau^{2}_{xy} + \tau^{2}_{yx} + \tau^{2}_{zy} + \tau^{2}_{zx} + \tau^{2}_{xz}\right]$$

(2.3-20)

and

$$\frac{\delta f}{\delta \sigma_{ij}} = \sigma_{ij}'$$

Eq. 2.3-19 may then be expressed as $d\epsilon_{ij}^{P} = d\lambda\, \sigma_{ij}'$ (2.3-21)

or

$$\frac{d\epsilon_{ij}^{P}}{\sigma_{ij}'} = \frac{\frac{1}{2} d\gamma_{ij}^{P}}{\tau_{ij}} = d\lambda$$

This may be expressed as

$$\frac{d\epsilon_r^{P} - d\epsilon_\theta^{P}}{\sigma_r - \sigma_\theta} = \frac{d\epsilon_\theta^{P} - d\epsilon_z^{P}}{\sigma_\theta - \sigma_z} = \frac{d\epsilon_z^{P} - d\epsilon_r^{P}}{\sigma_z - \sigma_r} = d\lambda \quad (2.3\text{-}22)$$

If Eq. 2.3-21 is expanded the total stress-strain relation which is known as the Reuss equation[33] may be written as:

$$d\epsilon_r = \frac{1}{E}[d\sigma_r - \mu d(\sigma_\theta + \sigma_z)] + \frac{1}{3} d\lambda (2\sigma_r - \sigma_\theta - \sigma_z)$$

$$d\epsilon_\theta = \frac{1}{E}[d\sigma_\theta - \mu d(\sigma_r + \sigma_z)] + \frac{1}{3} d\lambda (2\sigma_\theta - \sigma_r - \sigma_z) \quad (2.3\text{-}23)$$

$$d\epsilon_z = \frac{1}{E}[d\sigma_z - \mu d(\sigma_\theta + \sigma_r)] + \frac{1}{3} d\lambda (2\sigma_z - \sigma_r - \sigma_\theta)$$

The strain increment equations may be determined by relating $d\lambda$ with the octahedral shear stress τ_0 and the increment of plastic octahedral shear strain $d\gamma_0^{P}$ as follows:

The octahedral shear stress and strain are defined as

$$\tau_0 = \frac{1}{3}[(\sigma_r - \sigma_\theta)^2 + (\sigma_\theta - \sigma_z)^2 + (\sigma_z - \sigma_r)^2 + 6(\tau_{r\theta}^2 + \tau_{rz}^2 + \tau_{zr}^2)]^{1/2} \quad (2.3\text{-}24)$$

and the octahedral plastic shear strain increment as

$$d\gamma_0^P = \frac{2}{3}\left[(d\epsilon_r^P - d\epsilon_\theta^P)^2 + (d\epsilon_\theta^P - d\epsilon_z^P)^2 + (d\epsilon_z^P - d\epsilon_r^P)^2 \right.$$

$$\left. \frac{3}{2}(d\gamma_{r\theta}^{P2} + d\gamma_{\theta z}^{P2} + d\gamma_{zr}^{P2})\right]^{1/2} \qquad (2.3\text{-}25)$$

Substituting the value of Eq. 2.3-22 into the above equation, one obtains

$$d\gamma_0^P = \frac{2}{3}d\lambda[(\sigma_r - \sigma_\theta)^2 + (\sigma_\theta - \sigma_z)^2 + (\sigma_z - \sigma_r)^2 + 6(\tau_{r\theta}^2 + \tau_{\theta z}^2 + \tau_{zr}^2)]^{1/2}$$

(2.3-26)

Comparing this with the equation of the octahedral shear stress gives

$$d\lambda = \frac{1}{2\tau_0}\, d\gamma_0^P \qquad (2.3\text{-}27)$$

This shows the significance of the scalar function $d\lambda$ as a function of the octahedral shear stress and the increment of the octahedral shear strain.

If the derivative with respect to time is taken from the Reuss equation is divided by dt, then the total strain rate equation may be expressed as follows:

$$\frac{d\epsilon_r}{dt} = \frac{1}{E}\left[\frac{d\sigma_r}{dt} - \mu\frac{d}{dt}(\sigma_\theta + \sigma_z)\right] + \frac{1}{2\tau_0}\frac{d\gamma_0}{dt}\left(\frac{2\sigma_r - \sigma_\theta - \sigma_z}{3}\right)$$

$$\frac{d\epsilon_\theta}{dt} = \frac{1}{E}\left[\frac{d\sigma_r}{dt} - \mu \frac{d}{dt}(\sigma_r + \sigma_z)\right] + \frac{1}{2\tau_0}\frac{d\gamma_0}{dt}\left(\frac{2\sigma_r - \sigma_\theta - \sigma_z}{3}\right) \qquad (2.3\text{-}27)$$

$$\frac{d\epsilon_z}{dt} = \frac{1}{E}\left[\frac{d\sigma_z}{dt} - \mu \frac{d}{dt}(\sigma_r + \sigma_\theta)\right] + \frac{1}{2\tau_0}\frac{d\gamma_0}{dt}\left(\frac{2\sigma_z - \sigma_r - \sigma_\theta}{3}\right)$$

The total incremental strain rate equations are then related to the incremental change of the plastic octahedral shear strain. With this function the strain rate for a hollow thick-walled cylinder may be evaluated. Evaluation of creep equations as applied to laboratory experiments is considered later in Chapter VI.

Hill's[33] equation for work hardening has been used to check the possibility of the existence of work hardening in rock salt. From the plastic potential theory

$$d\epsilon_{ij}^{P} = \sigma_{ij}' \, d\lambda$$

The scalar function $d\lambda$ may be defined as

$$\frac{d\lambda}{d\bar{\epsilon}^{P}} = \frac{3}{2}\frac{1}{\bar{\sigma}} \qquad (2.3\text{-}28)$$

The quantity $d\bar{\epsilon}^{P}$ is known as the generalized plastic strain-increment and defined by

$$d\bar{\epsilon}^{P} = \frac{2}{3}\left(d\epsilon_{ij}^{P} \, d\epsilon_{ij}^{P}\right)^{1/2} = \frac{1}{\sqrt{3}} \, d\gamma_0^{P}$$

and $\bar{\sigma}$ is known as the generalized stress or effective stress and defined by

$$\bar{\sigma} = \sqrt{\frac{3}{2}} \left(\sigma_{ij}' \, \sigma_{ij}'\right)^{1/2} = \frac{3}{\sqrt{2}} \tau_0$$

If there is work hardening the plastic strain increment may be defined as Hill's[33] Eq. 30.

$$d\epsilon_{ij}^{P} = \frac{3}{2} \frac{\sigma_{ij}'}{\bar{\sigma}} \frac{d\bar{\sigma}}{H'} \qquad (2.3\text{-}29$$

where "H' is the slope of the equivalent stress/plastic strain curve."

From Eq. 2.3-29, $d\lambda = \frac{3}{2} \frac{d\bar{\sigma}}{\bar{\sigma} H'}$ and hence

$$H' = \frac{3}{2} \frac{d\bar{\sigma}}{\bar{\sigma} \, d\lambda} \qquad (2.3\text{-}30$$

If the values of $\bar{\sigma}$ and $d\lambda$ are known, then the slope of the stress-plastic strain curve may be determined. (See table 6.4, Chapter VI.)

2.3d Small strain plastic boundary motion in plane strain with maximum shear stress yield condition and plastic potential theory.

The displacement solution in the elastic domain may be obtained from Hooke's law as

$$\epsilon_\theta = \frac{u}{r} = \frac{1}{E} \left[\sigma_\theta - u \left(\sigma_r + \sigma_z\right)\right]$$

Substitute the value of σ_θ, σ_r and σ_z from the Eq. 2.3-10 and replace $E = 2G(1+u)$ to obtain the radial displacement u as a function of geometry conditions and external stress, such that

$$u_e = \frac{1}{2G} \left\{ \frac{\frac{3}{2\sqrt{2}} K_0}{2} \left[(2u - 1) \, r \, \frac{\rho^2}{r}\right] - (1 - 2\mu) P_0 r \right\} \qquad (2.3\text{-}31)$$

This holds for the region described $\rho \leq r \leq b$.

The small strain boundary motion solution in the region described by $a \leq r \leq \rho$ may be obtained by assuming elastic compressibility such that

$$\epsilon_r + \epsilon_\theta = \left(\frac{1-2\mu}{E}\right)(\sigma_r + \sigma_\theta + \sigma_z);\ \epsilon_z = 0 \qquad (2.3\text{-}32)$$

or

$$\frac{du}{dr} + \frac{u}{r} = \left(\frac{1-2\mu}{E}\right)[(1+\mu)(\sigma_r + \sigma_\theta)]$$

Substitute the value of the plastic stresses, Eq. 2.3-14, into the above equation to obtain

$$\frac{du}{dr} + \frac{u}{r} = \left(\frac{1-2\mu}{G}\right)\left[\frac{3}{2\sqrt{2}} K_0 \ln\frac{\rho}{r} - \frac{\frac{3}{2\sqrt{2}} K_0}{2}\frac{\rho^2}{b_0^2} - P_0\right] \qquad (2.3\text{-}33)$$

This may be reduced to the differential form such that

$$\frac{d}{dr}(ur) = \left(\frac{1-2u}{G}\right)\left[\frac{3}{2\sqrt{2}} K_0\, r \ln\frac{\rho}{r} - \frac{\frac{3}{2\sqrt{2}} K_0}{2}\frac{\rho^2}{b_0^2} r - P_0 r\right] \qquad (2.3\text{-}34)$$

integrate

$$u_p = \left(\frac{1-2\mu}{G}\right)\left[\frac{\frac{3}{2\sqrt{2}} K_0}{2}\left(r \ln\frac{\rho}{r} + \frac{r}{2}\right) - \frac{\frac{3}{2\sqrt{2}}}{4} K_0 \frac{\rho^2}{b_0^2} r - \frac{P_o r}{2}\right] + \frac{C}{r} \qquad (2.3\text{-}35)$$

This defines the radial displacement in the plastic domain (small strain). To determine the unknown constant of integration C, continuity at the elastic plastic boundary is assumed such that

$$u_e = u_p \quad \text{at} \quad r = \rho \tag{2.3-36}$$

Substitute $r = \rho$ and solve for C to get

$$C = -(1-\mu)\frac{\frac{3}{2\sqrt{2}}K_o}{2G}\rho^2$$

Therefore the radial displacement in the plastic region prescribed by $a \leq r \leq \rho$ is defined by

$$u_p = \frac{(1-2\mu)}{G}\left[\frac{\frac{3}{2\sqrt{2}}K_o}{2}\left(r \ln\frac{\rho}{r} + \frac{r}{2}\right) - \frac{\frac{3}{2\sqrt{2}}K_o}{4}\frac{\rho^2}{b_o^2}r - P_o\frac{r}{2}\right] - (1-\mu)\frac{\frac{3}{2\sqrt{2}}K_o}{2G}\frac{\rho^2}{r} \tag{2.3-37}$$

For the determination of displacement at the inside boundary, evaluate u_p at $r = a$

$$u_{r=a} = \frac{(1-2\mu)}{G}\left[\frac{3}{2\sqrt{2}}K_o\left(\frac{a}{2}\ln\frac{\rho}{a} + \frac{a}{4}\right) - \frac{\frac{3}{2\sqrt{2}}K_o}{4}\frac{\rho^2 a}{b_o^2} - \frac{P_o a}{2}\right] - (1-\mu)\frac{\frac{3}{2\sqrt{2}}K_o}{2G}\frac{\rho^2}{a} \tag{2.3-38}$$

The variation of u vs. P_o is plotted as shown in Fig. 2.4. With the exception of the "plastic radius" ρ, and P_o, all other parameters are known. The "plastic radius" ρ, could be expressed as a function of external pressure P_o, but under small strain condition this could be approximated by the original radius a_o where $a = a_o + u(a_o, \rho)$

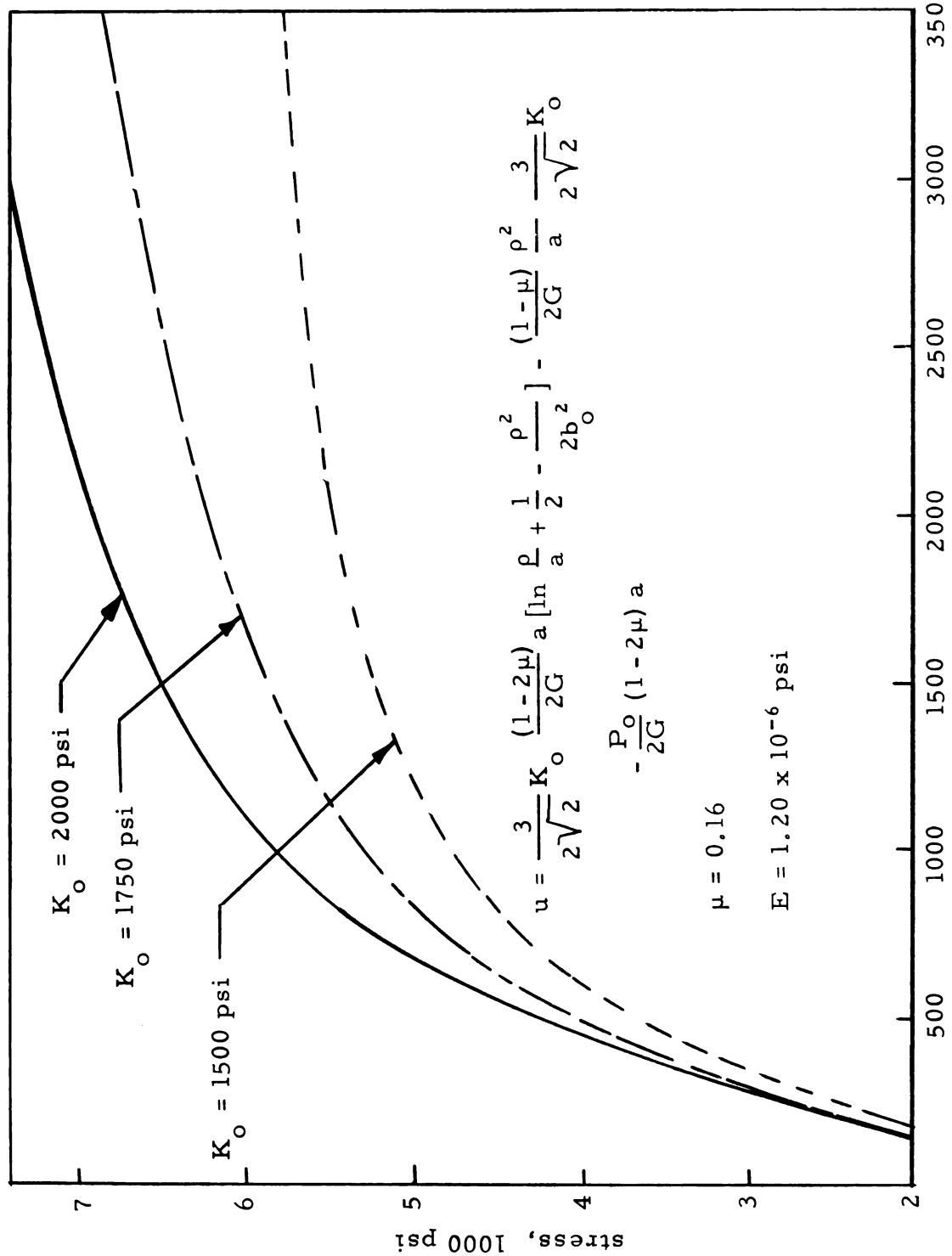

Fig. 2.4 Theoretical analysis of the radial displacement in thick walled cylinder with plane strain and triaxial compression

(where u is a negative quantity). A mathematical concept of a model salt cavity is presented in Fig. 2.5.

2.3e Determination of the inner radius of a hollow thick-walled cylinder for large-strain solution and plane strain.

If the compressibility equation is used and the movement of the plastic boundary radius, ρ, is taken as scale of "time" (see Hill[33], p. 100), the relation of inner radius to plastic radius is calculated as follows:[51]

$$d_r + d_\theta + d_z = \left(\frac{1-2\mu}{E}\right) \frac{d}{d\rho} (\sigma_r + \sigma_\theta + \sigma_z) \qquad (2.3\text{-}39)$$

where $\frac{d}{d\rho}$ is a material derivative applied to a function of ρ and r such that

$$\frac{d}{d\rho} = \frac{\partial}{\partial \rho} + V\left(\frac{\partial}{\partial r}\right)$$

$$V = \text{radial velocity} = \frac{dr}{d\rho},$$

where r is the coordinate of a moving particle.

$$d_r = \frac{dV}{dr}$$

$$d_e = \frac{V}{r}$$

It is known that $\sigma_z = \mu(\sigma_r + \sigma_\theta)$, in plane strain with maximum shear yield condition and plastic potential theory, where

$$\sigma_r + \sigma_\theta = \frac{3}{2\sqrt{2}} K_o \left(2 \ln \frac{\rho}{r} - \frac{\rho^2}{b_o^2}\right) - 2P_o$$

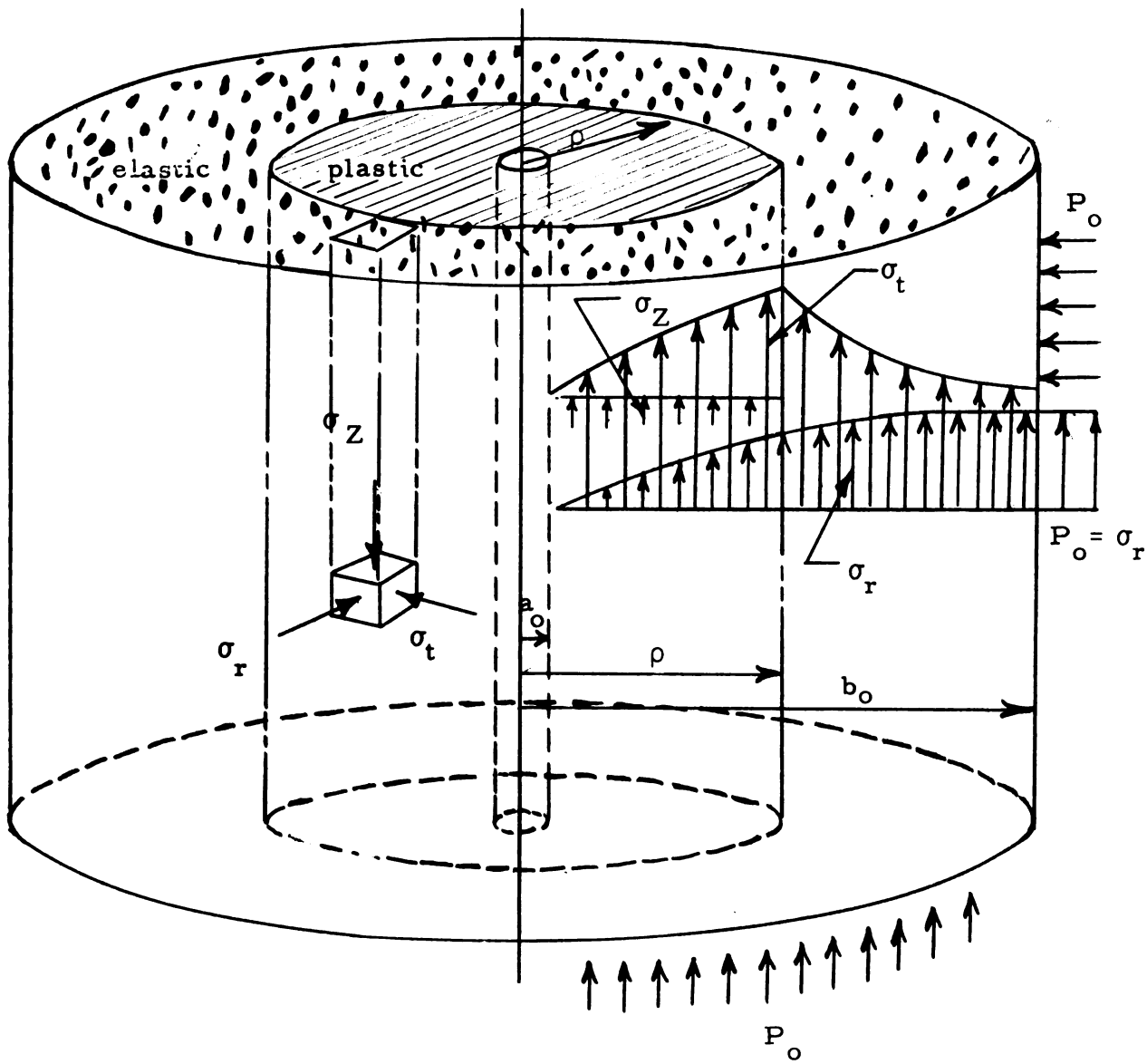

Displacement

$$u = \frac{(1-2\mu)}{G}\left[\frac{3}{2\sqrt{2}}K_o\left(\frac{r}{2}\ln\frac{\rho}{r}+\frac{r}{4}\right)-\frac{P_o r}{2}-\frac{\frac{3}{2\sqrt{2}}K_o\rho^2}{4\,b_o^2}\,r\right] - (1-\mu)\frac{\frac{3}{2\sqrt{2}}K_o}{2G}\frac{\rho^2}{r}-\mu r\,\epsilon_z$$

Fig. 2.5 Mathematical concept of model salt cavity

From above expression and using Eq. 2.3-39 for plane strain with $d_z = 0$, gives

$$\frac{dV}{dr} + \frac{V}{r} + 0 = \left(\frac{1-2\mu}{E}\right) \frac{d}{d\rho} \left[2 \frac{3}{2\sqrt{2}} K_o (1+\mu) \ln \frac{\rho}{r} - 2(1+\mu) P_o \right.$$

$$\left. - (1+\mu) \frac{3}{2\sqrt{2}} K_o \frac{\rho^2}{b_o^2} \right] \qquad (2.3\text{-}40)$$

Now let $2G = \frac{E}{1+\mu}$

$$P_o = \frac{3}{2\sqrt{2}} K_o \left[\ln \frac{\rho}{a} + \frac{1}{2} \left(1 - \frac{\rho^2}{b_o^2}\right) \right] \qquad (2.3\text{-}41)$$

$$\frac{dP_o}{d\rho} = \frac{3}{2\sqrt{2}} K_o \left(\frac{1}{\rho} - \frac{\rho}{b_o^2}\right)$$

Substitute the value of P_o back into Eq. 2.3-40 to eliminate P_o, then

$$\frac{V}{r} + \frac{dV}{dr} = \left(\frac{1-2\mu}{2G}\right) \frac{d}{d\rho} \left[\frac{3}{\sqrt{2}} K_o \ln \frac{\rho}{r} - \frac{3}{\sqrt{2}} K_o \left(\ln \frac{\rho}{a} + \frac{1}{2} - \frac{\rho^2}{2b_o^2} \right) \right.$$

$$\left. - \frac{3}{2\sqrt{2}} K_o \frac{\rho^2}{b_o^2} \right]$$

Taking the derivative with respect to "time," ρ, and collecting terms, it becomes

$$\frac{V}{r} + \frac{dV}{dr} = \frac{3}{2\sqrt{2}} K_o \left(\frac{1-2\mu}{G}\right) \left[\frac{1}{a} \frac{da}{d\rho} - \frac{1}{r} \frac{dr}{d\rho} \right] \qquad (2.3\text{-}42)$$

where $\frac{da}{d\rho}$ is the rate of change in internal radius with respect to

"time," ρ, which is the velocity expressed as $V(a)$, and $\frac{dr}{d\rho} = V$.

Hence

$$\frac{V}{r} + \frac{dV}{dr} = \frac{3}{2\sqrt{2}} K_o \left(\frac{1-2\mu}{G}\right)\left[\frac{V(a)}{a} - \frac{V}{r}\right] \qquad (2.3\text{-}43)$$

Let $M = \frac{3}{2\sqrt{2}} K_o \left(\frac{1-2\mu}{G}\right)$

so that Eq. 2.3-43 reduces to

$$\frac{dV}{dr} + (1+M)\frac{V}{r} = M\frac{V(a)}{a} \qquad (2.3\text{-}44)$$

Assuming M to be very small compared to unity, this is closely approximated by

$$\frac{dV}{dr} + \frac{V}{r} = M\frac{V(a)}{a}$$

or

$$r\frac{dV}{dr} + V = \frac{d}{dr}(Vr) = M\frac{V(a)}{a}\, r$$

whence

$$Vr = M\frac{V(a)}{a}\frac{r^2}{2} + c(\rho) \qquad (2.3\text{-}45)$$

Since V is a function of both r and ρ, $c(\rho)$ is the constant of integration, to be determined from the continuity conditions at the elastic-plastic boundary. Recalling that $r = \rho$ at the elastic-plastic boundary

$$V_e = V_P \text{ at } r = \rho$$

Assume ϵ_z is zero in plane strain and replaces P_o by its value as a

function of ρ. Then the elastic region radial displacement of Eq. 2.3-31 reduces, after collecting terms, to

$$u_e = -\frac{\frac{3}{2\sqrt{2}} K_o}{2G} \left[\frac{\rho^2}{2r} + (1-2\mu)\, r\left(\ln \frac{\rho}{a} + \frac{1}{2}\right)\right] \qquad (2.3\text{-}46)$$

Let

$$du = V\, d\rho$$

$$V = \frac{du}{d\rho} = \frac{\partial u}{\partial \rho} + V \frac{\partial u}{\partial r}$$

or

$$\frac{\partial u}{\partial \rho} = V\left(1 - \frac{\partial u}{\partial r}\right)$$

hence,

$$V = \frac{\partial u/\partial \rho}{1 - \frac{\partial u}{\partial r}} \qquad (2.3\text{-}47)$$

From Eqs. 2.3-46 and 2.3-47, the value V at the elastic-plastic boundary may be determined by taking derivatives $\frac{\partial u_e}{d\rho}$ and $\frac{\partial u_e}{d\rho}$ and substituting into Eq. 2.3-47 to get for $r = \rho$

$$V_e\,]_{r=\rho} = \frac{-\frac{\frac{3}{2\sqrt{2}} K_o}{2G} \left[1 + (1-2\mu)\left(1 - \frac{\rho}{a} V(a)\right)\right]}{1 + \frac{\frac{3}{2\sqrt{2}} K_o}{2G} \left[(1-2\mu)\left(\ln \frac{\rho}{a} + \frac{1}{2}\right)\right]} \qquad (2.3\text{-}48)$$

since

$$\frac{\frac{3}{2\sqrt{2}} K_o}{2G} (1-2\mu)\left(\ln \frac{\rho}{a} + \frac{1}{2}\right) << 1$$

we may approximate $V_e]_{r=\rho}$

$$V_{r=\rho} = -\frac{\frac{3}{2\sqrt{2}}K_o}{2G} - \frac{(1-2\mu)\frac{3}{2\sqrt{2}}K_o}{2G}\left(1-\frac{\rho}{a}V(a)\right)$$

or

$$V_{r=\rho} = -\frac{\frac{3}{2\sqrt{2}}K_o}{2G} - \frac{M}{2}\left(1-\frac{\rho}{a}V(a)\right) \qquad (2.3\text{-}49)$$

Now apply the condition that $V_e = V_p$ at the elastic-plastic boundary which implies that Eq. 2.3-45 is equal to Eq. 2.3-49 at $r = \rho$.

Therefore

$$c(\rho) = -\frac{\frac{3}{2\sqrt{2}}K_o\rho}{2G} - \frac{M}{2}\rho$$

if this value is substituted back into Eq. 2.3-45, the solution for plastic velocity is then

$$V = \frac{MV(a)}{2a}r - \left(\frac{\frac{3}{2\sqrt{2}}K_o}{2G} + \frac{M}{2}\right)\frac{\rho}{r} \qquad (2.3\text{-}50)$$

which describes the velocity at any point in the plastic region.

From the preceding results, an expression for the ratio $(\frac{a}{a_o})$ of the current inside radius to the original inside radius can be obtained in terms of the elastic plastic boundary radius.

Evaluating Eq. 2.3-50 at $r = a$ and substituting

$$V(a) = \frac{da}{d\rho}$$

yields

$$\frac{da}{d\rho}\left(1 - \frac{M}{2}\right) = -\frac{\frac{3}{2\sqrt{2}} K_o}{2G} \frac{\rho}{a} - \frac{M}{2} \frac{\rho}{a}$$

or

$$\int_{a_1}^{a} a\,da = \frac{1}{\left(1 - \frac{M}{2}\right)} \left(-\frac{\frac{3}{2\sqrt{2}} K_o}{2G} - \frac{M}{2}\right) \int_{a_1}^{\rho} \rho\,d\rho$$

where the limit on a is from initial yield internal radius a_1 to current internal radius a and the integral on ρ is from same point a_1 to current position ρ.

Integrating, and neglecting M in comparison to unity, yields

$$\frac{1}{2}\left(a^2 - a_1^2\right) = -\left(\frac{\frac{3}{2\sqrt{2}} K_o}{2G} + \frac{M}{2}\right)\left(\rho^2 - a_1^2\right)\frac{1}{2}$$

or

$$a^2 - \left(1 + \frac{\frac{3}{2\sqrt{2}} K_o}{2G} + \frac{M}{2}\right) a_1^2 = -\left(\frac{\frac{3}{2\sqrt{2}} K_o}{2G} + \frac{M}{2}\right) \rho^2 \qquad (2.3\text{-}51)$$

Now

$$a_1 = a_o + u_o,$$

where u_o is the boundary displacement at first yield.

$$a_1^2 = a_o^2 + 2a_o u_o + u_o^2;$$

Since $u_o \ll a_o$, a good approximation is

$$a_1^2 - a_o^2 = 2a_o u_o \qquad (2.3\text{-}52)$$

and u_o as a function of a_o may be obtained from the elastic solution

radial displacement at $\rho = a_o$ when

$$P_o = \frac{\frac{3}{2\sqrt{2}} K_o}{2} \left(1 - \frac{a_o^2}{b_o^2}\right)$$

the boundary conditions for the elastic solution being imposed as usual in the undeformed configuration with $a = a_o$. Substituting the value of P_o and collecting terms reduces the displacement given by Eq. 2.3-46 to

$$u_o = -\frac{a_o}{2}\left(\frac{\frac{3}{2\sqrt{2}} K_o}{2G} + M\right) \qquad (2.3\text{-}53)$$

Substitute this back into Eq. 2.3-52 to obtain

$$a_1^2 = a_o^2 \left(1 - \frac{\frac{3}{2\sqrt{2}} K_o}{2G} - \frac{M}{2}\right)$$

Hence an expression for current radius a in terms of initial radius a_o may be obtained by substituting the value of "a_1" into Eq. 2.3-51 to get

$$a^2 = a_o^2 \left[1 - \left(\frac{\frac{3}{2\sqrt{2}} K_o}{2G} + \frac{M}{2}\right)^2\right] - \left(\frac{\frac{3}{2\sqrt{2}} K_o}{2G} + M\right) \rho^2$$

Since

$$\left(\frac{\frac{3}{2\sqrt{2}} K_o}{2G} + \frac{M}{2}\right)^2 << 1$$

The above equation is closely approximated by

$$a^2 = a_o^2 - \left(\frac{\frac{3}{2\sqrt{2}} K_o}{2G} + \frac{M}{2}\right) \rho^2$$

or

$$\left[\frac{a^2}{a_o^2} = 1 - \frac{\frac{3}{2\sqrt{2}} K_o}{G} (1 - \mu) \frac{\rho^2}{a_o^2}\right], \quad \frac{\rho}{a_o} \geq 1 \qquad (2.3\text{-}54)$$

This equation describes the behavior of inside radius as a function of plastic radius and structural properties of the material. It is clear that as the plastic radius ρ, which is a function of loading, increases, the ratio of $\frac{a}{a_o}$ decreases. For $\rho = a_o$ at the initial yield, the ratio of $\frac{a}{a_o}$ is equal to the ratio of elastic radius a to initial radius a_o. This relation between the inside radius and plastic radius defines too, the stability of the cavity. As ρ increases, the outside pressure increases accordingly and hence the inside radius, a, decreases and thus the cavity remains stable. It should be remarked here that the second term on the right is small in comparison to unity until ρ becomes large in comparison to a_o.

2.4 Analysis of Completely Plastic Cylinder with Plane Strain

2.4a Stress distribution in completely plastic cylinder.

From equilibrium equation, we obtain, as in Eq. 2.3-12

$$\sigma_r = \frac{3}{2\sqrt{2}} K_o \ln r + B \qquad (2.4\text{-}1)$$

The constant of integration B is determined from the internal boundary condition that at $r = a$, $\sigma_r = - P_i$. Hence

$$B = \frac{3}{2\sqrt{2}} K_o \ln a - P_i$$

and

$$\sigma_r = \frac{3}{2\sqrt{2}} K_o (\ln \frac{a}{r}) - P_i$$

$$\sigma_\theta = \frac{3}{2\sqrt{2}} K_o (\ln \frac{a}{r} - 1) - P_i \qquad (2.4\text{-}2)$$

$$\sigma_z = 2\mu (\frac{3}{2\sqrt{2}} K_o \ln \frac{a}{r} - \frac{1}{2} - P_i)$$

Eq. 2.4-2 describes the plastic stress distribution in the domain where $a \leq r \leq b$. The outside pressure necessary to create a complete plastic state is determined by considering the boundary condition at $r = b$, $\sigma_r = - P_o$. Hence

$$- P_o = \frac{3}{2\sqrt{2}} K_o (\ln \frac{a}{b}) - P_i$$

or

$$P_o = \frac{3}{2\sqrt{2}} K_o \ln (\frac{a}{b}) + P_i \qquad (2.4\text{-}3)$$

The behavior of the inner radius in the plastic region may be expressed as

$$\frac{a}{b} = e^{- \frac{1}{\frac{3}{2\sqrt{2}} K_o} (P_o - P_i)} \qquad (2.4\text{-}4)$$

It is very convenient to obtain the octahedral shearing strength from the slope of this curve. The theoretical expression for the ratio a/b when plotted against the outside pressure on a semi-log paper gives a linear relation whose slope is $- 3/2\sqrt{2}\ K_o$, a function of the

octahedral shearing strength. The above equation will be used later to determine the shear strength of the material.

If incompressibility is assumed, the plastic strains and displacements may be calculated as follows:

$$\epsilon_r + \epsilon_\theta + \epsilon_z = 0$$

or

$$\frac{du}{dr} + \frac{u}{r} + \epsilon_z = 0$$

On integration this equation yields

$$u = -\frac{\epsilon_z r}{2} + \frac{c_1}{r}, \quad \epsilon_z = \text{constant} \tag{2.4-5}$$

The constant of integration c_1 is determined as a function of radial displacement at r = a where,

$$u_a = u_{r=a} = -\frac{\epsilon_z a}{2} + \frac{c_1}{a}$$

or

$$c_1 = \frac{\epsilon_z a^2}{2} + u_a a$$

Substituting this into Eq. 2.4-5) yields

$$u = \frac{\epsilon_z}{2}\left(\frac{a^2}{r} - r\right) + u_a \frac{a}{r} \tag{2.4-6}$$

The displacement at the elastic plastic boundary is obtained by substituting $r = \rho$ into above equation to give

$$u_\rho = \frac{\epsilon_z}{2}\left(\frac{a^2}{\rho^2} - \rho\right) + u_a \frac{a}{\rho} \tag{2.4-7}$$

Neglecting the first term on the right, which is zero in plane strain, the displacement at the innerface of the cavity may be expressed as

$$u_a = \left(\frac{\rho}{a}\right) u_\rho \tag{2.4-8}$$

Because of the continuity at the elastic plastic boundary, $u_\rho = u^e_{r=\rho}$

Hence by Eq. 2.3-31

$$u_a = \frac{\rho}{a} \cdot \frac{1}{2G}\left\{\frac{\frac{3}{2\sqrt{2}} K_o}{2}\left[(2\mu - 1)\frac{\rho^3}{b_o^2} - \rho\right] + (2\mu - 1)\rho P_o\right\} \tag{2.4-9}$$

This result was derived under the assumption of compressibility in the elastic region and incompressibility in the plastic region. Finally, the tangential and radial strains in the plastic region are also obtained from Eq. 2.4-6, such that

$$\begin{aligned} \epsilon_\theta &= \frac{u}{r} = \frac{\epsilon_z}{2}\left(\frac{a^2}{r^2} - 1\right) + u_a \frac{a}{r^2} \\ \epsilon_r &= \frac{du}{dr} = -\frac{\epsilon_z}{2}\left(\frac{a^2}{r^2} + 1\right) - u_a \frac{a}{r^2} \end{aligned} \tag{2.4-10}$$

where u_a is given by Eq. 2.4-9.

CHAPTER III

DETERMINATION OF THE MATERIAL PROPERTIES

3.1 Linear Viscoelastic Behavior of a Solid Cylinder with a Laterally Constrained Motion

3.1a General remarks

Elastic and plastic analysis of rock salt has been treated solely in the previous chapters with no reference to the viscous behavior of the material. The triaxial study of rock salt in the laboratory showed that rock salt exhibits certain plastic and viscoelastic properties. These properties are needed to describe the time dependent behavior of the hollow cylinder with mathematical formulas.

Solid materials that possess the characteristics to flow are called viscoelastic or viscoplastic materials. Such materials possess rigidity and at the same time flow and dissipate energy by internal friction. Under different external conditions, these materials may exhibit both solid and fluid characteristics simultaneously. This study is mainly concerned with those materials which possess characteristics of both the elastic (Hookean) solid and the viscous Newtonian fluid. The ideal linear elastic element is represented by a "spring" and a linear viscous element by a "dashpot." Since it is desired to look at the material behavior in between the spring and dashpot, different mechanical models were arranged to fit different

materials. There are several different possibilities for combining elasticity and viscosity, but two approaches have received special attention. Simplified forms of these are the elements in parallel (Voigt, Kelvin body) and the elements in series (Maxwell). The constitutive equations of the above two models are indicated respectively as

$$\sigma = (E + \eta D)\,\epsilon \qquad \text{(Kelvin)}$$

and

$$\dot{\epsilon} = \left(\frac{D}{E} + \frac{1}{\eta}\right)\sigma \qquad \text{(Maxwell)}$$

where η is the viscosity coefficient and $D = \frac{d}{dt}$. Both of the above equations contain the material time derivative of small strain and the Maxwell contains the material time derivative of stress. Both of these equations are not objective[52] and hence cannot be applied for unrestricted motions. However for symmetrical loading, where there is no rotation, the principle of objectivity is not involved.

3.1b General visco-plastic behavior of rock salt.

The physical behavior of a rock salt specimen subjected to homogeneous stresses of the type $\sigma_z \neq \sigma_x = \sigma_y$ is investigated. This investigation intends to describe the stress and strain behavior of rock salt by a mechanical model. Based on the triaxial behavior of a laterally confined specimen the following observations have been made:

1. Rapid plastic deformation occurs during loading and shortly afterwards and reaches its maximum value in a few hours period.
2. The amount of deformation in Part 1 is a relatively large part of the total deformation.
3. A slow deformation process continues to take place for a long period of time extending in some experiments up to a period of 40 days.

From the above observations, it was concluded that

1. A rapid plastic deformation takes place almost instantaneously during loading, and rapid deformation continues for a short period after load is kept constant, indicating a relatively small viscosity coefficient.
2. A slow viscoelastic deformation, whose effect is negligible in Part 1, continues to take place for a long period of time indicating a relatively larger viscosity coefficient than the previous part.

Such behavior suggested the following model:[69]

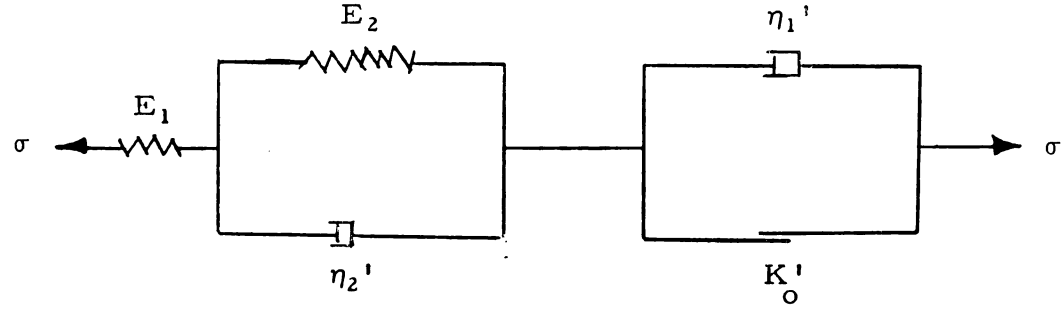

Fig. 3.1 Plastic viscoelastic model of rock salt (one dimensional)

where

σ = stress, psi

K_o' = maximum yielding strength

E_1 = Young's modulus, psi

E_2 = retarded Young's modulus, psi

η'_1 = linear plastic viscosity coefficient, poises in one dimension

η'_2 = viscoelastic viscosity coefficient, poises in one dimension

3.1c Plastic stress relaxation equation and the determination of the plastic constant η_1

The elastic and plastic model, which describes the rapid change during a short period after loading is represented as follows

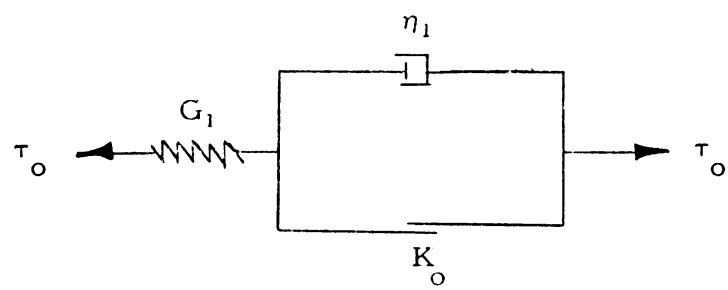

where

$G_i = \frac{E}{2(1+\mu)}$ elastic shear modulus

τ_o = octahedral shear stress

K_o = octahedral shearing strength

η_1 = viscosity coefficient in viscoplastic region

The nonhomogeneous constitutive equation of the above model may then be presented as follows:

$$\dot{\gamma}_o = \frac{\dot{\tau}_o}{G_1} + \frac{\tau_o - K_o}{\eta_1} \qquad (3.1\text{-}1)$$

where γ_o = octahedral shear strain.

The Levy-Mises equation presented before may be written in tensor notation so that

$$d\bar{\epsilon}_{ij} = \sigma'_{ij}\, d\lambda$$

where

$$\sigma'_{ij} = \sigma_{ij} - \frac{1}{3}\,\sigma_{kk}\,\delta_{ij}$$

$$\delta_{ij} = \begin{cases} 1 & i = j \\ 2 & i \neq j \end{cases}$$

with the understanding that if the deformation is small, the natural strain increment $d\bar{\epsilon}_{ij}$ may be represented by small strain increments $d\epsilon_{ij}$, where $d\epsilon_1$, $d\epsilon_2$ and $d\epsilon_3$ are the components of small strain increment. The meaning of the scalar function $d\lambda$ was explained in the previous chapter as a function of octahedral shear stress and the increment of the plastic octahedral shear strain is presented as follows:

$$d\lambda = \frac{1}{2\tau_o}\, d\gamma_o^{\,P}$$

Substituting this value into the Levy-Mises equation and dividing by dt yields the strain rate equations

$$\frac{d\epsilon'_{ij}}{dt} = \frac{1}{2\tau_o}\,\frac{d\gamma_o^{\,P}}{dt}\,\sigma'_{ij} \qquad (3.1\text{-}2)$$

where

$$d\epsilon'_{ij} = d\epsilon_{ij} - \frac{1}{3}\, d\epsilon_{kk}\,\delta_{ij}$$

The rate of the plastic octahedral shear strain is obtained from the plastic model such that

$$\frac{d\gamma_o^P}{dt} = \frac{\tau_o - K_o}{\eta_1} \quad \text{for } \tau_o > K_o$$

Substituting this value into the deviatoric strain rate equations gives

$$\frac{d\epsilon'_{ij}}{dt} = \frac{1}{2\eta_1}\left(1 - \frac{K_o}{\tau_o}\right)\sigma'_{ij} \tag{3.1-3}$$

This describes the three dimensional flow where incompressibility is assumed in the plastic state. The deviatoric stresses may be obtained as a function of the deviatoric strain rate, such that

$$\sigma'_{ij} = \frac{1}{\left(1 - \frac{K_o}{\tau_o}\right)} 2\eta_1 \frac{d\epsilon'_{ij}}{dt} \tag{3.1-4}$$

where the coefficients of the strain rates contain the viscosity term $2\eta_1$ and plasticity term K_o/τ_o.

Including the effect of the elastic strain rate in the deviatoric strain-rate equation, the result is as follows

$$\frac{d\epsilon'_{ij}}{dt} = \frac{1}{2\eta_1}\left(1 - \frac{K_o}{\tau_o}\right)\sigma'_{ij} + \frac{1}{2G_1}\frac{d\sigma'_{ij}}{dt} \tag{3.1-5}$$

where the last term on the right is contributed by the elastic strain rate. From this constitutive equation, it is desired to obtain the

stress relaxation equation in the viscoplastic region.

Assuming incompressibility, $d\epsilon'_{ij} = d\epsilon_{ij}$, reduces Eq. 3.1-5 to

$$\frac{d\epsilon_{ij}}{dt} = \frac{1}{2\eta_1}\left(1 - \frac{K_o}{\tau_o}\right)\sigma'_{ij} + \frac{1}{2G_1}\frac{d\sigma'_{ij}}{dt} \qquad (3.1\text{-}6)$$

The axial elastic plastic stress-strain relation is written from the above equation as

$$\frac{d\epsilon_z}{dt} = \frac{1}{2\eta_1}\left(1 - \frac{K_o}{\tau_o}\right)\sigma'_z + \frac{1}{2G_1}\frac{d\sigma'_z}{dt} \qquad (3.1\text{-}6)'$$

From boundary condition of solid cylinder, the following substitution can be made:

$$\tau_o = \pm \frac{\sqrt{2}}{3}(\sigma_L - \sigma_z)$$

$$\sigma'_z = \frac{2}{3}(\sigma_z - \sigma_L)$$

$$\frac{d\sigma'_z}{dt} = -\frac{2}{3}\frac{d\sigma_L}{dt}; \quad \sigma_z = \text{constant}$$

Experimental results for the tests described in sec. 6.3b indicate that $\frac{d\epsilon_z}{dt}$ is approximately zero. Hence, substituting the above quantities into Eq. 3.1-6' we obtain,

$$\frac{d\sigma_L}{dt} + \frac{G_1}{\eta_1}\sigma_L = \frac{G_1}{\eta_1}\left(\sigma_z \pm \frac{3}{\sqrt{2}}K_o\right)$$

Integrate to get

$$\sigma_L e^{\frac{G_1}{\eta_1}t} = \left(\sigma_z \pm \frac{3}{\sqrt{2}}K_o\right) e^{\frac{G_1}{\eta_1}t} + C \qquad (3.1\text{-}7)$$

From initial boundary conditions, at t = 0 after the initial purely elastic deformation, since $\epsilon_L = 0$,

then

$$\sigma_L = \frac{\mu}{1-\mu}\sigma_z$$

Thus, the integration constant, C, in Eq. 3.1-7 becomes

$$C = \sigma_z \left(\frac{\mu}{1-\mu} - 1\right) \mp \frac{3}{\sqrt{2}} K_o$$

Hence, the lateral stress relaxation equation in the viscoplastic region is described as follows:

$$\sigma_L = \left(\sigma_z \mp \frac{3}{\sqrt{2}} K_o\right) + \left[\left(\frac{\mu}{1-\mu} - 1\right) \sigma_z \mp \frac{3}{\sqrt{2}} K_o\right] e^{-\frac{G_1}{\eta_1} t} \qquad (3.1\text{-}8)$$

For the loading cycle equation 3.1-8 takes the form of

$$\sigma_L = \left(\sigma_z - \frac{3}{\sqrt{2}} K_o\right) + \left[\left(\frac{\mu}{1-\mu} - 1\right) \sigma_z + \frac{3}{\sqrt{2}} K_o\right] e^{-\frac{G_1}{\eta_1} t} \qquad (3.1\text{-}9)$$

As time approaches infinity

$$\sigma_L = \sigma_z \mp \frac{3}{\sqrt{2}} K_o \qquad (3.1\text{-}10)$$

Therefore, the tangent of the "plastic line" is

$$\frac{d\sigma_L}{d\sigma_z} = \tan B = 1 \qquad (3.1\text{-}11)$$

From Eq. 3.1-8, it is observed that the last term is a function of time and the plastic viscosity coefficient η_1. Hence, the one to one

relationship between lateral stress and axial stress demonstrated in Eq. 3.1-11 may be obtained by either letting t approach infinity or by assuming that η_1 is a very small number.

The change of lateral stress as a function of axial stress and at constant interval of time may be demonstrated from Eq. 3.1-9 as follows:

1. define t_o as the time measured after each increment of loading, i.e., $t_o = 0$ at points A, B, and C of Fig. 3.2.
2. $\sigma_{z_2} > \sigma_{z_1}$
3. t = constant

Then from Eq. 3.1-9

$$\Delta\sigma_{L_1} = \sigma_{L_1 t_1} - \sigma_{L_1 t_o} = [(\frac{\mu}{1-\mu} - 1)\,\sigma_{z_1} + \frac{3}{\sqrt{2}} K_o]\, D \qquad (3.1\text{-}12)$$

and

$$\Delta\sigma_{L_2} = \sigma_{L_2 t_2} - \sigma_{L_2 t_o} = [(\frac{\mu}{1-\mu} - 1)\,\sigma_{z_2} + \frac{3}{\sqrt{2}} K_o]\, D$$

where $D = e^{-\frac{G_1}{\eta_1} t}$; $t = t_1 - t_o = t_2 - t_o$

Therefore, from the above equation

$$\Delta\sigma_{L_2} > \Delta\sigma_{L_1}$$

Since

$$\sigma_{z_2} > \sigma_{z_1}$$

This indicates that $\Delta\sigma_L$ is a linear function of σ_z and may be represented graphically by Fig. 3.2.

In the laboratory, an experimental stress relaxation equation equivalent to that of Eq. 3.1-9 was determined as

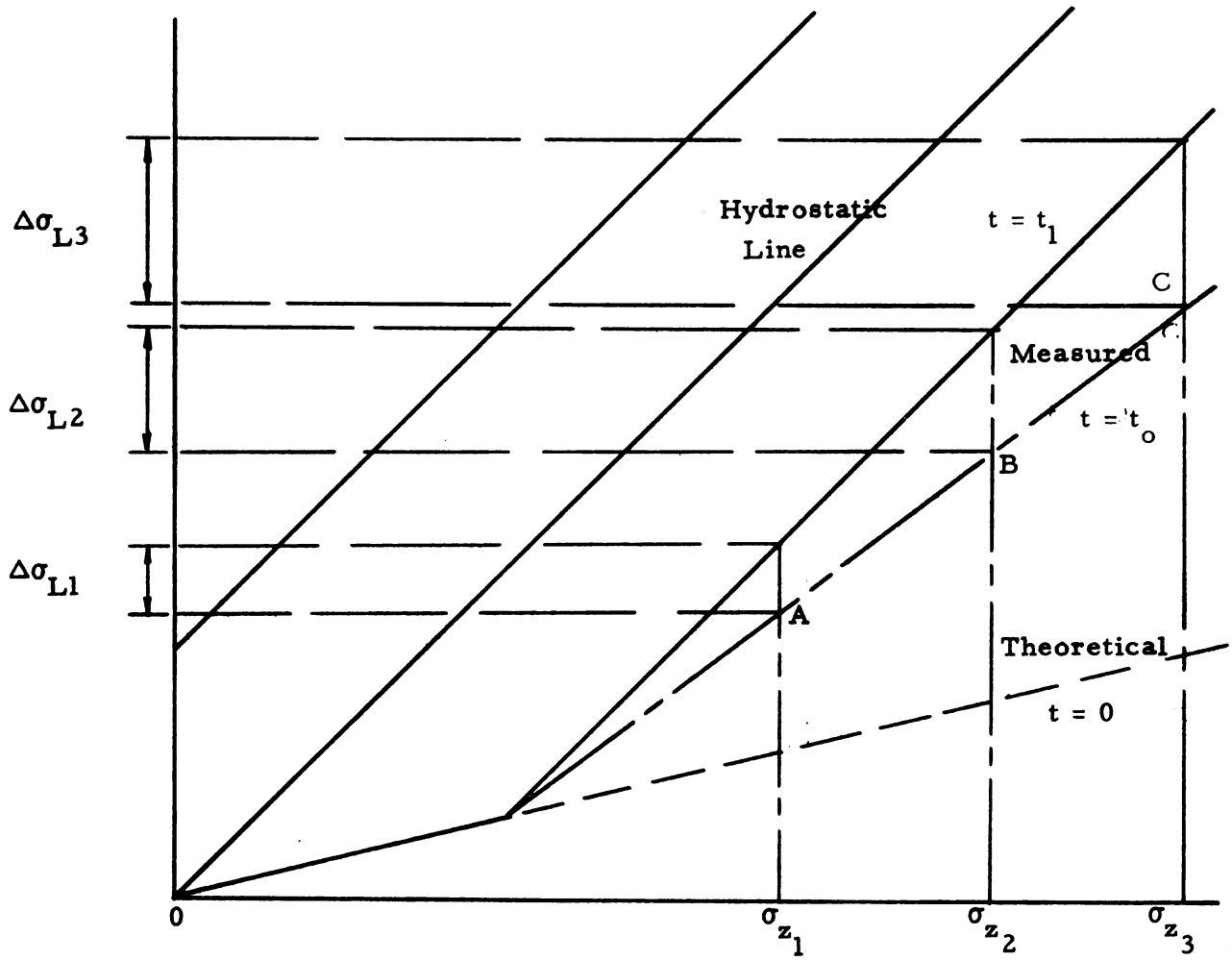

Fig. 3.2 Theoretical prediction of the change of lateral stress in viscoplastic region

$$\sigma_L = \sigma_z - \frac{3}{\sqrt{2}}\tau_f - \frac{3}{\sqrt{2}}(\tau_i - \tau_f)e^{-a_1 t} \qquad (3.1\text{-}13)$$

where,

τ_f = octahedral shear stress at t = ∞

τ_i = octahedral shear stress at t = 0

a_1 = material constant

Comparison between Eq. 3.1-9 and Eq. 3.1-13 gives

$$\eta_1 = \frac{G_1}{a_1} \qquad (3.1\text{-}14)$$

where a_1 is determined experimentally from the slope of plastic deformation.

3.1d Viscoelastic stress relaxation equation and the determination of viscosity constant, η_2

For a Kelvin body and spring in series, Fig. 3.1, the one dimensional constitutive equation, is presented as follows:

$$\frac{d\sigma}{dt} + \left(\frac{E_1 + E_2}{\eta'_2}\right)\sigma = E_1 \frac{d\epsilon}{dt} + \frac{E_1 E_2}{\eta_2'} \qquad (3.1\text{-}15)$$

An equivalent three-dimensional constitutive equation may be written as,

$$\frac{d\tau_o}{dt} + \left(\frac{G_1 + G_2}{\eta_2}\right)\tau_o = G_1 \frac{d\gamma_o}{dt} + \frac{G_1 G_2}{\eta_2}\gamma_o \qquad (3.1\text{-}16)$$

where

G_1 = shear modulus

G_2 = retarded shear modulus

η_2 = viscosity coefficient in viscoelastic region

Eq. 3.1-16 may be solved either for creep or stress relaxation response depending on the condition prescribed. For a laterally confined solid cylinder with homogeneous stress distribution, it is assumed that

$$\gamma_o = \gamma_i\, u(t)$$

$u(t)$ = unit step function

$$\dot{u}(t) = \delta(t) \text{ where} \int_o^t \delta(t)\,dt = \begin{cases} 1, & t = 0 \\ 0, & t > 0 \end{cases}$$

Hence,

$$\frac{d\tau_o}{dt} + \left(\frac{G_1 + G_2}{\eta_2}\right)\tau_o = \frac{G_1 G_2}{\eta_2}\gamma_i\, u(t) + G_1\gamma_i\delta(t)$$

integrating

$$\tau_o\, e^{\left(\frac{G_1+G_2}{\eta_2}\right)t} = \left(\frac{G_1 G_2}{G_1 + G_2}\right)\gamma_i\, e^{\left(\frac{G_1+G_2}{\eta_2}\right)t}\, u(t) + G_1\gamma_i u(t) + C$$

From initial conditions

at $t = 0$, $\tau_o = G_1\gamma_i$, then

$$C = -\left(\frac{G_1 G_2}{G_1 + G_2}\right)\gamma_i$$

Substitute this back into the above equation and arrange terms to get τ_o:

$$\tau_o = G_1\gamma_i\, e^{-\left(\frac{G_1+G_2}{\eta_2}\right)t}\, u(t) + \left[1 - e^{-\left(\frac{G_1+G_2}{\eta_2}\right)t}\right]\frac{G_1 G_2}{G_1 + G_2}\,\gamma_i u(t) \quad (3.1\text{-}17)$$

As time approaches infinity

$$\tau_o = \tau_f = \frac{G_1 G_2}{G_1 + G_2} \gamma_i = \text{constant} \qquad (3.1\text{-}18)$$

where τ_f is the minimum value of τ_o below which yielding never occurs.

The lateral stress relaxation is obtained from the relation

$$\sigma_L = \sigma_z \pm \frac{3}{\sqrt{2}} \tau_o$$

$$\sigma_L = \sigma_z \pm \frac{3}{\sqrt{2}} \left[[G_1 \gamma_i e^{-(\frac{G_1+G_2}{\eta_2})t} u(t) + [1 - e^{-(\frac{G_1+G_2}{\eta_2})t}] \frac{G_1 G_2}{G_1+G_2} \gamma_i u(t) \right] \qquad (3.1\text{-}19)$$

at $t = 0$

$$\sigma_L = \sigma_z \pm \frac{3}{\sqrt{2}} (G_1 \gamma_i) = \sigma_z \pm \frac{3}{\sqrt{2}} \tau_o$$

which indicates that on the lateral vs. axial stress diagram, stress relaxation in viscoelastic region starts from 45^o line to reach a constant value at $t = \infty$, indicated by

$$\sigma_L = \sigma_z \pm \frac{3}{\sqrt{2}} \left(\frac{G_1 G_2}{G_1 + G_2} \right) \gamma_o u(t) \qquad (3.1\text{-}20)$$

Eq. 3.1-20 will be used to obtain the retarded shear modulus G_2 and to verify the constant stress relaxation region as indicated in Fig. 6.13.

In the laboratory, a stress relaxation equation equivalent to Eq. 3.1-17 was determined such that

$$\tau_o = \tau_f + (\tau_i - \tau_f) e^{-\alpha_2 t}$$

where a_2 is a material constant defined by the slope of the stress relaxation curve in the viscoelastic region.

A comparison of Eq. 3.1-17 and Eq. 3.1-21 gives

$$\eta_2 = \frac{G_1 + G_2}{a_2} \tag{3.1-22}$$

Eq. 3.1-14 and Eq. 3.1-22 define the viscosity in the plastic and viscoelastic region respectively.

CHAPTER IV

THEORETICAL BEHAVIOR OF A CYLINDRICAL CAVITY UNDER CONSTANT TRIAXIAL STRESS

The creep formulas, for the same thick walled cylinder treated in Chapter II, are derived for the purpose of measuring the strain rate of a model salt cavity in the laboratory. The derivation is based on the following assumptions:

1. Deformation is uniform and sufficiently small to produce no appreciable change in geometry of the cavity.
2. At a constant external stress, the deformation occurs in such a way that the stress distribution across the cylindrical surface remains constant with time and that the octahedral shear stress may be expressed as $\tau = \tau_o u(t)$.
3. The material has a different creep rate depending on the state of stress and the temperature employed. The temperature is kept constant across the thickness of the cylinder.
4. The mechanical model presented in Chapter III describes the viscous behavior of rock salt.

4.1 Strain Rate Equations in a Hollow Thick Walled Cylinder.

Several theories have been proposed for predicting creep strains in terms of stresses for the combined states of stress. Most of these theories are based on an assumed tensile creep stress-strain relation.

A generalized stress-strain relation based on Hooke's law and the basic laws of plastic flow is described in Eq. 2.3-27 where the elastic stresses and the octahedral shear strain are functions of time. The characteristic feature for large deformation in a thick walled cylinder is that for every increment of time there is not only a set of increments of plastic strains but also a set of increments of stresses. By assuming small deformation with stress increment $\cong 0$, the octahedral creep strain function, $\gamma_o(t)$, for rock salts may be determined from the mechanical model as follows:

The three dimensional constitutive equation for the viscoelastic part of the model is given by

$$\frac{d\tau_o}{dt} + \left(\frac{G_1 + G_2}{\eta_2}\right)\tau_o = G_1 \frac{d\gamma_{12}}{dt} + \frac{G_1 G_2}{\eta_2}\gamma_{12} \qquad (4.1\text{-}1)$$

where

$\gamma_{12} = \gamma_1 + \gamma_2$

γ_1 = octahedral shear strain in elastic element

γ_2 = octahedral shear strain in viscoelastic element

Taking $\tau = \tau_o u(t)$, then

$$\frac{d\gamma_{12}}{dt} + \frac{G_2}{\eta_2}\gamma_{12} = \frac{\tau_o \delta(t)}{G_1} + \frac{G_1 + G_2}{G_2 \eta_2}\tau_o u(t)$$

solving this equation to get,

$$\gamma_{12}\, e^{\frac{G_2}{\eta_2}t} = \frac{\tau_o}{G_1} u(t) + \frac{G_1 + G_2}{G_1 \eta_2} \cdot \frac{\eta_2}{G_2} e^{\frac{G_2}{\eta_2}t} u(t) + C$$

At t = 0

$$\gamma_{12} = \frac{\tau_o}{G_1}$$

Then

$$C = -\frac{G_1 + G_2}{G_1 G_2}\tau_o$$

Thus, the viscoelastic creep response function is derived as,

$$\gamma_{12} = \frac{\tau_o}{G_1} e^{-\frac{G_2}{\eta_2}t} u(t) + \frac{G_1 + G_2}{G_1 G_2}\tau_o u(t) - \frac{G_1 + G_2}{G_1 G_2} e^{-\frac{G_2}{\eta_2}t} \tau_o u(t)$$

Collecting terms, it reduces to

$$\gamma_{12} = [\frac{G_1 + G_2}{G_1 G_2} - \frac{1}{G_2} e^{-\frac{G_2}{\eta_2}t}] \tau_o u(t) \qquad (4.1\text{-}2)$$

Similarly, the octahedral shear strain from the viscoplastic part, γ_3, can be derived as follows:

$$\gamma_3 = \int_o^t (\frac{\tau_o - K_o}{\eta_1}) dt \quad \text{for} \quad \tau_o > K_o$$

$$\gamma_3 = (\frac{\tau_o - K_o}{\eta_1}) t \qquad (4.1\text{-}3)$$

Hence, the total creep response for the model in plastic and viscoelastic regions is derived as,

$$\gamma_o = [\frac{G_1 + G_2}{G_1 G_2} - \frac{1}{G_2} e^{-\frac{G_2}{\eta_2}t}]\tau_o u(t) + (\frac{\tau_o - K_o}{\eta_1}) t \qquad (4.1\text{-}4)$$

By taking time derivative, this function yields

$$\frac{d\gamma_o}{dt} = \frac{G_1 + G_2}{G_1 G_2} - \frac{1}{G_2} e^{-\frac{G_2}{\eta_2} t}] \tau_o \delta(t) + \frac{1}{\eta_2} e^{-\frac{G_2}{\eta_2} t} \tau_o u(t) + \frac{\tau_o - K_o}{\eta_1} \qquad (4.1\text{-}5)$$

For $t > 0$

$$\frac{d\gamma_o}{dt} = \left(\frac{\tau_o - K_o}{\eta_1}\right) + \frac{1}{\eta_2} e^{-\frac{G_2}{\eta_2} t} \tau_o u(t) \qquad (4.1\text{-}6)$$

where the first term on the right is constant with time and contributed from plastic flow just after load is applied.

When stresses are constant with time, the general stress-strain relation is

$$\frac{d\epsilon_r}{dt} = \frac{1}{2\tau_o} \frac{d\gamma_o}{dt} \cdot \frac{1}{3}(2\sigma_r - \sigma_\theta - \sigma_z)$$

$$\frac{d\epsilon_\theta}{dt} = \frac{1}{2\tau_o} \frac{d\gamma_o}{dt} \cdot \frac{1}{3}(2\sigma_\theta - \sigma_r - \sigma_z) \qquad (4.1\text{-}7)$$

$$\frac{d\epsilon_z}{dt} = \frac{1}{2\tau_o} \frac{d\gamma_o}{dt} \cdot \frac{1}{3}(2\sigma_z - \sigma_r - \sigma_\theta)$$

Substitute the value of $\frac{d\gamma_o}{dt}$ into the above equation to obtain

$$\frac{d\epsilon_r}{dt} = \frac{1}{2\tau_o} \left[\frac{\tau_o - K_o}{\eta_1} + \frac{1}{\eta_2} e^{-\frac{G_2}{\eta_2} t} \tau_o u(t)\right] \frac{2}{3} \left[\sigma_r - \frac{1}{2}(\sigma_\theta + \sigma_z)\right]$$

$$\frac{d\epsilon_\theta}{dt} = \frac{1}{2\tau_o}\left[\frac{\tau_o - K_o}{\eta_1} + \frac{1}{\eta_2} e^{-\frac{G_2}{\eta_2}t} \tau_o u(t)\right] \frac{2}{3}\left[\sigma_\theta - \frac{1}{2}(\sigma_r + \sigma_z)\right]$$

which reduces to

$$\frac{d\epsilon_r}{dt} = \frac{1}{2}\left[\frac{1}{\eta_1}\left(1 - \frac{K_o}{\tau_o}\right) + \frac{1}{\eta_2} e^{-\frac{G_2}{\eta_2}t}\right] \sigma_r'$$

$$\frac{d\epsilon_\theta}{dt} = \frac{1}{2}\left[\frac{1}{\eta_1}\left(1 - \frac{K_o}{\tau_o}\right) + \frac{1}{\eta_2} e^{-\frac{G_2}{\eta_2}t}\right] \sigma_\theta' \qquad (4.1\text{-}8)$$

where the deviatoric stresses are:

$$\sigma_r' = \frac{2}{3}\left[\sigma_r - \frac{1}{2}(\sigma_\theta + \sigma_z)\right]$$

$$\sigma_\theta' = \frac{2}{3}\left[\sigma_\theta - \frac{1}{2}(\sigma_r + \sigma_z)\right]$$

For the case where $\tau_o = K_o$, the first term on the right of Eq. 4.1-8 vanishes and

$$\frac{d\epsilon_r}{dt} = \sigma_r' \cdot \frac{1}{2\eta_2} e^{-\frac{G_2}{\eta_2}t}$$

$$\frac{d\epsilon_\theta}{dt} = \sigma_\theta' \cdot \frac{1}{2\eta_2} e^{-\frac{G_2}{\eta_2}t} \qquad (4.1\text{-}9)$$

As time approaches infinity, the strain rates approach zero. This

is true only in the viscoelastic region. The strain rate equation for any cylindrical cavity may then be defined by substituting the values of the deviatoric stresses for any particular cavity. These stresses are usually defined as a function of the boundary conditions, octahedral shear strength and applied external loads.

From Eqs. 4.1-5 and 4.1-8, it is observed that the plastic deformation at t = 0 consists of an instantaneous elastic part and a plastic part described by

$$\frac{d\epsilon_r}{dt} = \frac{1}{2\tau_o}\left[\frac{G_1 + G_2}{G_1 G_2} - \frac{1}{G_1} + \frac{1}{\eta_1}\left(1 - \frac{K_o}{\tau_o}\right)\sigma_r' \tau_o u(t)\right] \qquad (4.1\text{-}10)$$

At t > 0, the elastic deformation vanishes and the above equation reduces to the triaxial plastic flow where the plastic strain rates are linearly proportional to the deviatoric stresses, such that

$$\frac{d\epsilon_r}{dt} = \frac{1}{2\eta_1}\left(1 - \frac{K_o}{\tau_o}\right)\sigma_r' \qquad (4.1\text{-}11)$$

4.2 Comparison of Theoretical and Empirical Equations Describing the Creep Behavior of the Model Cavity

From the viscoelastic state, the tangential strain rate equation is defined as

$$\frac{d\epsilon_\theta}{dt} = \sigma_\theta' \cdot \frac{1}{2\eta_2} e^{-\frac{G_2}{\eta_2} t}$$

The total amount of tangential strain in the opening can be calculated by integrating the above equation such that

$$\epsilon_\theta = \int_{t_1}^{t_2} \sigma_\theta' \cdot \frac{1}{2\eta_2} e^{-\frac{G_2}{\eta_2} t}$$

By integrating between $t_1 = t$ and $t_2 = \infty$, gives

$$\epsilon_{\theta t} - \epsilon_{\theta \infty} = -\frac{\sigma_\theta'}{2G_2} e^{-\frac{G_2}{\eta_2} t} \qquad (4.2\text{-}1)$$

where

$$\epsilon_{\theta \infty} = \frac{3}{4} \sigma_\theta' \frac{1}{2\eta_2}$$

The radial displacement, u, at $r = a_o$ is obtained from the above equation such that,

$$\frac{u_t - u_\infty}{a_o} = -\frac{\sigma_\theta'}{2G_2} e^{-\frac{G_2}{\eta_2} t} \qquad (4.2\text{-}2)$$

where u is defined as $a - a_o$, the above equation reduces to

$$\frac{a - a_f}{a_o} = -\frac{\sigma_\theta'}{2G_2} e^{-\frac{G_2}{\eta_2} t} \qquad (4.2\text{-}3)$$

where,

a_f = reduced radius a at $t = \infty$.

By comparing Eq. 4.2-3 with the following empirical relation obtained in the laboratory,

$$\frac{a - a_f}{a_o} = C\, e^{-pt} \qquad (4.2\text{-}4)$$

The following relationship is found:

$$C = -\frac{\sigma_\theta'}{2G_2}$$

and

$$P = \frac{G_2}{\eta_2}$$

Since the values of the above relationships are constant for a given material and geometry, the empirical and the theoretical equations are essentially the same. This has been proven by a different method as discussed in the following chapters.

The plastic deformation is assumed to occur at the early stage of the creep since the viscosity coefficient of the plastic flow, η_1, is very much smaller than that of the viscoelastic flow. Just after loading, the plastic flow dominates the creep and the strain rate may be described by

$$\frac{d\epsilon_\theta}{dt} = \frac{1}{2\eta_1}\left(1 - \frac{K_o}{\tau_o}\right) \cdot \sigma_\theta'$$

The total strain is then

$$\epsilon_\theta = \frac{1}{2}\eta_1 \int_o^t \left(1 - \frac{K_o}{\tau_o}\right) \sigma_\theta'\, dt$$

where τ_o and σ_θ' are not constant with time. Assuming t is very small, then the change in τ_o and σ_θ' is insignificant, hence

$$\epsilon_\theta = \frac{u}{r} = \frac{1}{2}\,\eta_1\,\sigma_\theta'\,(1 - \frac{K_o}{\tau_o})\,t \qquad (4.2\text{-}5)$$

at $r = a_o$, this reduces to

$$\frac{a - a_o}{a_o} = \frac{1}{2}\,\eta_1\,(1 - \frac{K_o}{o})\,t\,\sigma_\theta' \qquad (4.2\text{-}6)$$

Eq. 4.2-6 holds true only in a short period after the load is applied.

PART TWO

EXPERIMENTAL INVESTIGATION

CHAPTER V

APPARATUS AND EXPERIMENTAL PROCEDURE

5.1 General Remarks

5.1a Testing techniques and their objectives

Two basically different testing techniques were utilized for testing the theories of rock salt behavior. The first one used a hollow thick-walled cylindrical specimen triaxially compressed in a high pressure vessel developed by Serata. The confining pressure of the vessel may reach up to 10,000 psi. The vessel was used for a long term triaxial creep test with confining pressure of up to 8,000 psi. This high pressure vessel was used to study the distribution of stress and strain in a hollow thick-walled cylinder; the general setup is shown in Fig. 5.1.

The second technique is the confining cylinder of the "transition test technique" developed by Serata. The axial load was applied by a Forney's press tester whose capacity is 250,000 pounds. This technique was developed to study the triaxial behavior of rocks for the purpose of simulating underground stress field in relation to time, material property and loading conditions; a general setup of this apparatus is shown in Fig. 5.2.

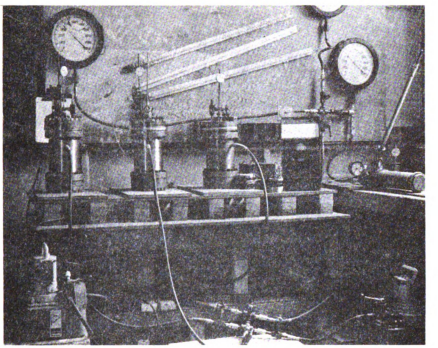

Figure 5. 1. High pressure testing system providing versatile triaxial loads up to 200, 000 pounds with automatic loading control.

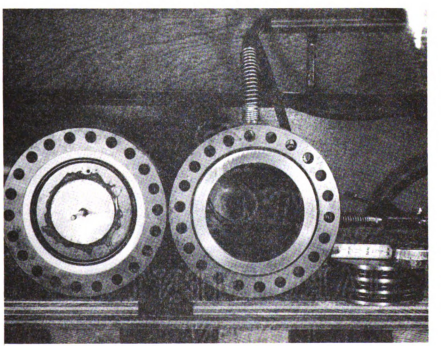

Figure 5. 1. a. Top view of high pressure vessel showing ring and cap-plate.

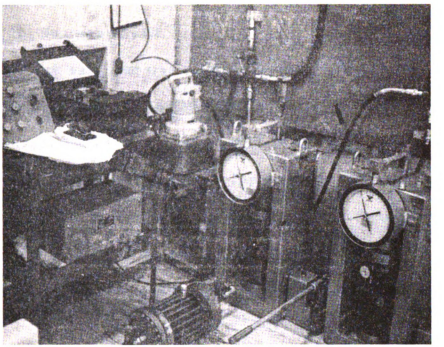

Figure 5. 2. General set up of transition test showing 250, 000 pounds press tester, shock absorber, pressure gage, strain indicator and automatic loading control.

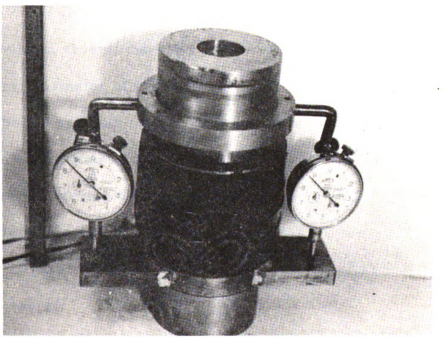

Figure 5. 3. Thick walled cylinder cell with enclosed specimen, plungers and dial gages used for triaxial transition tests.

5.1b Sources of salt

The rock salt used was obtained from three different locations: Saskatchewan, Louisiana and Michigan. The specimens designated by SS came from the Yorkton Saskatchewan mine of the International Minerals and Chemical Company. The salt was obtained from a depth of 3020 feet. These samples were pink in color and contained small inclusions of foreign materials. The salt crystals ranged in mean diameter from 0.15 to 0.75 inches with an average of about 0.45 inches.

The specimens designated by LS were mined from the International Salt Company mine in Avery Island, Louisiana. The samples were obtained from a drill core at a depth of 600 feet. This salt was white in color and contained much less impurities than the SS salt. The maximum crystal diameter of LS salt was about 0.50 inches with an average diameter of 0.31 inches.

The MS salt was obtained from the Detroit Salt Mines. The samples were obtained from a depth of 1000 feet. The salt was white in color with varying degrees of impurities. It was more homogeneous and clearer than the SS salt. The average crystal diameter was about 0.50 inches. Michigan and Louisiana salt were used for most of these tests.

The first number following the lettering SS, MS or LS indicates the sample block from which the specimen was cut and the second number indicates the test number.

5.2 Transition Test

5.2a Testing devices

1. Thick-walled cylinder

The cylinder is a stainless steel tubing with a length of 3.250 inches, inside diameter of 3.250 inches and outside diameter of 4.00 inches. The cylinder assembly is shown in Fig. 5.3. The two Ames dial gages were used to obtain average values of the axial deformations.

2. Creep measuring devices

The strains of the cylinder were measured by SR-4 strain gages with the Baldwin SR-4 type M indicator. An A.C. voltage regulator was also used to eliminate fluctuation of the supply voltage to the strain indicator. The use of a regulated power supply reduced the instrumental drift in the extended creep measurement to an insignificant value. The usual indication of instability is a shift of the null balance point, which is known as instrumental drift or zero drift. This kind of drift was eliminated by studying its possible sources which are suggested by Perry and Lissner[60] as follows:

1. Incomplete temperature compensation of the active strain gage.
2. Instability of the wheatstone bridge, power supply and amplifier.
3. Improperly bonded strain gages.
4. Creep of one or more strain gages.
5. Insufficient protection from humidity, or reduction in the impedance between the gage wires and ground.

6. Variation in the impedance of the lead wires.

It is necessary in the long-term creep tests to obtain continuous records based on an initial zero reference point.

Three rosette SR-4 strain gages, type FABX-50-12, were attached symmetrically (i.e., 120^{o} apart) to the external surface of the cylinder. The rosette gages were oriented with their two directions of the wire resistance parallel and perpendicular to the axis of the cylinder. To prevent creep in the gage cement, the following curing cycle was adopted (Boldwin-Lima-Hamilton).

> "The absolute minimum curing cycle is 1 hour at 175^{o} F followed by 2 hours of 250^{o} F with temperature brought up slowly to each baking point over a 1 hour period. Performance is improved considerably by an additional 2 hours at 300 to 350^{o} F either before or after removing the pressure clamp."

The instrumental drift for long-term creep tests was detected by a switch, which alternates the positions of the active and dummy gages to reverse the apparent sign of strain. An average of the two absolute values was taken as the true creep strain (Fig. 6.9).

The lateral stress in the specimen was determined from the tangential strain (ϵ_{ts}) measurement on the external surface of the cylinder. The distribution of a tangential stress in a hollow cylinder subjected to uniform pressure on the internal and external surfaces is given by

$$\sigma_{\theta s} = \frac{a_o^2 b_o^2 (P_o - P_i)}{r^2 (b_o^2 - a_o^2)} + \frac{P_i a_o^2 - P_o b_o^2}{b_o^2 - a_o^2}$$

where,

a_o = internal radius of cylinder = 1.625 inches

b_o = external radius of cylinder = 2.00 inches

P_i = radial internal pressure = σ_L

P_o = radial external pressure = 0

$\sigma_{\theta s}$ = tangential stress on the surface of thick-walled cylinder

Substituting $P_o = 0$ and $P_i = -\sigma_L$ at $r = b_o$ into the above equation,

gives

$$\sigma_L = -\left(\frac{b_o^2 - a_o^2}{2a_o^2}\right) \sigma_{\theta s}$$

but $\sigma_{\theta s} = E_s \epsilon_{ts} + \mu_s (\sigma_{rs} + \sigma_{zs})$

where,

μ_s = Poisson's ratio of steel

σ_{rs}, σ_{zs} = radial and axial stresses on the outer surface of steel

$\sigma_{rs} = \sigma_{zs} = 0$

Hence, E_s = Young's modulus of steel = 30×10^6 psi

$$\sigma_L = -\frac{b_o^2 - a_o^2}{2a_o^2} E_s \epsilon_{ts}$$

Substitute the values of b_o, a_o and E_s to get

$$\sigma_L = -7.722 \epsilon_{ts}$$

This is used to determine lateral stress from strain gage readings as will be shown in several diagrams later.

5.2b Specimen preparation

The specimens used for the transition tests were solid cylinders with a diameter of 3.240 inches. The ends of all specimens were made perpendicular to the axis of the cylinder to insure uniform loading. All imperfections existing in the surface after machining were filled with plaster of paris to insure an ideal model shape. The imperfections were usually caused by small crystals chipping out of the surface in the machining operation.

Thin films of the friction reducer (grease-graphite mixture) were sandwiched between two layers of thin plastic film and one layer of tin-foil. Each set of these layers was placed on the top and bottom ends of the cylindrical specimen to reduce lateral friction. A thin film of friction reducer was placed on both sides of a thin plastic sheet. The plastic was then wrapped around the cylindrical surface with great caution to eliminate any air bubbles or wrinkles and any excess grease between the plastic sheets and the cylinder.

5.2c Testing procedure

The general objective of this series of tests was to define, then determine the necessary material constants to describe time- and stress-dependent behavior of the material. The test involved the following four procedures:

1. Lateral stress-axial stress relationship

Axial pressure to the solid cylinder specimen placed in a confined cell was gradually increased at 600 psi intervals up to 13,400 psi and lowered gradually to zero. Strain-gage measurements, $\epsilon_{\theta s}$, and dial-gage measurements, ϵ_z, were recorded at each stress level. The process was repeated for several cycles in each test.

The purposes of these tests were to study the instantaneous transition behavior between the elastic and plastic states of stress and determine the mechanical properties of rock salt.

2. Stress relaxation tests

The axial load was gradually increased from zero in 600 psi intervals up to 10,400 psi. The axial load was maintained at that level for about 20 days by an automatic pressure control system. After that period, the load was increased gradually from 10,400 psi up to 13,400 psi and kept at that level for another 20-day period.

The purposes of these tests were to: (a) study the lateral stress relaxation behavior as a function of time, (b) determine the slopes of the visco-plastic and visco-elastic stress relaxation curves and (c) verify that the state of stress after 20 days is elastic, so that further loadings always start from an elastic region.

3. Constant stress region

The axial load was gradually increased at 600 psi intervals up to 13,400 psi with immediate strain-gage readings taken at each stress level. The load was then decreased at 1200 psi intervals down to 6000 psi and maintained at each of these stress levels for a period of 90 minutes.

The purpose was to study the lateral stress relaxation around the hydrostatic line and to verify the existence of a constant lateral stress region defined by Eq. 3.1-20.

4. Visco-plastic stress relaxation tests

The axial load was increased gradually at 600 psi intervals up to 12,000 psi and lowered back to zero. At each stress level, the load was maintained constant for a period of 10 minutes. Strain gage readings were taken as soon as the stress level was reached at the end of this waiting period.

The purpose of this test was to verify the theoretical Eq. 3.1-8 which indicates that the slope of the line of lateral-axial stress relation is not 45^{o} if instantaneous readings were recorded. However, because η_1 is very small, this one to one relationship will be attained in a short period of time.

5.3 Hollow Cylinder Test

5.3a Testing devices

1. High pressure vessel and assembly

The components of the high pressure vessel are shown in detail in Fig. 5.4 and Table 5.1. The vessel is pressure sealed to withstand an internal operational pressure up to 10,000 psi. The cylinder is made of stainless steel, which was quenched at an air temperature of 1800° F and drawn at 1100° F to develop a Brinell 310-Rockwell C-34 hardness with a yield strength of 1.2×10^5 psi. Provisions for hydraulic pressure input and deformation measurements are illustrated in the previous figure. A cylindrical rock specimen is held in the vessel (Fig. 5.4) by means of a tightly fitted plastic jacket. The peripheral ends of the plastic jacket are held tightly between the circumference of the cylinder top and the cap plate. The O-rings and the teflon rings, shown in the figure, serve as an oil seal. As pressure increases, they flatten out and more sealing effect is produced. The specimen is subjected to a lateral confining pressure of up to 10,000 psi. The load is applied by an automatic pump through the pressure control system which is illustrated in Fig. 5.1.

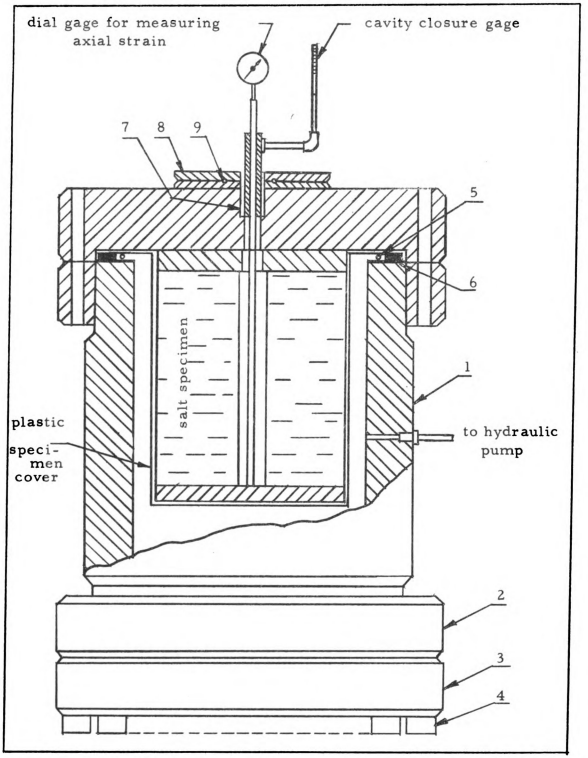

Fig. 5.4 Cross-sectional view of high pressure vessel, showing various components and arrangement of specimen

Table 5.1 Components of high pressure vessel

Item No.	No. required	Description	Material
1	1	Cylinder: 5" I.D. x 7" O.D. x 11" L.	AISI 420 stainless steel
2	2	Bolt ring: 8 5/8" O.D. x 1 1/4" thick	AISI 420 stainless steel
3	2	Cap plate: 8 5/8" O.D. x 1 1/16" I.D. x 1 1/4" thick	AISI 420 stainless steel
4	48	1/2 20 NF x 2 1/4 Soc. HD cap screw	
5	2	Teflon ring	Teflon
6	2	O-ring	
7	2	3/8 ASA taper pipe thread	
8	2	Pressure release plate: 2" x 2"	
9	11	Circular grove 1/4" dia.	

2. Pressure control system

A schematic diagram of the triaxial testing assembly, Fig. 5.5, shows the pressure control system and the testing vessel. The automatic pump "Vanguard" operates in a range of 100 to 10,000 psi. A hand pump is connected to the pressure system to provide a slow loading and a fine control.

The shock absorber system is devised in order to reduce the surging wave produced by the automatic pump during a constant loading in the creep tests. The system consists of a shock absorber unit and several damping chambers with needle size orifices shown in Fig. 5.6. This arrangement reduced the shock wave amplitude from approximately 700 psi to 150 psi. This system is particularly important for creep experiments.

5.3b Specimen preparation

The same process of specimen preparation discussed in sec. 5.2b was followed here. The only difference was that the friction reducers were placed at top and bottom edges of the cylindrical specimens.

The specimens used for the cavity closure tests were hollow cylinders with a diameter of 4.625 inches and a length of 4.625 inches. The bore of the cylinders ranged from 0.75 inches to 1.50 inches for different tests. A few specimens of diameter 3.25 inches, length of 3.25 inches and a bore of 0.65 inches were used.

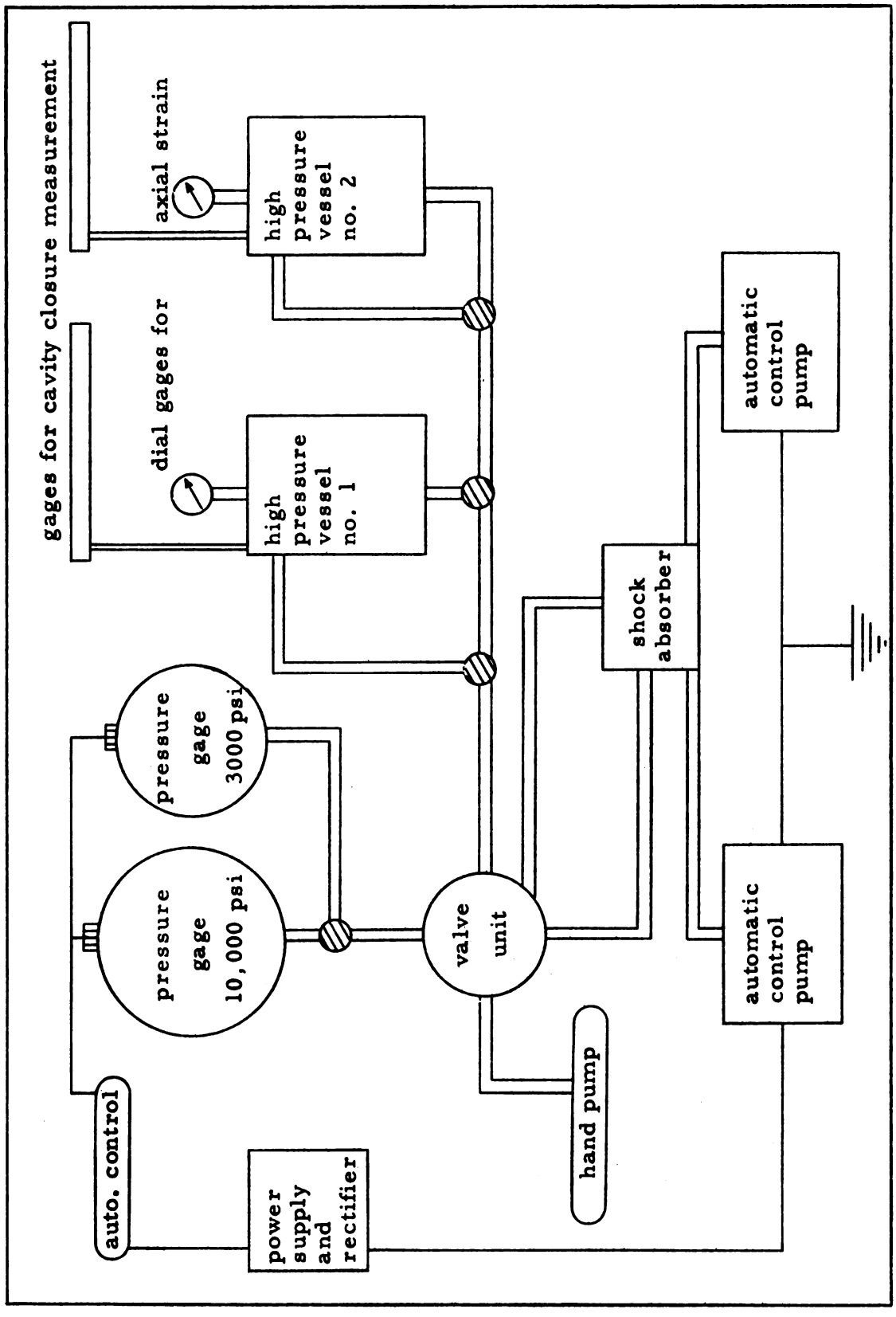

Figure 5.5 Schematic diagram of triaxial assembly.

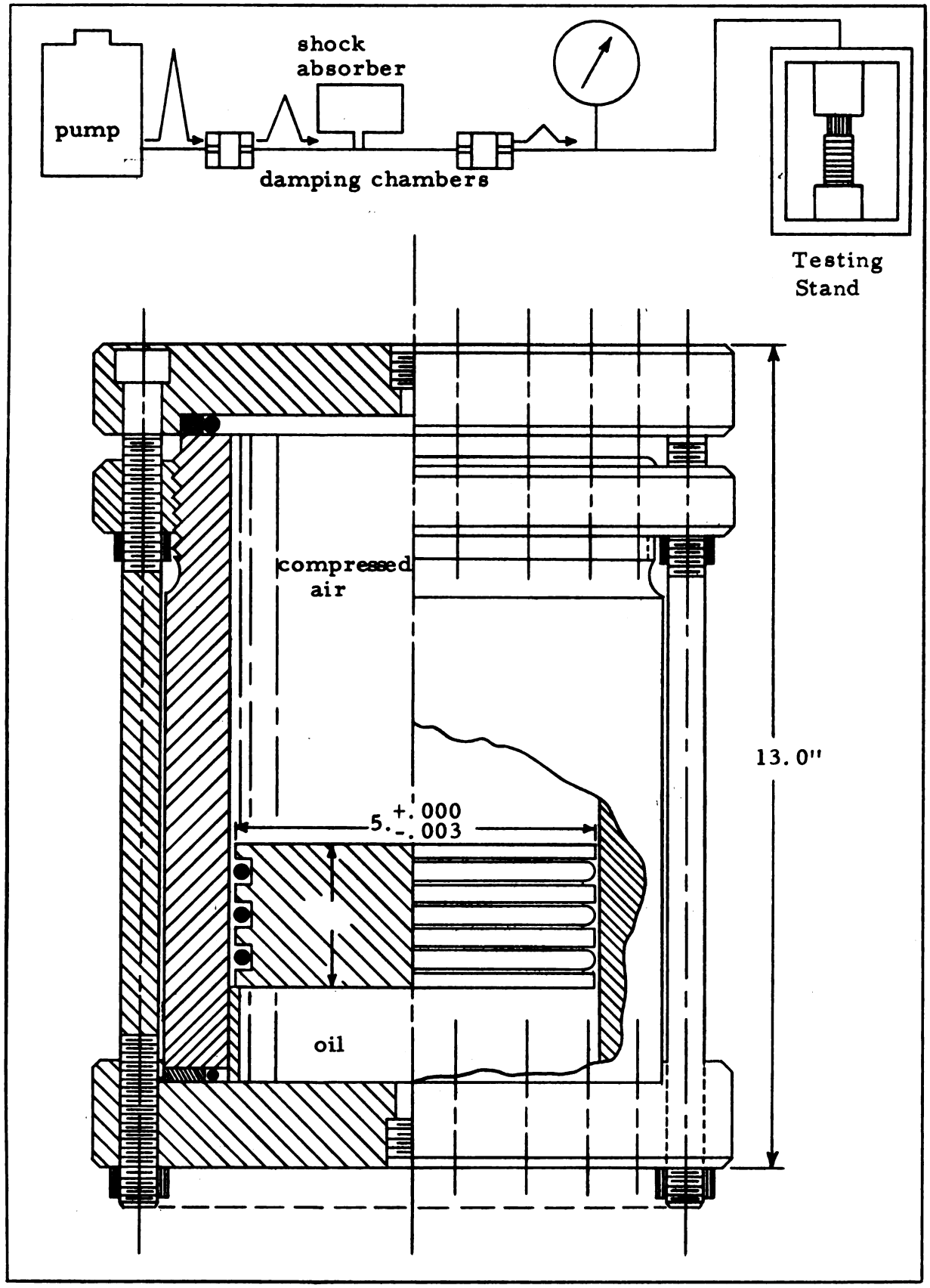

Fig. 5.6. Schematic diagram of pulse reduction and cut-aways view of shock absorber.

5.3c Jacketing of a hollow cylindrical specimen

Considerable time and energy were spent in order to develop a jacket that will transmit the liquid pressure to the specimen and yet will not permit the liquid to enter its pores. Such a jacket should be impermeable, ductile, strong enough to resist shear and not be affected by liquid medium.

The following materials were tried unsuccessfully:

1. Several layers of thin wrapping plastic were found not strong enough to prevent the hydraulic oil from having access to the specimen.
2. A thick, 1/4 inch, rubber jacket was made to fit tightly on the specimen, but it was soluble in mineral oil if kept in the oil for long-term creep tests. It was also permeable at high pressures.
3. Thin copper tubings were made to fit 4 9/16 x 4 9/16 inches specimens. These were found unsuccessful, because of the difficulty of obtaining a strong weld at the top and bottom ends of the jackets. Besides, a large amount of air, which is undesirable for accurate measurements, was found to be trapped between the specimen and the jacket.

Finally, a successful jacket was made of 7-mil thick plastic material, known by the trade name of Plexiglass. This material proved to be impermeable, strong enough to resist shear, and flexible at low confining pressure. The jacket is also very easy to make.

Fig. 5.7 shows the plastic jackets and the cylindrical form used to make them. The form was of the same dimensions as the specimens. The plastic was cut and wrapped around the circumference and bottom of this frame. All seams were cemented with plastic cement. Steel rings were then tightened around all seams. Final sealing was accomplished by heating the rings to the melting point of the plastic.

A tight fit was secured by moderately heating the plastic jacket and placing it around the specimen. Thus, most of the air usually trapped between specimen and jacket is eliminated before specimen is immersed in the confining liquid.

Several tests were performed with these jackets at an axial load of up to 200, 000 pounds and lateral liquid pressure of 10, 000 psi. These jackets are reusable, if handled properly during installation and removal of the specimen.

5.3d Closure measuring system

The closure of the salt cavity under triaxial compression was measured by mercury displacements into graduated tubes. The tubes are of 4 mm. inside diameter and calibrated to read to one-tenth of a millimeter. A zero reading was recorded at a zero liquid pressure. As liquid pressure increases, deformation at the inner face of the cavity occurs and the corresponding mercury displacement was measured.

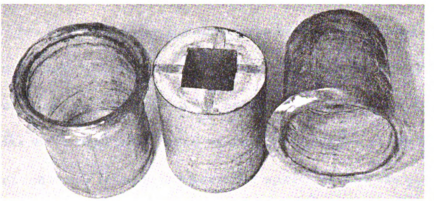

Figure 5. 7. Plastic jackets with form.

Figure 5. 7. a. Various wall thickness of hollow cylinders.

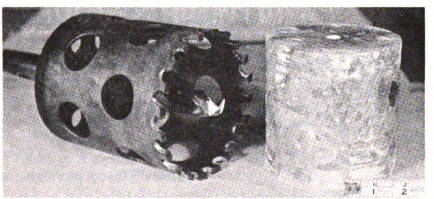

Figure 5. 7. b. Specimen cutting auger.

Mercury was chosen as the measuring medium because of its inert chemical characteristics and its heavy density that might occupy any present pores or crevices in the bores of the salt cylinders. Thin rubber tubes were efficiently used to line the surfaces of the cavity and prevent mercury leakage between the specimen and the jacket. Any air trapped inside the cavity, when mercury was poured in, was eliminated by an air relief mechanism indicated by components 8 and 9 in Fig. 5.4.

The reduced radius of the cavity, a, was measured from the displacement of mercury, ΔV, by the following relation.

$$a = \sqrt{\frac{V_o - \Delta V}{\pi h}}$$

where

a = reduced cavity radius

V_o = original volume of the cavity

ΔV = change in volume

h = height of cylindrical cavity

Also, the radial displacement, u_r, was calculated from the relation

$$u_r = a - a_o$$

where

a = reduced cavity radius

a_o = initial radius of cavity

The axial deformation measurements were performed by a dial gage that fits on the top of a perpendicular steel rod connected to the bottom of specimen, Fig. 5.4.

5.3e Testing procedure

The procedure followed in studying the behavior of a model cavity under triaxial compression was divided into three main categories:

1. Elastic-plastic deformation tests: The objectives of these tests were to determine: (a) the structural properties of rock salt such as Young's modulus E, and octahedral shear strength K_o, (b) the development of the plastic zone as a function of cavity depth and strength of salt, and (c) to verify the mathematical equations describing the variation of cavity closure based on theories of elasticity and plasticity.

   The pressure was raised uniformly in steps of 500 to 1000 psi. Immediate mercury displacements were recorded over a pressure range of 500 to 9000 psi.

2. Cyclic tests: In this part, the interest was to study the effect of triaxial compression tests on the properties of rock salt.

   The pressure was raised uniformly in steps of 200 psi up to 2000 psi and unloaded uniformly to zero. The process was repeated for about 15 cycles; in a few of these the load was

maintained at that level for 5 minutes till the plastic flow effect was decreased and then unloaded to zero.

The cyclic effect on Young's modulus and octahedral shear strength were observed and compared with the first cycle.

Immediate mercury displacements were recorded for the loading and unloading cycles. Results were plotted in several diagrams and the cyclic effect on Young's modulus and octahedral shear strength were observed and compared with the values of Young's modulus from the first cycle.

3. Creep test: The objectives in this series of tests were to study (a) the creep behavior of a hollow cylinder under multiaxial compression, (b) creep rate equations and material constants, and (c) the effect of geometry, external pressure and time on these behaviors. The outside dimensions of the specimen were all the same, but the inside diameters varied between 0.50 inches and 1.50 inches for different tests.

The pressure was raised at a uniform rate from zero up to 3000, 5000 or 7000 psi. It was maintained at these stress levels by the automatic control system. Creep measurements were calculated from mercury displacement over a period of 10 to 40 days.

PART THREE: EVALUATION

CHAPTER VI

EXPERIMENTAL RESULTS AND DISCUSSION

6.1 Fundamental Structural Properties of the Material

The structural properties of most materials are usually defined by fundamental coefficients, such as Young's modulus, E, Poisson's ratio, μ, octahedral shear strength, K_o, viscosity coefficient, η, and retarded shear modulus. These coefficients vary from one material to the other. They also vary within the same material if subjected to various factors such as strain hardening, physio-chemical interaction, radiation, heat . . . etc. However, under normal laboratory conditions these coefficients are constant and essential to describe the physical behavior of most engineering materials. The reaction of different materials to different stress conditions depends entirely on their mechanical properties. These properties are divided into two groups: first, time-depencence constants such as viscosity coefficients and retarded shear modulus that are discussed in sec. 6.3 and second, time-independent property constants such as Young's modulus, Poisson's ratio and octahedral shear strength. The two main constants that have been investigated in this section under triaxial compression are Young's modulus and octahedral shear strength, also the strain hardening was investigated.

6.1a Young's modulus

For a material that obeys Hooke's law, Young's modulus is defined as the proportionality constant between the stress and strain in uniaxial loading, or it may be defined as the slope of a straight line which includes most of the linear part of the stress-strain curve below its yield limit. The values of Young's modulus varied depending upon the testing procedures used. Values of Young's modulus determined by different test procedures are listed by Serata.[70]

Young's modulus under triaxial compression was determined in the laboratory by using equation of a thick walled hollow cylinder, Eq. 2.2-8,

$$\frac{\Delta u}{\Delta p_o} = \frac{1}{E} \frac{(1-\mu)}{(1-\frac{a_o^2}{b_o^2})} \left[\frac{a_o^2}{r} + (1-2\mu)\, r\right]$$

where $\frac{\Delta u}{\Delta p_o}$ is the slopw of the curve of displacement versus external pressure. This equation describes the radial displacement in the elastic region as a function of cavity geometry and external stress, p_o. If the geometry and Poisson's ratio are known, Young's modulus may be obtained by determining the slope of the displacement-stress curve at r = a. The displacement-stress curves for different specimens of hollow thick-walled cylinder subjected to triaxial compression and plane strain are shown in Fig. 6.1. This figure is characterized by the following features:

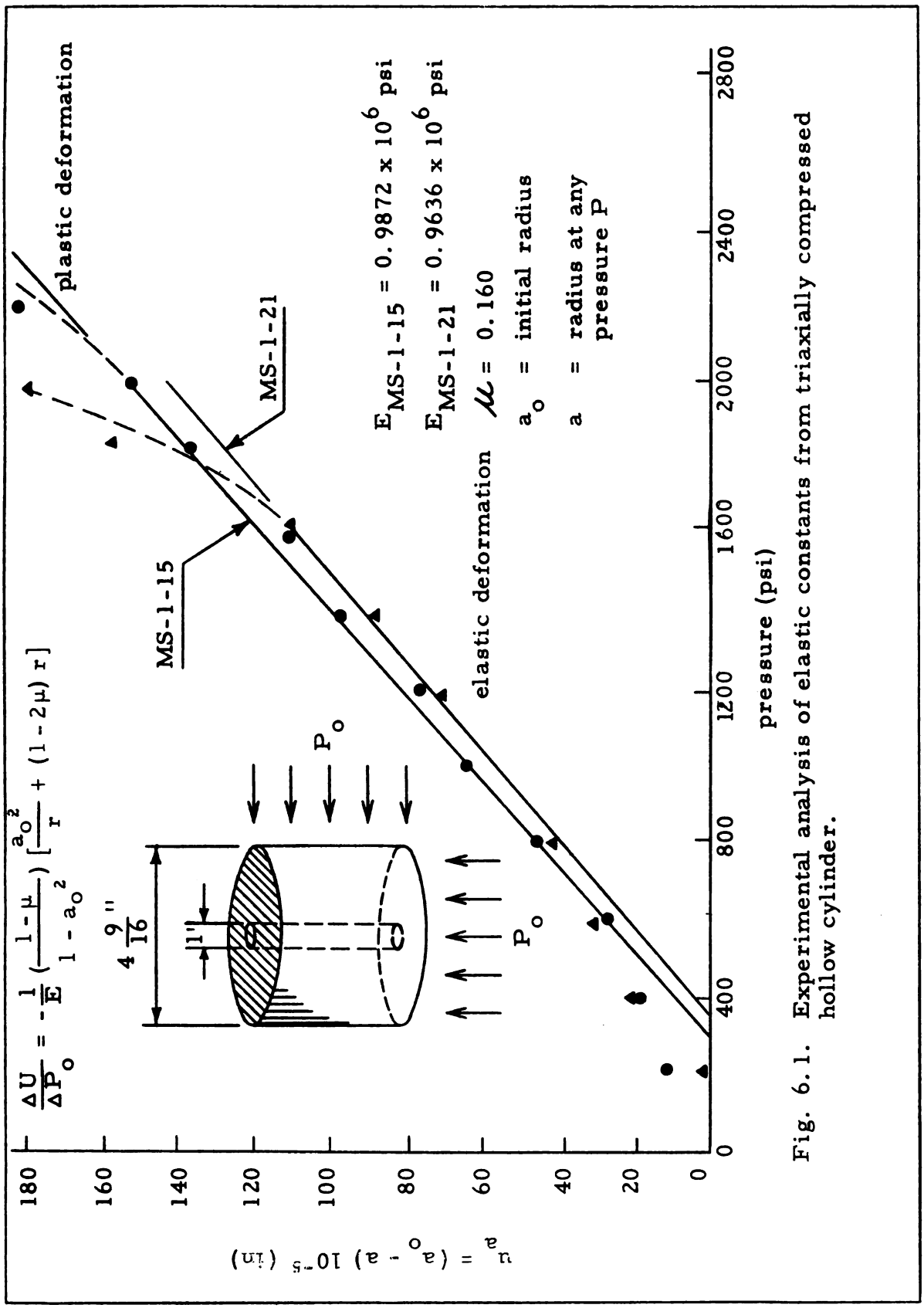

Fig. 6.1. Experimental analysis of elastic constants from triaxially compressed hollow cylinder.

1. There is a definite elastic straight line.

2. p_o = 1600 to 2000 psi when yield first occurred.

3. Rapid changes in slope occur approximately after these limits, which may indicate the beginning of the plastic deformation.

Values for Young's modulus obtained from this and similar curves by using the above mentioned equation are tabulated as follows:

Table 6.1 Values of Young's modulus as obtained from hollow cylinder (first cycle)

Test No.	Young's modulus Ex 10^6 psi	Size of specimen
MS-1-15	0.987	Di = 1.0"; Do = 4 9/16"; ho = 4 9/16"
MS-1-16	0.749	Di = 1.0"; Do = 4 9/16"; ho = 4 9/16"
MS-1-18	0.40	Di = 1 15/16"; Do = 4 9/16"; ho = 4 9/16"
MS-1-21	0.964	Di = 1.0"; Do = 4 8/16"; ho = 4 9/16"
MS-1-24	1.137	DI = 1 16/64"; Do = 4 9/16"; ho = 4 8/16"

These results are based on data obtained from the first cycle. The above values compare closely with the results reported by Serata.[70] Higher values of Young's modulus were observed in the subsequent cycles as indicated in Fig. 6.2.

Another testing method, the transition test technique, was used to determine Young's modulus. In this method, a triaxially stressed solid cylinder was used to determine the lateral stress axial stress

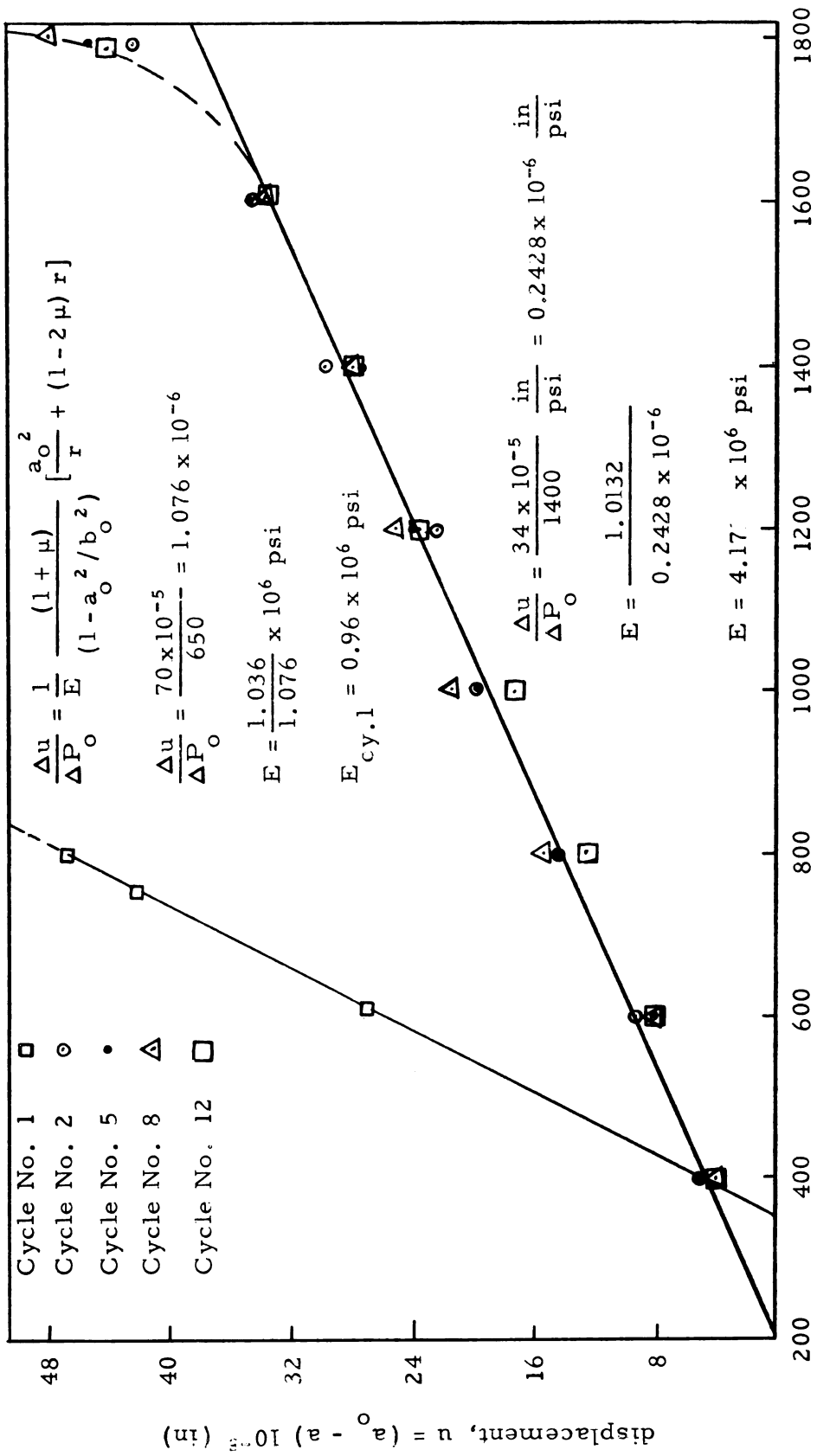

Fig. 6.2 Analysis of Young's modulus from experimental results of triaxially compressed hollow cylinders

relation. Using these results and the equation of Young's modulus (Eq. 2.1-2), indicated on page 13, values of Young's modulus were calculated as shown in Table 6.2.

Table 6.2 Values of Young's modulus obtained from transition tests

Test No.	Young's modulus (10^6 psi)				
	Cycle I	Cycle II	Cycle III	Cycle IV	Aver-age
MS-1-26	----	2.0	2.68	2.45	2.378
LS-1-1	----	2.71	2.83	----	2.77
LS-1-3	----	2.23	2.83	----	2.53
LS-1-4	0.4×10^6	3.0	----	----	----

These values are higher than those obtained from the first cycle of the hollow cylinder tests, Table 6.1, but they are smaller than the values obtained from second and subsequent cycles (Fig. 6.2). This discrepancy can be explained by the difference in the boundary conditions and in the strain measuring technique of the transition test compared to that of hollow cylinder test. In the latter, slip on the crystal interfaces is relatively free to occur as the material adjusts to the differential stress. On the other hand, the lateral restraint of strain in the transition test prevents most of this behavior and creates a more compact crystal arrangement. Therefore, this wide variation of results is mainly attributed to the difference between the two

testing procedures. Similar observation has been reported by various investigators as reported by Serata.[70]

A certain amount of variation is expected to occur in a material like rock salt due to the following reasons:

1. Different stress history of the specimen
2. Deviation from isotropy and homogeneity of the specimen tested
3. Various grain size of the specimen
4. Degree of impurity concentration

6.1b Strength of salt

The strength theories of solids may be described in terms of state of stress, state of strain and energy of distortion. Some of the theories which are relevant to this work were used to define the strength of rock salt. The octahedral shear strength was chosen to describe the strength of salt under triaxial compression. However, in the uniaxial test the maximum strength is usually used. Two different procedures were used to determine the octahedral shear strength. These are described as follows:

1. Hollow cylinder test

In thick-walled cylinder the maximum shear theory was used to evaluate the octahedral shear strength, K_o. The ratio of the inner radius of the cylinder "a" to that of the external radius "b" is related to the external pressure P_o and the octahedral shear strength K_o as follows:

$$\frac{a}{b} = e^{-\frac{1}{\frac{3}{2\sqrt{2}}K_o}(P_o - P_i)}$$

or

$$\ln e \left(\frac{a}{b}\right) = -\frac{1}{\frac{3}{2\sqrt{2}}K_o}(P_o - P_i) \qquad (2.4\text{-}4)$$

This indicates that the logarithm of the plastic front ratio, a/b, is directly proportional to the stress difference between the external and internal pressures. If this relation is plotted on a semi-log paper, the slope would yield the octahedral shear strength of rock salt for completely plastic state.

Experimental data obtained from three identical specimens are shown in Fig. 6.3. The results indicate that the elastic limit is about 2000 psi for MS-1-15 and MS-1-16 and about 2500 psi for MS-1-21. An elastic-plastic state extends from these two limits up to approximately 7500 psi. A large deformation region is expected to exist beyond this value.

The octahedral shear strength is calculated from the slopes of the curves of the plastic region which extend beyond 7500 psi. For MS-1-15 and MS-1-16, the octahedral shear strength K_o is approximately 2300 psi. This value is based on the asymptote to the last few points of the curve. More accurate data could have been obtained if the capacity of the high pressure vessel is larger than 9000 psi, so

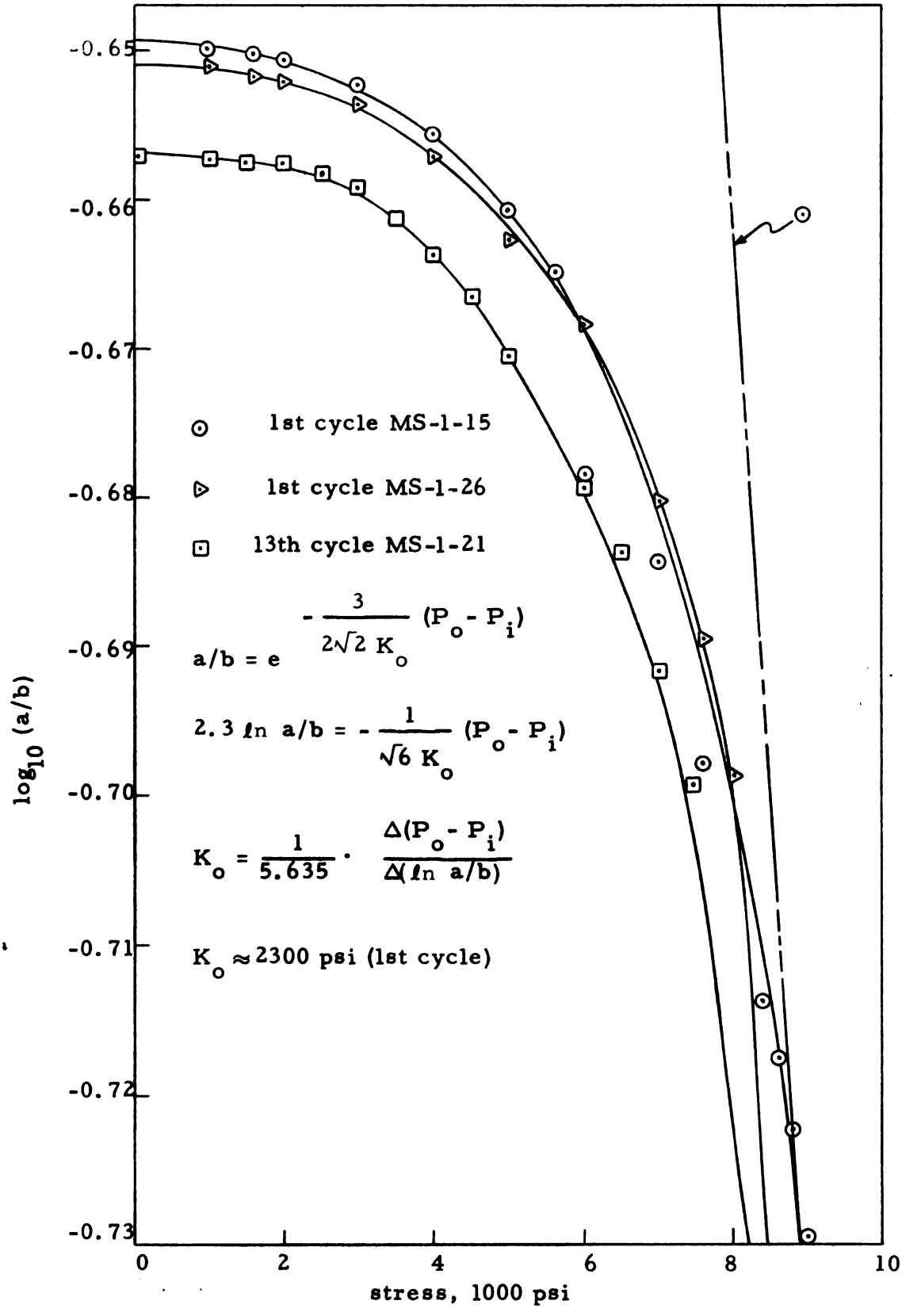

Fig. 6.3 Experimental analysis of large deformation in hollow cylinder

that more readings could have been obtained in the plastic region. Moreover, instantaneous readings at such high stresses should be considered to eliminate any time effect of plastic flow.

2. Transition test

In a continuous medium such as a homogeneous rock material imbedded in the earth crust, the conditions of triaxial pressure and restraint are similar to those of the transition test. The mechanical property of octahedral shear strength was obtained from this testing procedure.

In Fig. 2.1 of the transition test, it may be readily seen that the vertical distances between the lines of plastic states and the hydrostatic line are $\frac{3}{\sqrt{2}} K_o$. Table 6.3 gives the values of K_o obtained for each cycle of loading on each specimen. It is seen that the octahedral shear strength of specimen MS are larger than that of LS. Both kinds of rocks approach approximately to the same octahedral shear strength value after several cycles of loading. The values of the second cycle are 2000 psi and 1625 psi for rock MS and LS respectively. In general, the values from the second cycle agree very closely with the value obtained from hollow cylinder tests. It is observed that the values obtained from first and second cycles for LS-1-1, LS-1-2, LS-1-3, and LS-1-4 were almost exactly the same. This reflects the consistency and homogeneity of the specimen used.

Table 6.3 Octahedral shear strength obtained from transition tests

Test No.	K_o	No. of cycles
MS-1-26	1650	1
"	2000	2
"	2100	4
LS-1-1	1375	1
"	1625	2
"	1955	3
LS-1-2	1365	1
LS-1-3	1400	1
"	1650	2
LS-1-4	1300	1
"	1695	2

6.1c Cyclic stress tests and the effect of strain hardening.

It was observed from repeated loading procedure on both the hollow and solid cylinders that the values of the mechanical properties such as K_o and E increase after the first cycle. This behavior may be explained as an effect of work hardening of the material.

In metal testing, the raising of the elastic limit by increasing deformation of the piece in the plastic range is defined as strain-hardening or work hardening. This phenomenon may be explained that, if a slip is stopped from being propagated at a grain boundary because it is impeded by another dislocation or an impurity, then regions of high strain will be created within each crystal. Hence, an increase in stress will be required to facilitate more progress of dislocations. The stress needed to move a dislocation will depend on

grain boundaries, impurities and closeness of other dislocations. By increasing the temperature and activation of the dislocation to overcome these obstacles and causing slip to spread out at less stress, the effect of strain hardening will diminish. The effect of cycling and strain hardening was studied in both the hollow cylinder test and the transition test.

3. Hollow cylinder test

In testing a thick-walled salt cavity, as shown in Fig. 6.4, a similar increase in the elastic limit to that of metal is found by cyclic loading. The unloading lines are mainly straight lines parallel to those obtained in the first loading region. This may be explained by the fact that the interatomic forces that pull the atoms together when load is removed are the same forces that have to be overcome in the first elastic elongation. Hence, the slopes of the loading and unloading lines are the same and the lines are parallel.

During the first stages of unloading, it was observed that the lateral strain remains constant. No elastic recovery was observed as stress is reduced. This behavior in polycrystalline material like rock salt, is due to permanent slip and dislocations that cuase plastic flow to occur at higher loads and prevent atoms from returning to their equilibrium position upon unloading. In the laboratory, the load was raised to 2000 psi and maintained at that level for five

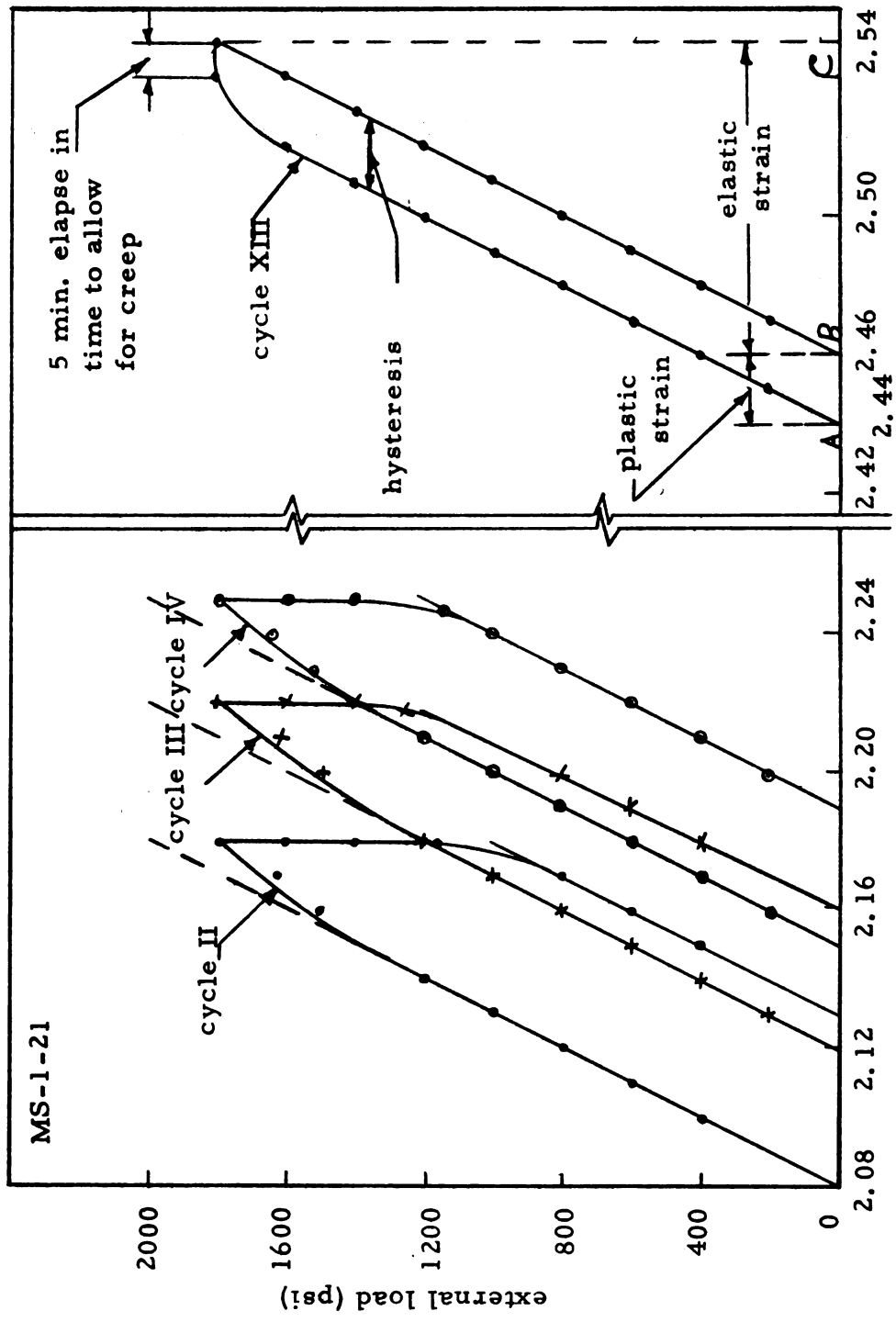

Fig. 6.4 Experimental analysis of cycling effect on strain of triaxially compressed hollow cylinders.

minutes and then unloaded. The results are shown in Fig. 6.4, where elastic recovery responded immediately since the rapid plastic flow had clearly diminished and only the elastic recovery was being measured.

The deformation of the compressed cylinder beyond the proportionality limits is partially elastic or recoverable and partially plastic or permanent. This is shown in Fig. 6.4, where the region AC represents the total deformation, $\epsilon = \epsilon^e + \epsilon^P$. Region AB is the unrecoverable part, ϵ^P, and BC is the recoverable part, ϵ^e.

4. Transition test

The effects of cyclic loading and strain hardening are shown in Tables 6.2 and 6.3. From these tables, it is clearly seen that the values of K_o and E increased with the number of loading cycles. Most of the increase occurs between the first and second cycles and approaches a small value after a certain number of cycles. The increase in K_o for MS-1-26 between the first and second cycles was about 17 percent, while only 5 percent between the second and the fourth cycles. Similarly, a large increase in E value was observed between the first and second cycles and was almost the same for the subsequent cycles (Fig. 6.2).

Theoretically, the strain hardening of rock salt in a triaxially compressed state may be described as illustrated in Eq. 2.3-30 by

using the Levy-Mises relation and the work hardening hypothesis suggested by Hill.[33] From these relations, an expression for the slope of work hardening material is expressed as follows:

$$H' = \frac{3}{2} \frac{d\bar{\sigma}}{\bar{\sigma} d\lambda}$$

where

H' = slope of the effective stress - effective strain curve

$\bar{\sigma}$ = effective stress

$$= \frac{1}{2} [(\sigma_x - \sigma_y)^2 + (\sigma_y - \sigma_z)^2 + (\sigma_z - \sigma_x)^2]^{1/2}$$

$d\bar{\sigma}$ = incremental change in the effective stress

$d\lambda$ = proportionality function = $\frac{3}{2} \frac{d\bar{\epsilon}^P}{\bar{\sigma}}$

$$d\bar{\epsilon}^P = \frac{\sqrt{2}}{3} [(d\epsilon_x - d\epsilon_y)^2 + (d\epsilon_y - d\epsilon_z)^2 + (d\epsilon_z - d\epsilon_x)^2]^{1/2}$$

By using the experimental results from test MS-1-26, the strain hardening characteristics of rock salt were obtained as presented in Table 6.4. As the effective stress increases beyond the proportionality limit, the material hardens with increasing effective strains. The slope of the strain hardening portion H' decreases rapidly until it approaches zero. This behavior is demonstrated in Fig. 6.8, Chapter VI. The slope H' decreases rapidly to zero as the axial stress increases approximately between 8000 to 11,000 psi. Fig. 6.8 shows that this is the transition region between the elastic and plastic states.

Table 6.4 Experimental analysis of strain hardening characteristics of rock salt

σ_z psi	$\bar{\sigma}$ psi	$\Delta\bar{\sigma}$ psi	$d\lambda\ 10^{-6}$	$1.5\frac{\Delta\bar{\sigma}}{\bar{\sigma}}$	H'
		Cycle II			
7839	5828	742	2652	0.190	72
9045	6470	642	2908	0.149	51
10251	6988	518	3280	0.111	33
11457	7359	0			0
		Cycle III			
8442	6315	757	1570	0.175	114
9648	6980	665	1720	0.142	83
10251	7274	712	2276	0.138	61
11457	7691	0			0

Beyond this value the "plastic line" reaches 45° which describes the perfectly plastic state with $\Delta\bar{\sigma} = H' = 0$.

6.2 General Behavior of a Cylindrical Cavity with Loading

6.2a Experimental verification of theoretical cavity behavior.

The strength of an elastic-plastic deformation of a cavity created in a salt medium has been studied in the laboratory by a model cylindrical cavity. Closure of a cavity with respect to loading is illustrated in Fig. 6.5. The pressure was increased uniformly at

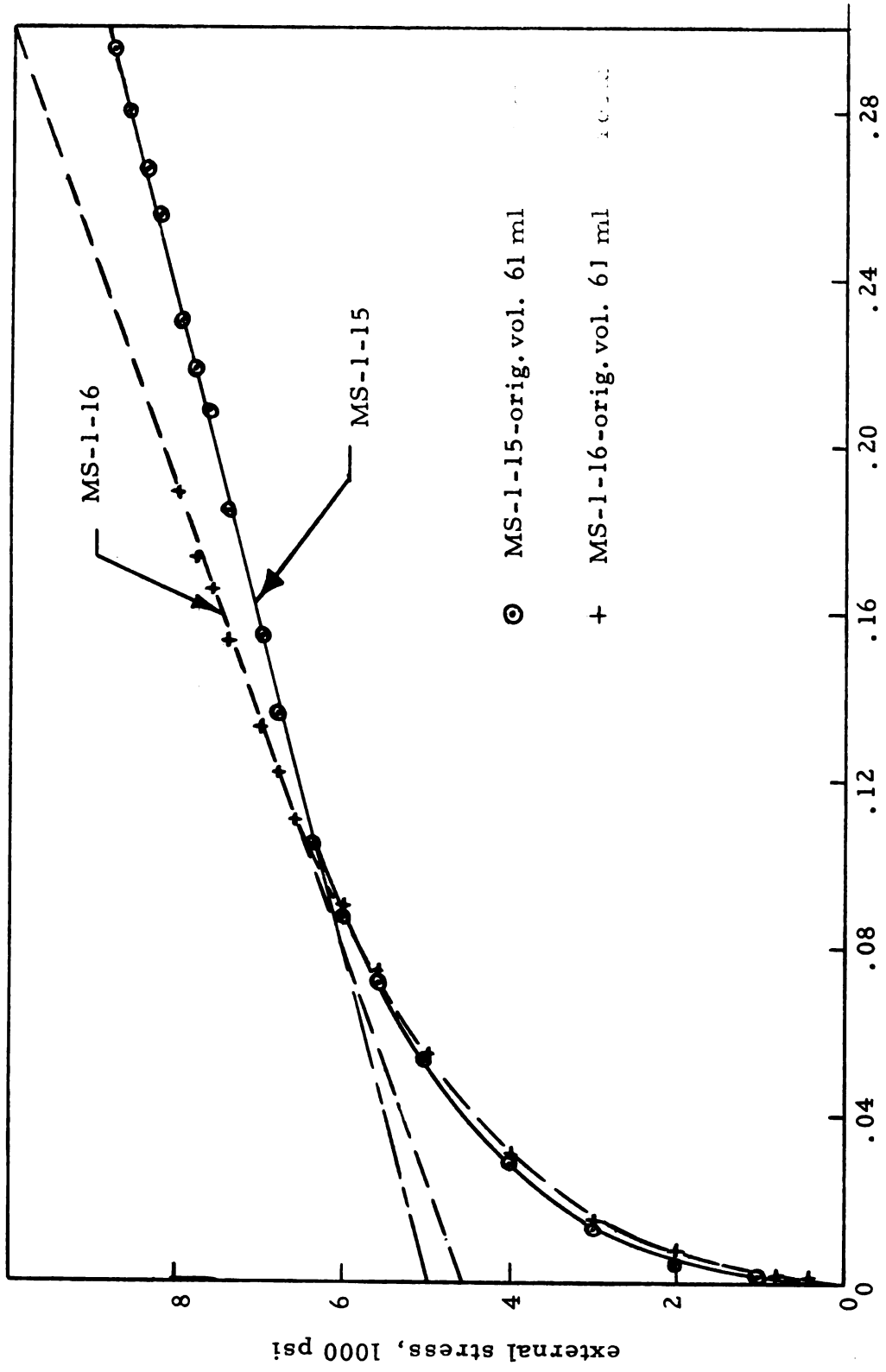

Fig. 6.5 Closure of model salt cavity

equal intervals of stress from zero up to 9000 psi and the corresponding cavity closure was recorded. A maximum closure of approximately 30 percent was registered at an external pressure of 9000 psi, and less than 5 percent at a stress of 3000 psi. This closure is an important factor in the design of salt cavities when these are created at a depth of more than 3000 ft.

Theoretical stress distribution around a cylindrical cavity has been developed in the elastic, elastic-plastic and completely plastic states as indicated by Eqs. 2.3-10, 2.3-14 and 2.4-2, respectively. Based on these equations, the theoretical radial displacement at $r = a$ is calculated and compared with experimental results. The conditions imposed on the displacement equations are either elastic compressibility in plastic regions or compressibility in elastic region and incompressibility in plastic region as indicated by the following equations.

For elastic compressibility in elastic region, the radial displacement is:

$$u_{r=a} = \left(\frac{1-2\mu}{G}\right)\left[\frac{\frac{3}{2\sqrt{2}}K_o}{2}\, a\left(\ln\frac{\rho}{a}+\frac{1}{2}\right) - \frac{\frac{3}{2\sqrt{2}}K_o}{4}\,\frac{\rho^2 a}{b_o^2} - \frac{P_o a}{2}\right]$$

$$- (1-\mu)\,\frac{\frac{3}{2\sqrt{2}}K_o}{2G}\,\frac{\rho^2}{a} \qquad (2.3\text{-}38)$$

For compressibility in elastic region and incompressibility in plastic

region, the radial displacement is:

$$u_{r=a} = \frac{\rho}{a} \cdot \frac{1}{2G}\left\{\frac{\frac{3}{2\sqrt{2}}K_o}{2}\left[(2\mu-1)\frac{\rho^3}{b_o^2} - \rho\right] + (2\mu-1)\,\rho\,P_o\right\} \qquad (2.4\text{-}9)$$

The theoretical behavior of the radial displacement as a function of applied stresses and plastic radius is worked out for values of ρ that varied between 0.50 inches to 2.20 inches. The steps involved for computation of the radial displacement are as follows:

1. The material properties are obtained from the previous laboratory data where, $E = 1.2 \times 10^6$ psi and $\mu = 0.16$.
2. For assumed values of ρ, values of "a" are calculated from Eq. 2.3-54.
3. By using the values of ρ and "a" obtained from step 2, values of external stresses necessary to create the given plastic radius, ρ, are calculated from Eq. 2.3-15.
4. By substituting the values of ρ, a, and P_o into Eq. 2.3-37 and Eq. 2.4-9, the theoretical radial displacements at each stress point are calculated. A sample of the calculation is presented in Table 6.5. Three different values of K_o of 1500 psi, 1750 psi and 2000 psi were used in Eq. 2.3-38. The stress-displacement curves thus obtained were presented in Fig. 2.4.

In the laboratory, radial displacements were measured for different specimens at equal intervals of pressure between 0 and

Table 6.5 Theoretical analysis of the behavior of a thick walled cylinder
(External diameter of 4 9/16" and internal diameter of 1 inch)

ρ	ρ^2	$\frac{1-0.03267}{\rho^2}$	$\frac{a}{a_o}$	a	$\frac{\rho^2}{b_o^2}$	ln ρ	ln a	P_o	$\frac{\rho^2}{2b_o^2}$	$\frac{\rho^2}{a}$	$P_o a$	*	u (10^{-7})
0.50	0.25	0.99235	0.9963	0.50842	0.04803	-0.693	-0.676	2249	.02401	.49171	1143	.23335	-19483
0.60	0.36	0.98899	0.99446	0.50748	0.06917	-0.511	-0.678	3098	.03458	.70938	1572	.32094	-28114
0.80	0.64	0.98043	0.99016	0.50528	0.12297	-0.223	-0.683	4441	.06148	1.26662	2244	.45400	-50376
1.00	1.00	0.96943	0.98459	0.50244	0.19215	0.000	-0.688	5350	.09607	1.99028	2688	.54862	-79019
1.20	1.44	0.95580	0.97765	0.49890	0.27670	0.18232	-0.695	6070	0.13835	2.88634	3028	.61812	-114658
1.40	1.96	0.94009	0.96962	0.49480	0.37662	0.33647	-0.7034	6622	0.18831	3.96119	3276	.66875	-157424
1.60	2.56	0.92174	0.96006	0.48992	0.49191	0.4700	-0.7132	7041	0.24595	5.22534	3449	.70413	-707728
1.80	3.24	0.90095	0.94918	0.48437	0.62258	0.58779	-0.7249	7356	0.31129	6.6891	3563	.72723	-265992
2.00	4.00	0.87772	0.93686	0.47809	0.76862	0.69315	-0.7371	7574	0.38431	8.36662	3621	.73909	-332762
2.20	4.84	0.85204	0.92310	0.47106	0.93003	0.78846	-0.7527	7722	0.46501	10.2746	3637	.74246	-408718

* $a\,(\ln \rho - \ln a - \rho^2/2b_o^2 + 0.5)$

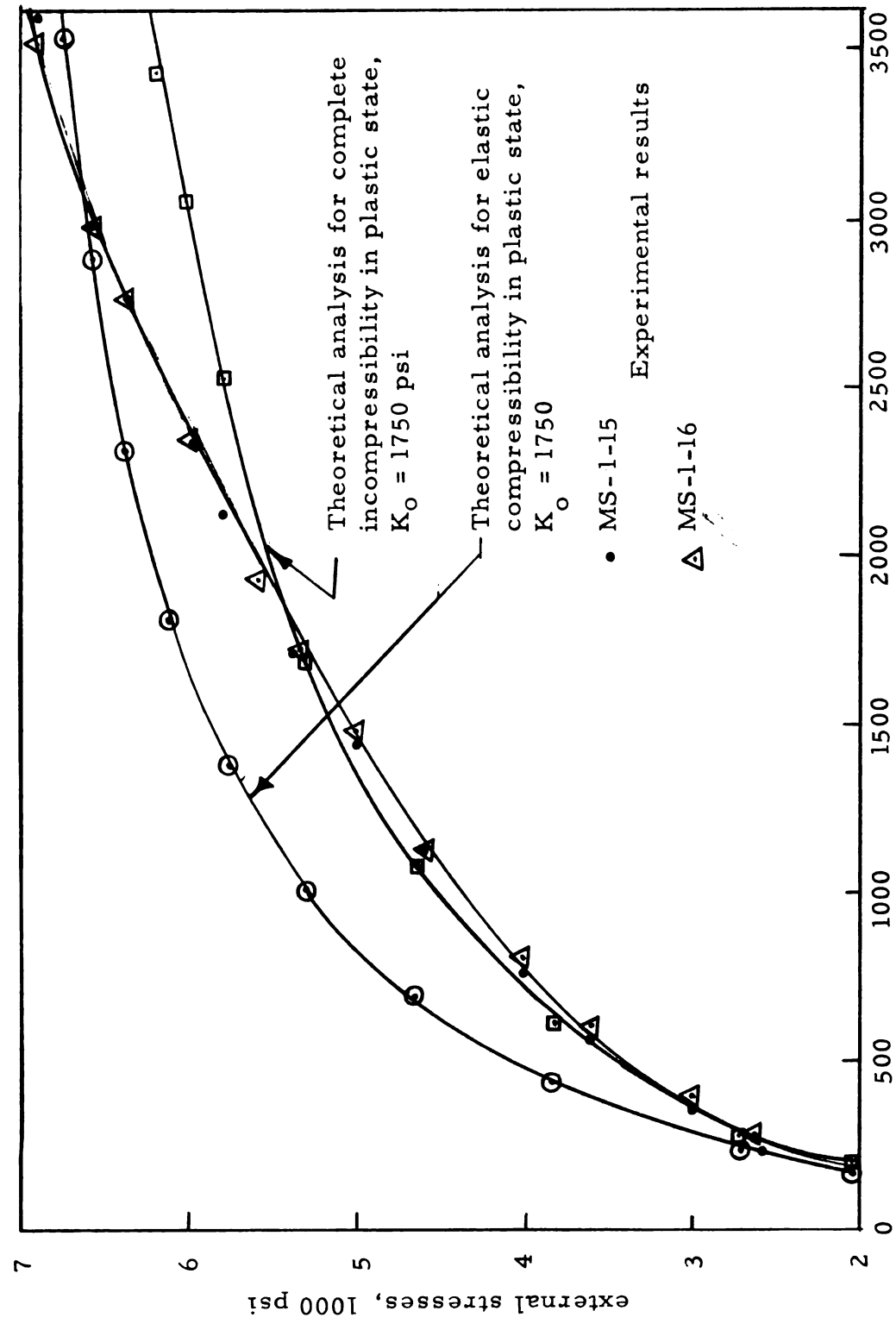

Fig. 6.6 Theoretical stress-strain relation of a model cylindrical cavity compared to experimental results

9000 psi. At each interval, the load was maintained at that level for a period of one minute before the data were recorded. A sample of the experimental results was compared with the theory of Eqs. 2.3-38 and 2.4-9 (for K_o = 1750 psi) as shown in Fig. 6.6. A general close agreement has been observed between the experimental results and the curve of complete incompressibility in the plastic region up to approximately 5500 psi. Above this stress level, the theoretical curve flattens out quickly and the degree of variation between the two curves increases. If sufficient time is allowed for salt to flow, the experimental results might have approached the theoretical curve. On the other hand, a good agreement was observed between the theory of Eq. 2.3-38 and experimental results up to approximately 4000 psi. Above this stress level, the degree of variation between the experimental and theoretical curves increases due to rapid plastic deformation. Whenever the plastic stress state is reached, the discrepancy between theoretical and experimental results was found especially when the experimental results were taken one minute after the load was reached.

Similarly, the relationship between the reduced cavity radius, a, and the external pressure was calculated simultaneously from Eq. 2.3-54 and Eq. 2.3-15. A comparison between the theoretical reduced radius, a, and its value obtained from experimental results is illustrated in Fig. 6.7. Close agreement between experimental and

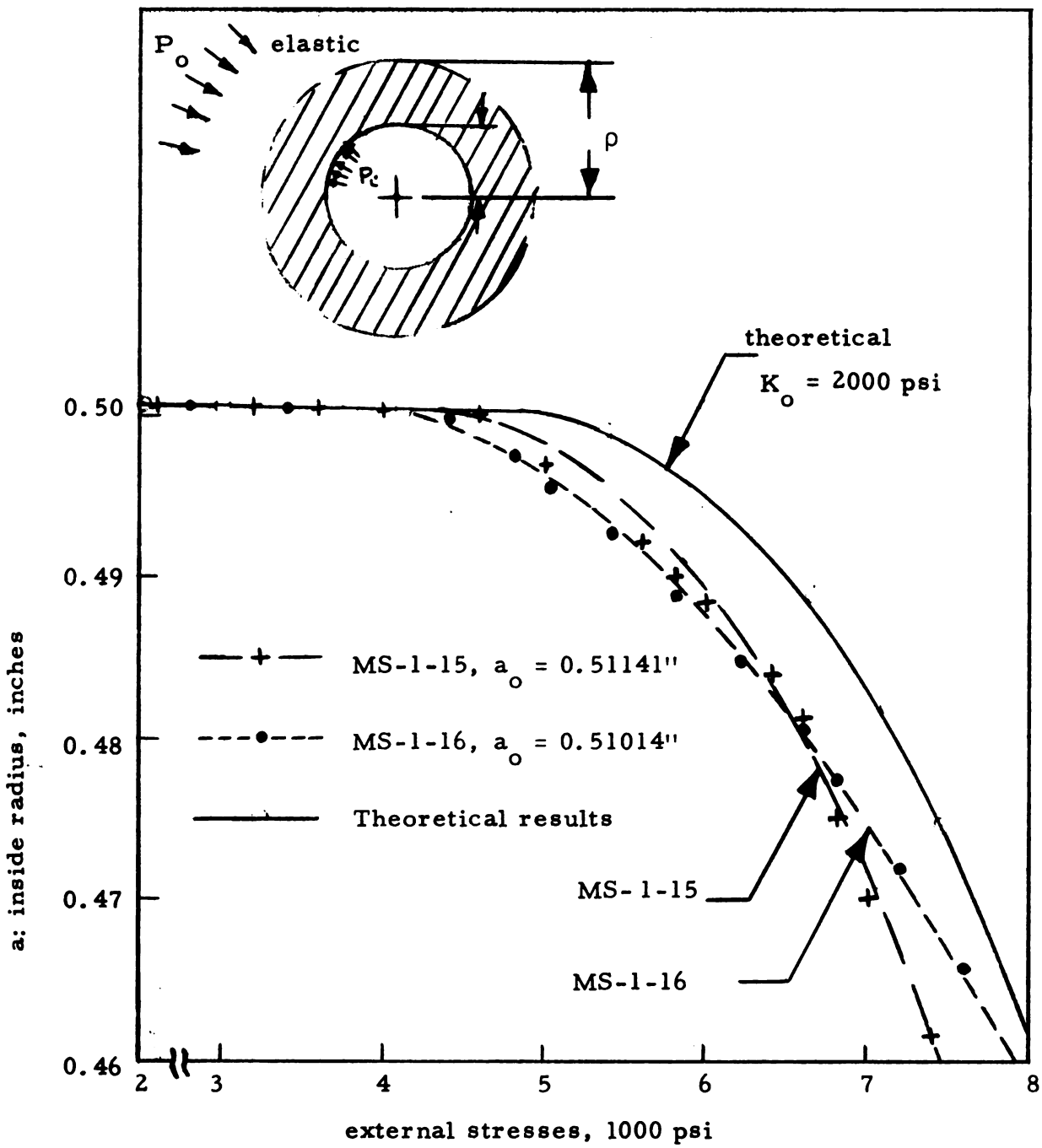

Fig. 6.7 Variation of the modified inner radius, a, of a cylindrical cavity compared to experimental results

theoretical values was observed up to a pressure of approximately 4000 psi, where the variation of the inside reduced radius is very small. At higher pressures the experimental values seemed to be lower than the theoretical ones. This might be explained by the fact that the experimental values were recorded one minute after the pressure was reached. It is reasonable to assume then that the experimental values would have been closer to the theoretical values had the readings been taken instantaneously.

6.2b Stability conditions

These analyses have demonstrated the important fact that a salt cavity will eventually reach a state of equilibrium between the advancing plastic zone and the elastic part. The advancement of the plastic zone is defined by Eq. 2.3-15 where

$$\rho = a \exp. \frac{1}{\frac{3}{2\sqrt{2}} K_o} \left\{ \left[(P_o - P_i) - \frac{1}{2} \left(1 - \frac{\rho^2}{b_o^2}\right) \right] \right\}$$

If an infinite medium is considered where $b_o >> \rho$, then

$$\ln \left(\frac{\rho}{a}\right) \frac{1}{\frac{3}{2\sqrt{2}} K_o} (P_o - P_i) - \frac{1}{2}$$

It should be noted that the natural log of (ρ/a) is directly proportional to the stress difference and inversely proportional to octahedral shear strength. Hence, the development of the plastic zone is

controlled by: (1) increasing the external load or (2) decreasing the internal pressure. With the increase of external pressure, the plastic radius increases and accordingly the internal radius decreases as shown in Eq. 2.3-54, where

$$\frac{a^2}{a_o^2} = 1 - \frac{\frac{3}{2\sqrt{2}} K_o}{G} (1 - \mu) \frac{\rho^2}{a_o^2}$$

and thus a state of stable equilibrium exists.

In the case of completely plastic state and for $\sigma_r \geq \sigma_z \geq \sigma_\theta$, the relation between external pressure and the reduced cavity radius is

$$P_o = \frac{3}{2\sqrt{2}} K_o \left(\ln \frac{b}{a}\right)$$

where for incompressibility conditions,

$$P_o = \frac{3}{2\sqrt{2}} K_o \ln \left[1 + \frac{b_o^2 - a_o^2}{a^2}\right]^{1/2}$$

From which it is clearly observed that as the inner cavity radius "a" decreases, the cavity gain ability to withstand a greater external pressure and thus the system is stable.

6.3 Transition Test

6.3a Axial stress-lateral stress relationship

In the laboratory, the lateral stress-axial stress relationship has been determined by Fig. 6.8. The stress conditions produced by

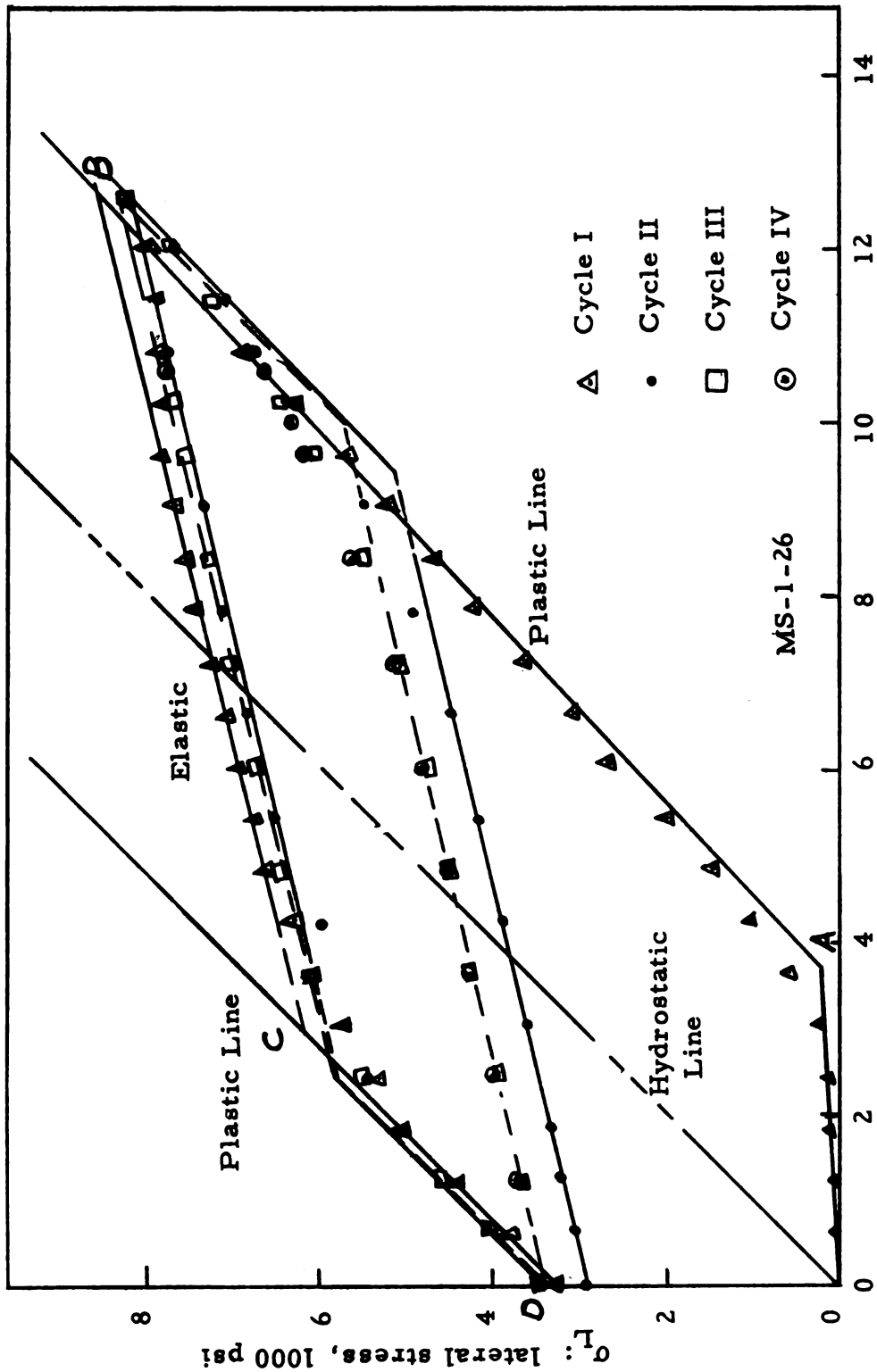

Fig. 6.8 Lateral stress-axial stress diagram illustrating the typical results of transition tests, in which solid cylinder is restrained from lateral expansion

a loading cycle can be illustrated as follows: during the initial loading up to point A on the stress diagram, the material behaves elastically. As the axial stress increases, the material changes rather abruptly to a plastic state of stress represented by line AB. The stress condition which the material experiences as the axial load is gradually reduced is illustrated by the elastic stress line, BC, and the plastic stress line, CD. The line DO represents the residual stress caused by creep and plastic deformation during the cycles of loading and unloading. The change in the residual stress becomes very small after the first cycle as indicated in the figure. However, the distance between the "hydrostatic line" and the "plastic line," which is related to the octahedral shear strength of the material, increases with the number of cycles.

It was observed from laboratory results that the transition from the elastic state OA to the plastic state AB is rather abrupt. Experimental results obtained by Raman[63] from limestone and granite as indicated in Figs. 2.2 and 2.3 show the gradual transition between the elastic and plastic states. This difference in the transition state between salt and the previously mentioned materials may be attributed to the viscosity constant of the materials. In case of rock salt, the transition was abrupt as indicated by line AB and this reflects a low viscosity constant. On the other hand, dolomite and limestone show a gradual change between the elastic and plastic states and this indicates a large viscosity value.

The discrepancy observed at the beginning of the unloading line BC may be due to viscous plastic deformation. As the axial stress is gradually reduced, for the first few readings, no strain recovery was observed. This was explained by the hypothesis that at high axial stress levels, plastic deformation is still taking place and thus cancelling the strain recovery produced by unloading.

6.3b Stress relaxation equations

The triaxial stress relaxation test involves the application of a constant load to the test specimens and the measurement of the deformation over a long period of time. Instrument creep was eliminated by taking the mean indicator reading illustrated in Fig. 6.9.

Fig. 6.10 illustrates the general stress relaxation behavior for a triaxially compressed and laterally confined rock salt specimen. It is observed that the octahedral shear stress decreases rapidly at the beginning of the creep period and relaxes asymptotically to a constant value as time increases.

The experimental equation describing this behavior is presented as follows:

$$\tau_o = \tau_f + (\tau_i - \tau_f)\, e^{-\alpha t} \qquad (3.1\text{-}13)$$

Rearranging this equation, it reads

$$\ln\left(\frac{\tau_o - \tau_f}{\tau_i - \tau_f}\right) = -\alpha t$$

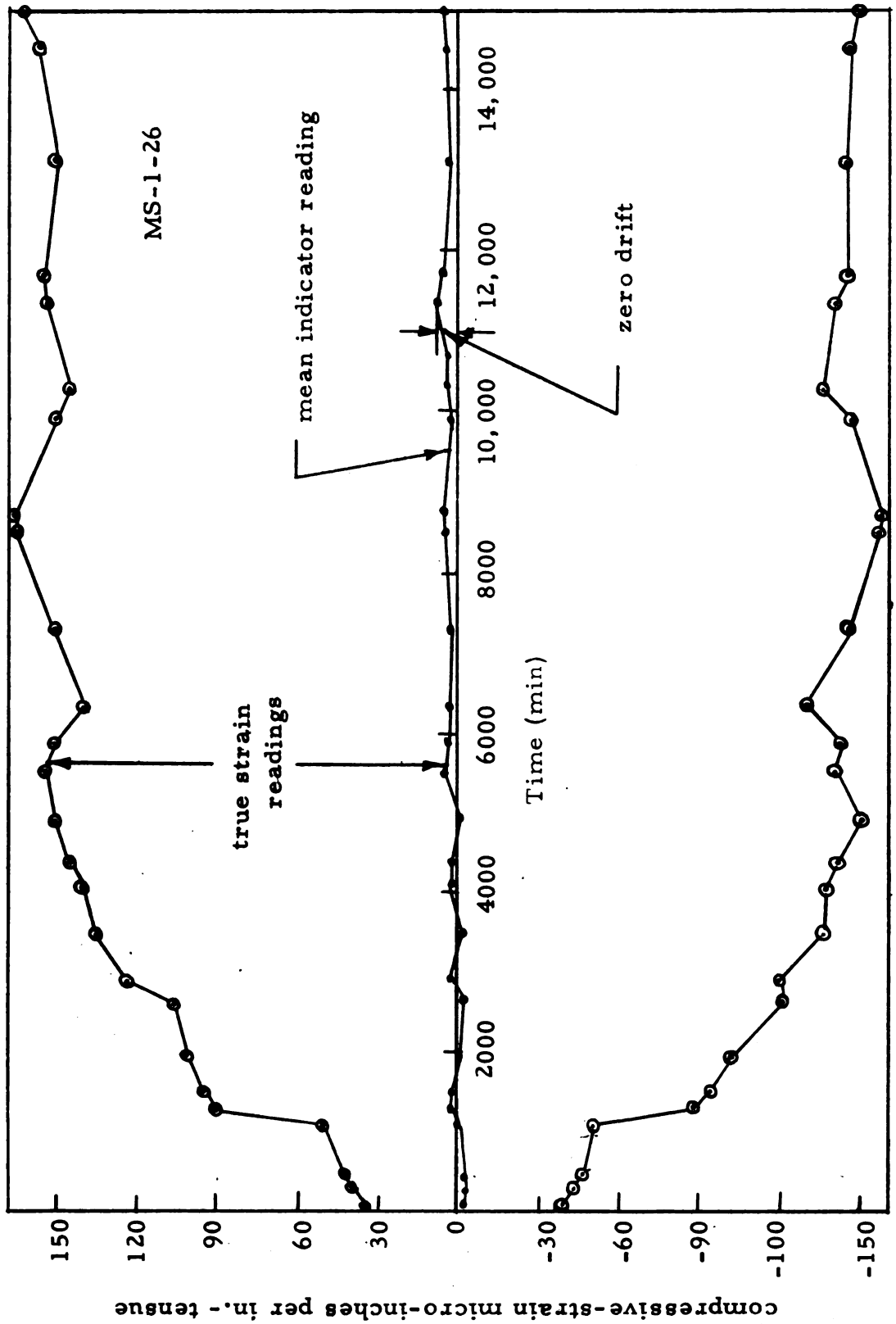

Fig. 6.9 Plot of strain readings illustrating the technique of determining zero drift by electrically reversing active and dummy gages

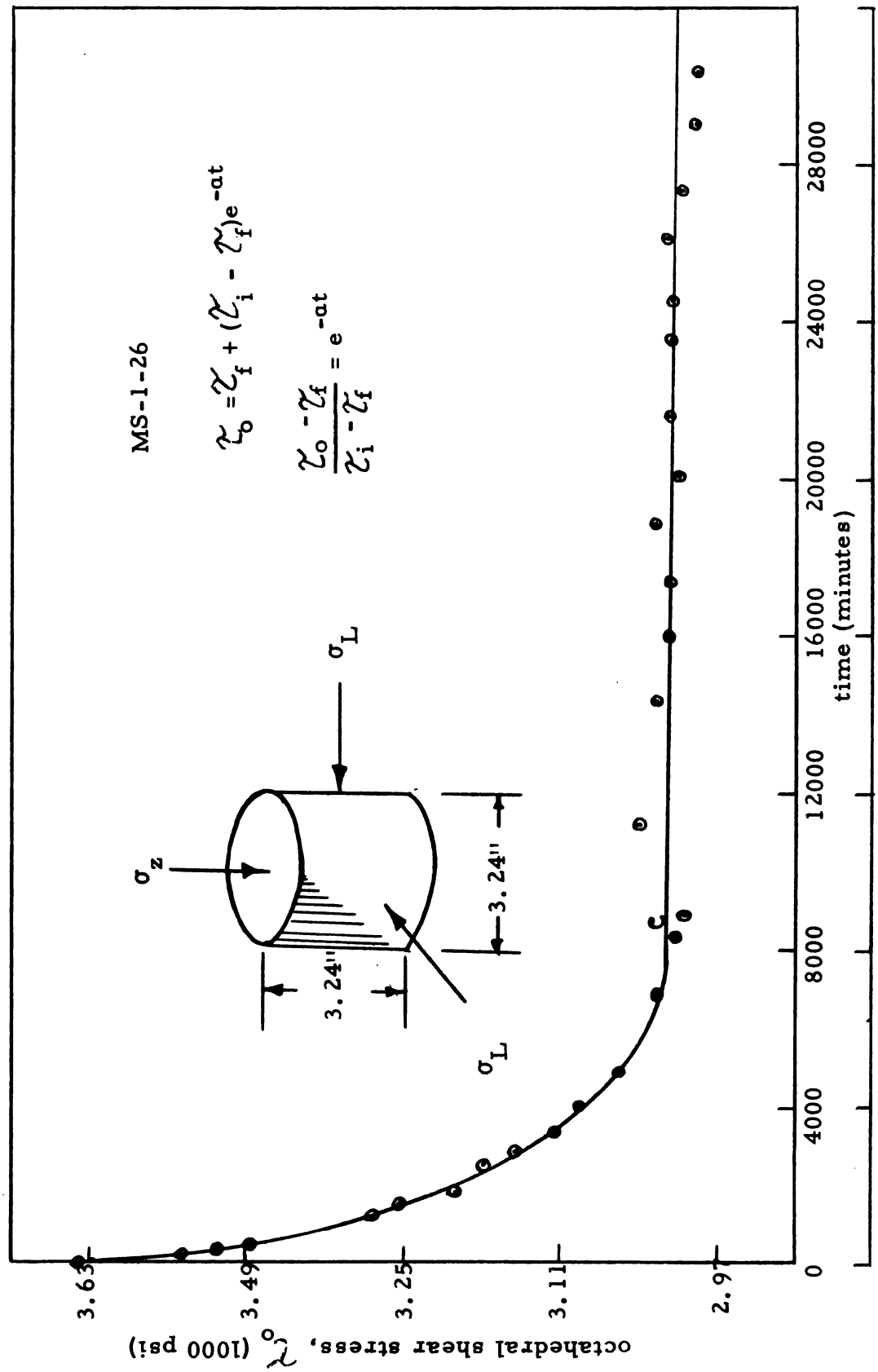

Fig. 6.10 Stress relaxation behavior in transition test

which indicates a linear relationship between octahedral shear stress and time on semi-log paper.

Laboratory results from stress relaxation tests were plotted as shown in Fig. 6.11. This showed that there are two independent stress relaxation equations represented in the same stress relaxation figure. A straight line was drawn asymptotically to the curve at large values of time. This represents the linear relationship of the viscoelastic stress relaxation. The difference between the values of the total stress relaxation curve and the line of the viscoelastic relaxation measured from the abscissa represents the stress relaxation curve of the viscoplastic state. This difference was found to be another straight line. The tangents of the angles of inclinations of these two lines, denoted by α_1 and α_2, are related to the viscosity coefficients of the material.

Theoretically, the stress relaxation behavior in the viscoplastic and viscoelastic regions is described by Eqs. 3.1-8 and 3.1-19 respectively, so that

$$\sigma_L = \left(\sigma_z \pm \frac{3}{\sqrt{2}} K_o\right) + \left[\left(\frac{\mu}{1-\mu} - 1\right) \sigma_z \mp \frac{3}{\sqrt{2}} K_o\right] e^{-\frac{G_1}{\eta_1} t}$$

and

$$\sigma_L = \sigma_z \pm \frac{3}{\sqrt{2}} \left[G_1 \gamma_o e^{-\frac{G_1+G_2}{\eta_2} t} u(t) + \left[1 - e^{-\frac{G_1+G_2}{\eta_1} t}\right] \frac{G_1 G_2}{G_1 + G_2} \gamma_o u(t) \right]$$

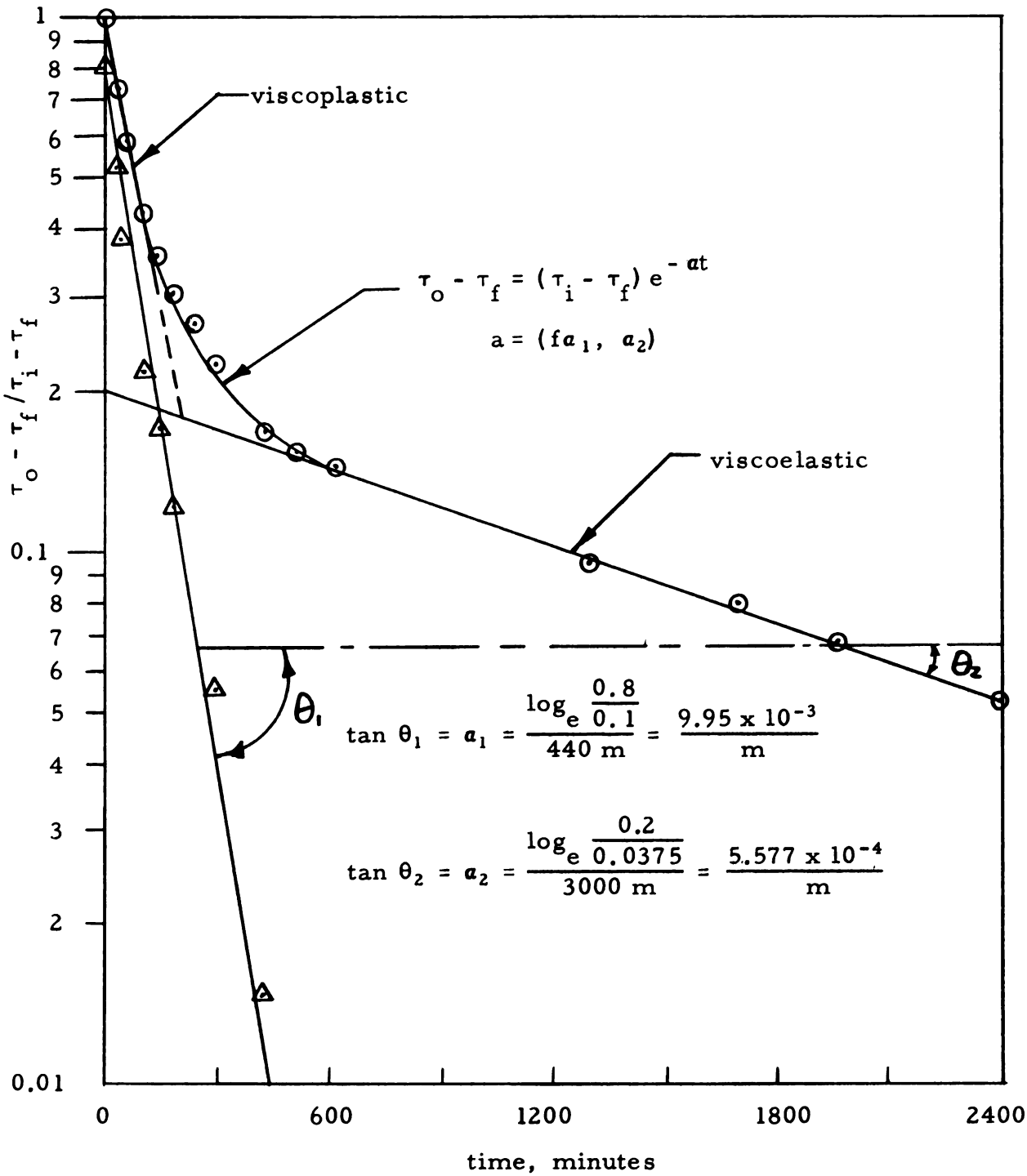

Fig. 6.11 Stress relaxation behavior in transition test illustrating contribution of viscoelastic and viscoplastic flow and determination of their coefficients

where

$$a_1 = \frac{G_1}{\eta_2}$$

and

$$a_2 = \frac{G_2 + G_1}{\eta_2}$$

These constants are used in sec. 6.3d to determine the time-dependent constants.

6.3c Plastic and viscoelastic states

1. Plastic state

It has been shown from theoretical analysis (Eq. 3.1-12) that the incremental change in the lateral stress is a linear function of the axial stress. Besides, the slope of the "plastic line" in a lateral stress-axial stress diagram is given by:

$$\frac{\Delta\sigma_L}{\Delta\sigma_z} = 1 + \left(\frac{\mu}{1-\mu} - 1\right) e^{-\frac{G_1}{\eta_1} t}$$

From these relations, it was concluded that:

1. $\frac{\Delta\sigma_L}{\Delta t}$ is a linear function of σ_z when all other variables are constant.

2. The "plastic line" approaches the 45^o line as t approaches infinity or when η_1 is a very small number, such that $\sigma_L = \sigma_z \pm \frac{3}{\sqrt{2}} K_o$ and $\frac{\Delta\sigma_L}{\Delta\sigma_z} = 1$.

3. The instantaneous slope of the "plastic line" deviates from 45^{o} by a factor described by

$$(\frac{\mu}{1-\mu} - 1)\, e^{-\frac{G_1}{\eta_1} t}$$

In the laboratory, tests were performed to verify these theoretical results. Experimental data shown in Fig. 6.12 indicate that the instantaneous readings represented by line AB and DE deviate from 45^{o} by about 5 percent. However, readings taken at the same axial load but at 10 minutes later formed 45^{o} lines represented by AC and DF. The exponential term in the lateral stress expression had nearly vanished in the first 10 minute period, and the lateral stress was reduced to $\sigma_L = \sigma_z + \frac{3}{\sqrt{2}} K_o$ or $\frac{\Delta\sigma_L}{\Delta\sigma_z} = 1$. This leads to the conclusion that η_1 is a very small number.

2. Viscoelastic state

In this region, the slope of the "plastic line," $\frac{\Delta\sigma_L}{\Delta\sigma_z}$, is always 45^{o} and moves parallel to the initial straight line as time increases. As time approaches infinity, the lateral stress approaches a constant value indicated by:

$$\sigma_L = \sigma_z \pm \frac{3}{\sqrt{2}} (\frac{G_1 G_2}{G_1 + G_2}) \gamma_o\, u(t)$$

In the laboratory, stress relaxation tests were performed to verify this behavior. Fig. 6.13 shows the lateral stress - axial stress

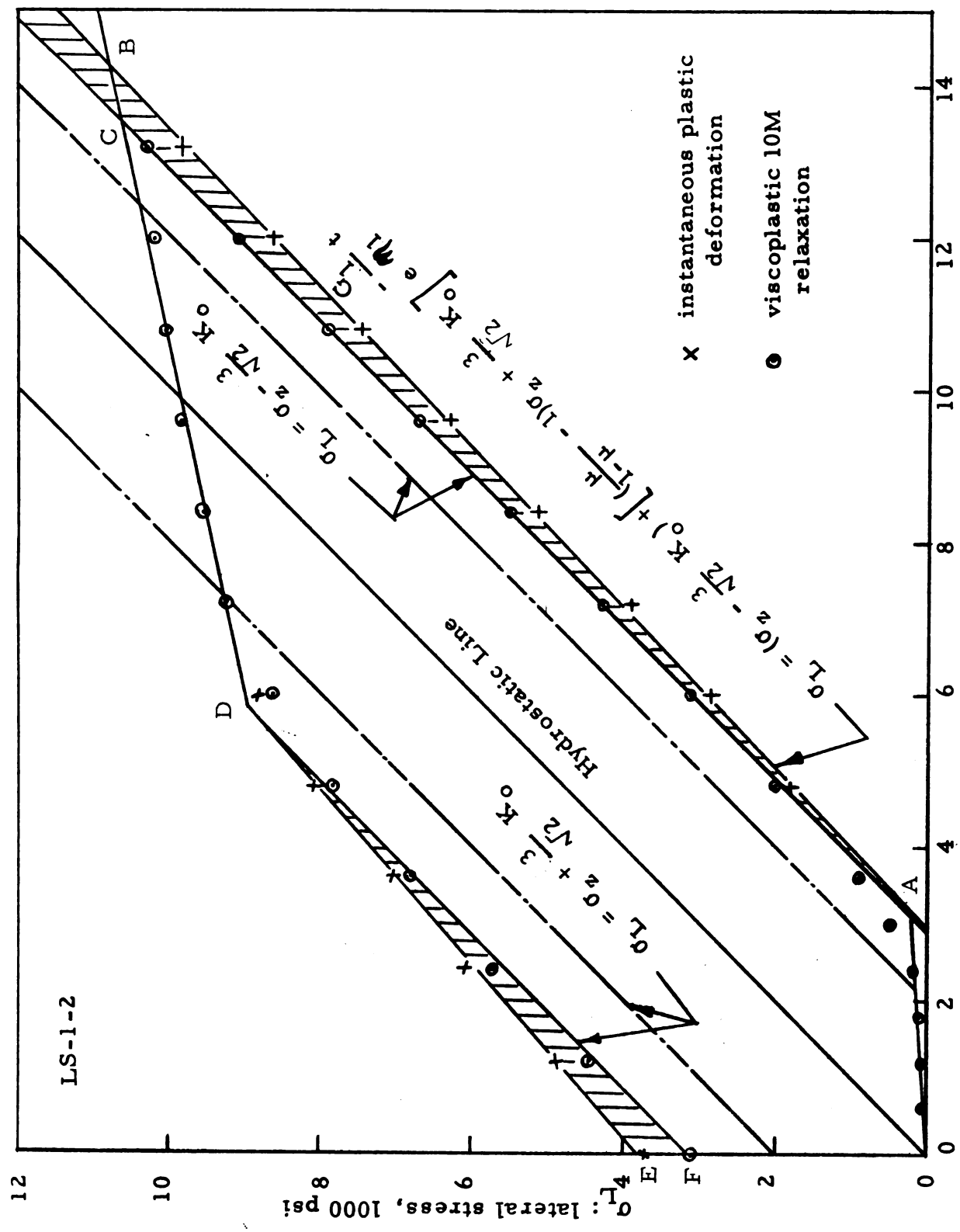

Fig. 6.12 Lateral stress-axial stress diagram illustrating the stress relation in viscoplastic region in transition test

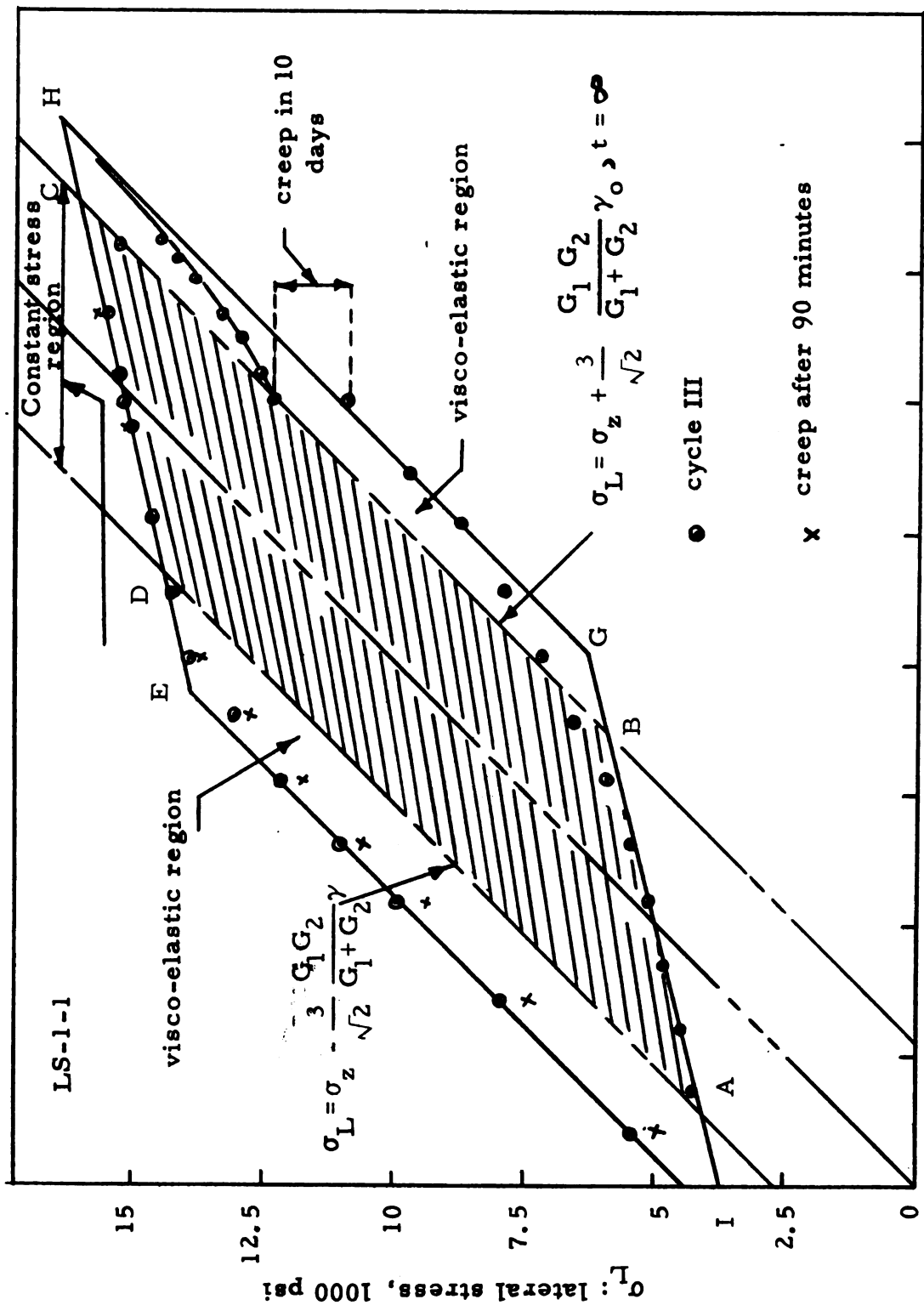

Fig. 6.13 Experimental analysis of constant stress region compared with the general theory of stress relaxation

relation for the third cycle. The axial load was raised to 15,000 psi and maintained at that level till the lateral stress reaches a constant value.

Through this point, a line was drawn parallel to GH intersecting IG and EH at B and C respectively. This line, BC, represents the constant stress σ_L, such that,

$$\sigma_L = \sigma_z \pm \frac{3}{\sqrt{2}} \left(\frac{G_1 G_2}{G_1 + G_2}\right) \gamma_o \, u(t)$$

A similar line AD was drawn parallel to BC and at equal distance from the hydrostatic line representing the change in lateral stress during unloading cycle. Accordingly, if lines BC and AD represent the constant lateral stress as time approaches infinity, then region ABCD is a constant stress region and no change in lateral stress with respect to time is expected along AB and DC.

To prove this constant stress region, the load was raised uniformly from 15,000 psi up to approximately 18,000 psi as indicated in Fig. 6.13. At that stress level, the axial stress was maintained constant for a period of 90 minutes. Then it was reduced to zero. At each stress level, during this unloading cycle, the load was maintained constant for a period of 90 minutes to allow for any stress relaxation.

The results showed that stress relaxation occurs only at 18,000 psi with a lateral stress change of 500 psi. As unloading proceeds

through the region indicated by line CD, no appreciable variation occurred. At point D, stress relaxation in an opposite direction to that of the loading cycle starts to increase as the axial stress approaches zero.

6.3d Determination of time-dependence constants from stress relaxation equations

Assuming rock salt has standard structural properties, the time-dependence constants are evaluated as indicated in the following example:

Test No. LS-1-1

Young's modulus, $E = 2.83 \times 10^6$ psi (3rd cycle)

Poisson's ratio, $\mu = 0.16$

Shear modulus, $G_1 = \frac{E}{2(1+\mu)} = 1.219,827$ psi

As time approaches infinity, the stress relaxation is described by Eq. 3.1-20, where

$$\sigma_L = \sigma_z \pm \frac{3}{\sqrt{2}} \left(\frac{G_1 G_2}{G_1 + G_2} \right) \gamma_o \, u(t)$$

The retarded shear modulus G_2 is the only unknown quantity, since σ_L, σ_z, G_1 and γ_o may be calculated.

From Fig. 6.13, as time approaches infinity

$\sigma_z = 15,000$ psi

$\sigma_L = 12,500$ psi

for laterally confined strain, $\epsilon_x = \epsilon_y = \epsilon_L$. Therefore,

$$\gamma_o = \pm \frac{2\sqrt{2}}{3} (\epsilon_L - \epsilon_z)$$

$$\gamma_o = \pm 8439 \times 10^{-6} \text{ in/in}$$

on loading cycle γ_o is a negative quantity if both σ_L and σ_z are positive. The retarded shear modulus may be expressed as

$$G_2 = \frac{G_1 (\sigma_L - \sigma_z)}{-\frac{3}{2\sqrt{2}} G_1 \gamma_o - (\sigma_L - \sigma_z)}$$

$$G_2 = \frac{1,219,827 \text{ (psi)} (-2500 \text{ psi})}{-\frac{3}{\sqrt{2}} (1,219,827)(\text{psi})(8439 \times 10^{-6}) + 2500 \text{ (psi)}}$$

$$G_2 = \underline{\underline{148,000 \text{ psi}}}$$

The plasticity constant η_1 was described by Eq. 3.1-14, such that

$$\eta_1 = \frac{G_1}{a_1}$$

where $a_1 = 995 \times 10^{-5}/\text{min}$.

Therefore,

$$\eta_1 = 122.6 \times 10^6 \frac{\text{min - lbs}}{\text{in}^2}$$

Using conversion factors from min - lbs/in^2 to dynes-sec/cm^2 to get:

$$\eta_1 = 122.6 \frac{\text{min-lbs}}{\text{in}^2} \times 60 \frac{\text{sec}}{\text{min}} \cdot \frac{10^6}{2,248} \frac{\text{dynes}}{\text{lbs}} \times \frac{1}{6.45 \frac{\text{cm}^2}{\text{in}^2}}$$

$$\eta_1 = \underline{\underline{5.0 \times 10^{14} \text{ poises}}}$$

Similarly, the viscoelasticity coefficient was described by Eq. 3.1-22, such as

$$\eta_2 = \frac{G_1 + G_2}{a_2}$$

where $a_2 = 5.577 \times 10^{-4}$/min

Therefore $\eta_2 = 23.2 \times 10^8$ min-lbs/in^2

or $\eta_2 = \underline{96 \times 10^{14} \text{ poises}}$

This indicates that η_2 is almost 20 times larger than η_1.

The ratio, $\frac{G_2}{\eta_2}$, that will be used in sec. 6.4 to verify the creep equation of a cylindrical cavity, is presented as follows:

Table 6.6 Values of the ratio $\frac{G_2}{\eta_2}$, as obtained from transition tests

Test No.	E x 10^6 psi	G_1 x 10^6 psi	G_2 x 10^6 psi	$\eta^2 \times 10^4$ min-lbs/in^2	$\frac{G_2}{\eta_2}$ per min 10^{-4}
LS-1-1	2.83	1,220,000	148,000	232,000	0.63
MS-1-26	2.45	1,060,000	166,900	224,000	0.74
LS-1-3	2.83	1,220,000	128,000	239,000	0.54

Accuracy of the time-dependence constants determined by the above procedure are affected by the accuracy of the time-independent property constant G_1. This does not minimize the applicability of this method to determine the viscosity constants η_1 and η_2, particularly if the structural properties are well defined.

6.4 Creep of Model Cavity

When a constant stress is applied to a material the atomic or molecular structures of the material readjust themselves with sustained loading. This readjustment of the internal structure of the material produces deformation as time passes on. The deformation produced is called creep. In other words, creep is the property of solids to change their shape with time under constant loads. ASTM defines creep as "the time-dependent part of the strain resulting from stress." The phenomenon of creep is the most complex of all mechanical behavior of materials. Freudenthal[24] refers to the complexity of creep as being in direct relation with the complexity of the internal structure of matter itself. This phenomenon is observed in metals, ionic and covalent crystals and in amorphous materials such as glasses and high polymers.

6.4a Factors affecting creep

Temperature plays an important role for creep responses of metal, rocks and amorphous material. Those having low melting points tend to creep extensively at elevated temperatures. Heat is the most critical factor affecting the structural property of rock salt. High temperatures in salt cause thermal stresses, increased creep rate and reduced strength. Serata[70] reported that at a temperature of 500^{o} F, rock salt exhibits a uniaxial yielding strength around 1000

1500 psi instead of 2300 psi. He further reported that, under triaxial compression, the differential stress reduced from 1700 to 1000 psi, and remained nearly constant for temperatures varying from 500° F up to 1475° F (melting point of rock salt).

The extent of creep is also affected by the grain size, microstructure, previous strain history and boundary characteristics. The latter are usually influenced by impurities and, with a large concentration of them, the cohesive force of the aggregate material might increase.

6.4b Mechanism of creep

1. Uniaxial

On the basis of the mechanism of creep, the total creep of any instant is divided into three groups by Richard.[67] First, is the elastic plus plastic creep that occurs immediately after applying the load. Second, is the transient or cold creep. Finally a combination of transient and steady state creep, usually referred to as a viscous creep or hot creep. The components are illustrated for comparison in Fig. 6.14a, b. The last two components of creep are of prime importance and represent basically two different phenomena. They are treated separately as follows.

2. Transient creep

Decreasing rate is the principal characteristic of transient

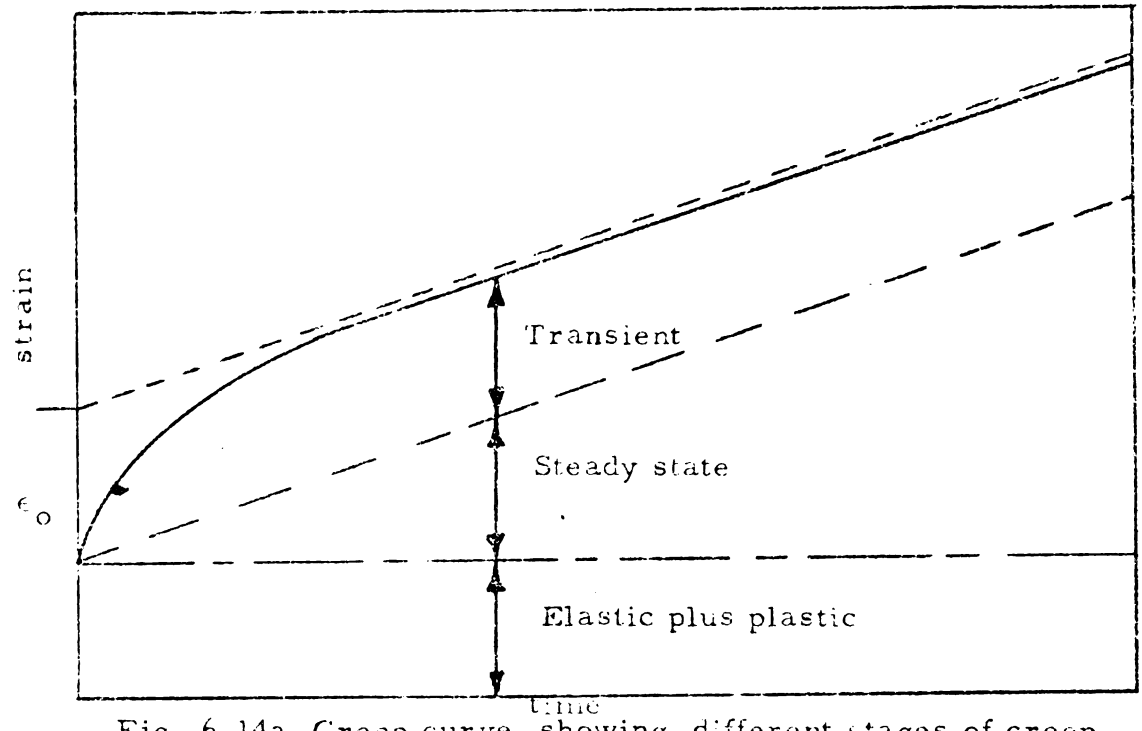

Fig. 6.14a Creep curve showing different stages of creep

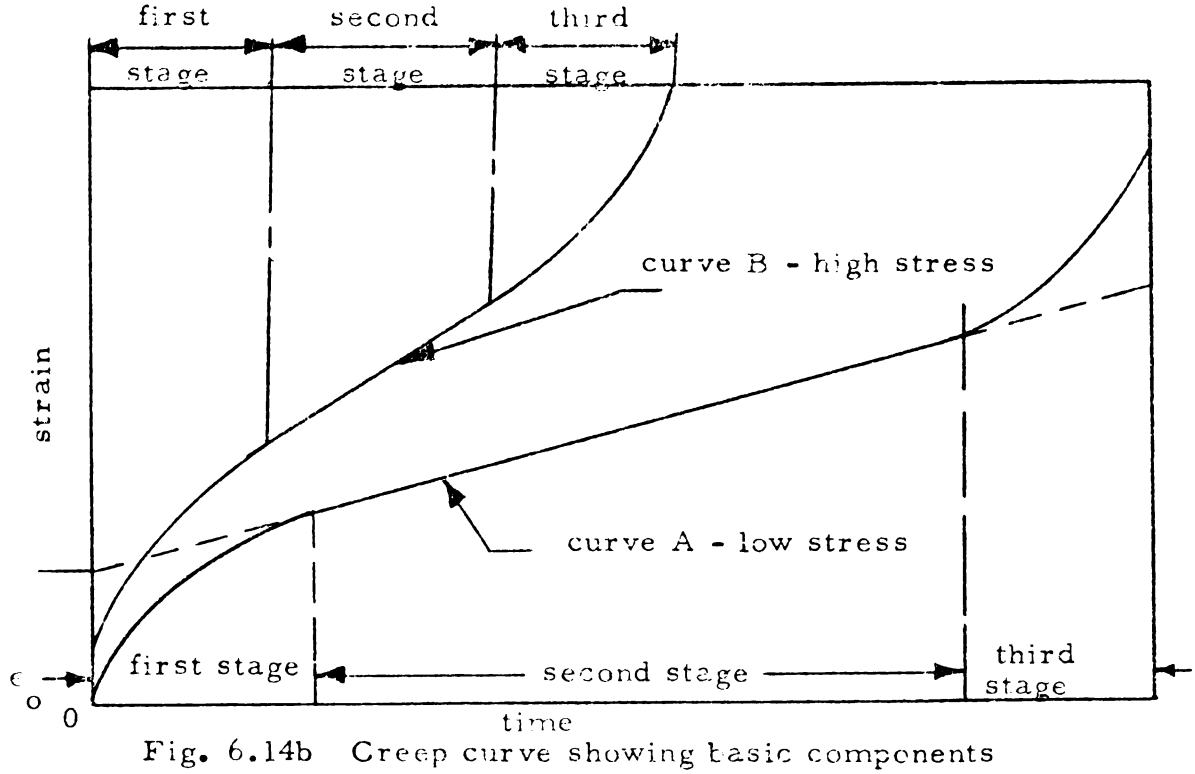

Fig. 6.14b Creep curve showing basic components

creep. The deformation rapidly increases but the flow rate gradually slows down and finally the creep deformation approaches its maximum value. In non-crystalline material, as in amorphous materials, elastic after-effects often constitute a major part of the total creep. In crystalline material, however, elastic after-effect is small and insignificant compared with the other creep deformation mechanisms, especially at high stress levels. In this range, the transient creep consists largely of yielding produced by plastic stresses and thermal activation. The plastic deformation is accompanied by initial plastic strain which decreases as the stresses are balanced by strain-hardening.

3. Viscous creep

Ideal viscous flow is characterized by steady increase of deformation at constant stress. In nonstrain-hardening materials like thermoplastic or amorphous polymers, viscous flow is the natural form of inelastic deformation. It is produced by permanent change in the molecular structure of the material. The changed molecules slip past each other, constantly breaking and regrouping with no strengthening results. In strain hardening material, like most crystalline materials, viscous flow takes place when the strain hardening effect is just balanced by the softening effect of heat. This softening is produced by atoms of the crystals which migrate

or diffuse to positions of lower energy. Thus, dislocations are made more mobile and can detour around obstacles or take them along, given a little time. Also, in polycrystalline materials, viscous creep is produced by what is called grain-boundary shearing which is due to flow of grains themselves as a semi-rigid body.

4. Triaxial

In triaxial stress state such as creep of a thick walled cylinder subjected to uniform external pressure, the transient state is defined "as that portion of the deformation history of the tube when the stresses throughout the cylinder vary with time."[12] This transient state may start when loads are just applied and is considered completed when the complex creep-relaxation process in the thick walled cylinder adjusts itself such that all the stress distribution is constant with time. Eventually, a steady state of stress will be reached and from then on the stress distribution will remain constant with time.

The creep rate characteristics of a region such as a thick walled cylinder with external pressure are that the transient creep rate decreases from large to a small value in a short period of time. However, after stress reaches a constant value, the creep rate continues to decrease slowly until it reaches an asymptotic value at $t = \infty$.

6.4c Creep analysis of a cylindrical model and verification of theoretical creep equations

The development of the mathematical theory of creep has been rather slow. This is due to the difficulty of obtaining experimental data for the entire life of the material concerned. Most of the research so far has been in the direction of developing empirical relations that fit the available data. A sound mathematical theory based on logical assumptions and guided by practical experience to describe the complex physical phenomena of creep is yet to be developed.

1. General creep behavior of a salt cavity

In the laboratory, as discussed earlier, a creep testing device has been setup to determine the creep characteristics of salt. This triaxial creep test involves the application of constant load to the test specimen and the measurement of deformation at a long period of time.

A sample of creep behavior of salt is presented in Fig. 6.15. The creep in these samples was divided mainly into two stages. The first stage is the one during which most of the transient creep takes place. This type of creep is usually called transient creep. When the transient creep has reached a substantially constant value, the strain continues to increase at a more or less decreasing creep rate, under the action of the viscoelastic component. This type of creep continues at a decreasing rate until eventually it reaches its minimum

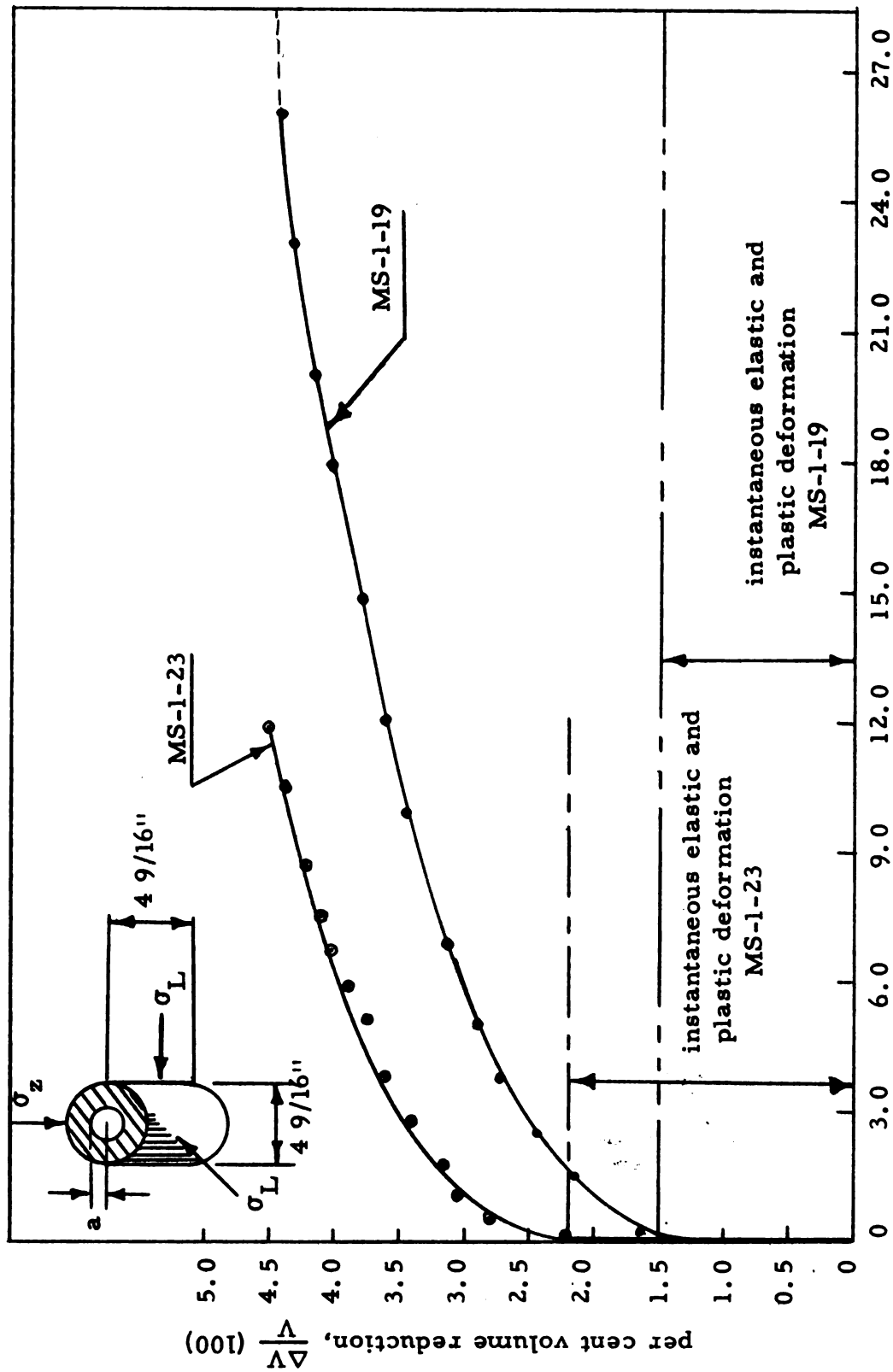

Fig. 6.15 Closure rate of model salt cavity

creep rate at a large value of time. Because of the nature of the loading, the third stage of creep discussed in uniaxial creep is difficult to observe in this study.

2. Transient and plastic deformation

In the laboratory, the deformation rate at the early stages of creep decreases rapidly from some large value to a small value (Fig. 6.15). To analyze this type of deformation, the change in cavity radius, a, was plotted as a function of time as indicated in Fig. 6.16. This figure shows that the cavity radius decreases rapidly to a small value within a short period of time. At this state of creep, where the deformation rates are large, the stresses in the salt are not constant even though the external pressure was maintained at the same level. For each increment of time, there is not only an increment of plastic strains but also an increment of stress which eventually reaches zero with time. The relation of cavity radius as a function of time and stresses in plastic region is demonstrated theoretically by Eq. 4.2-6, where

$$\frac{a_o - a}{a_o} = \frac{1}{2\eta_1}\left(1 - \frac{K_o}{\tau_o}\right)\sigma_\theta' \, t$$

The relation between a and t is difficult to obtain without determining the variation in the deviatoric stresses. However, for small values of t, the changes in σ_θ' and τ_o are small and a linear relation may be

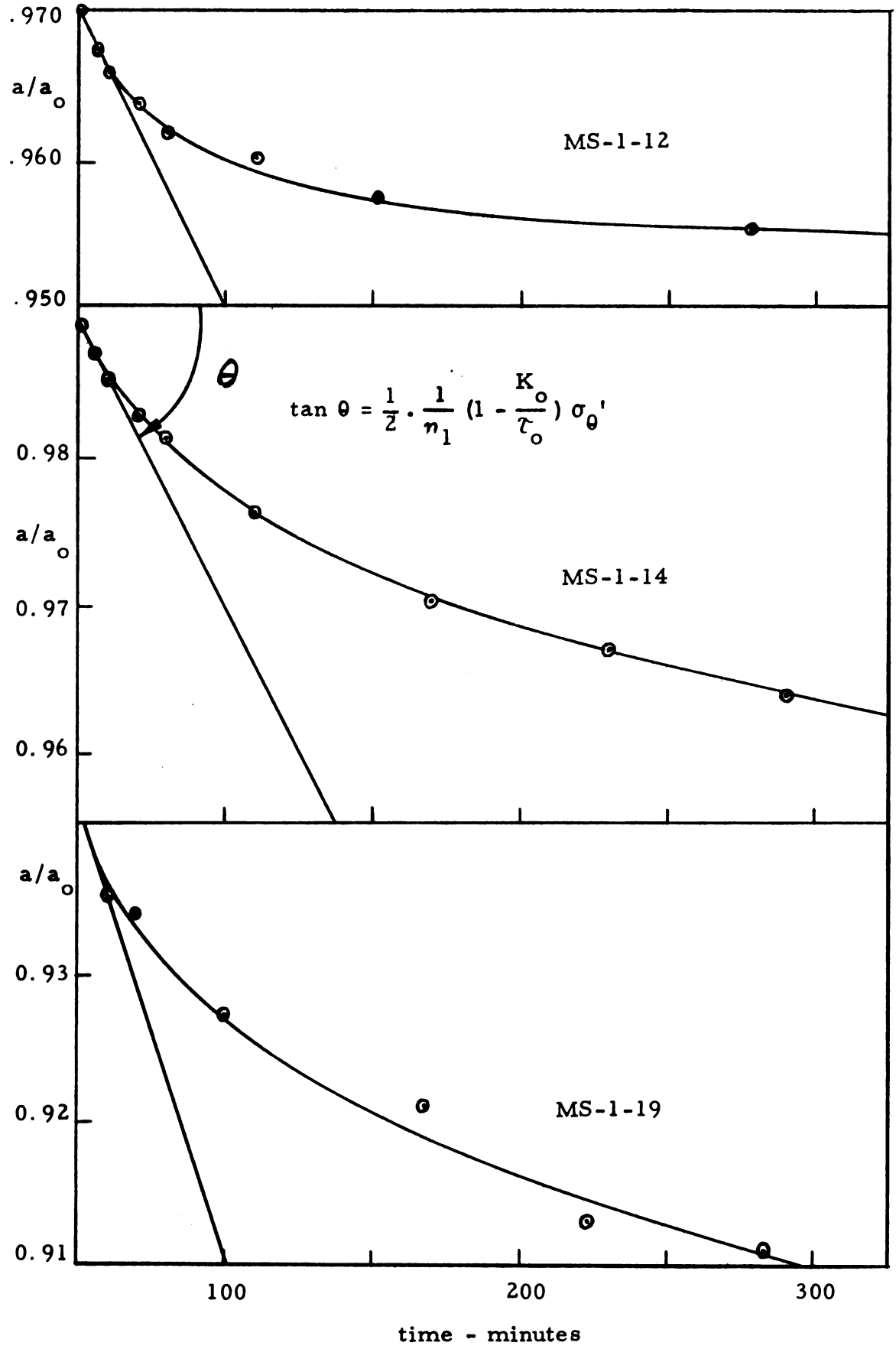

Fig. 6.16 Reduction of a model cavity reduces as a function of viscoplastic deformation

approximated only by drawing a tangent to the curve at time approximately equal to zero. The slope of this linear relation is described by

$$\tan \theta = \frac{1}{2\eta_1} \left(1 - \frac{K_o}{\tau_o}\right) \sigma_\theta'$$

if these variables are known the viscoplasticity constant η_1 may be approximated from the tangent of these curves.

3. Viscoelastic deformation

It has been observed from several test results that the creep curves of salt have some common features. Thus, they may be expressed by a common creep curve. Although no mathematical expression as yet describes the exact process of creep, many empirical relations have been suggested and used to fit the creep data obtained.

An empirical creep function that fits very closely the creep data for a cylindrical cavity was proposed. The proposed function may be written as:

$$a - a_f = a_o e^{-Pt}$$

where

a = reduced cavity radius at time t

a_f = reduced cavity radius as time approaches infinity

P = material constant

a more general formulation of this equation is

$$a - a_f = a_o e^{-Pt^n}$$

where n is equal to unity in a linear material. The advantage of this empirical equation is that the coefficients can be determined from simple graphical methods as illustrated in Fig. 6.17.

This figure indicates that the empirical equation fits very closely the viscoelastic creep data of the salt cavity. The discrepancy observed at the early stages of creep may be attributed mostly to the plastic deformation. At the end of the plastic deformation period, salt exhibits a linear behavior as demonstrated in the above figure. The material constant P, which is related to the viscosity of the material, was determined from the slopes of the curves.

It has been noted that the proposed creep function developed as a result of laboratory creep measurements is essentially the same equation obtained from the mathematical analysis of a cylindrical cavity in a linear viscoelastic material. In particular, a conclusion was reached such that $P = \frac{G_2}{\eta_2}$. To prove that these equations are the same, the value of P, as determined from creep analysis of a cylindrical salt cavity, should be equal to the value of $\frac{G_2}{\eta_2}$ as determined from stress relaxation equations of the transition tests.

From Fig. 6.17 and Table 6.6, the values of P and $\frac{G_2}{\eta_2}$ are calculated and presented in Table 6.7.

Table 6.7 Comparison of the values of P and $\frac{G_2}{\eta_2}$ as obtained from two different testing techniques

P from cavity creep tests	$\frac{G_2}{\eta_2}$ from transition tests
0.34×10^{-4} per min (MS-1-12)	0.63×10^{-4} per min (LS-1-1)
0.67×10^{-4} per min (MS-1-14)	0.74×10^{-4} per min (MS-1-26)
0.72×10^{-4} per min (MS-1-19)	0.54×10^{-4} per min (LS-1-3)

The above comparison of the two different experimental results shows a close agreement between the values of P and $\frac{G_2}{\eta_2}$, verifying that Eqs. 4.2-3 and 4.2-4 are essentially the same. This further supports the validity of the general assumptions made in developing the theory of creep behavior of a salt cavity. Therefore, by using these coefficients the creep rate of underground cylindrical cavity can be described, provided the conditions of the cavity agree with the basic assumptions of the study.

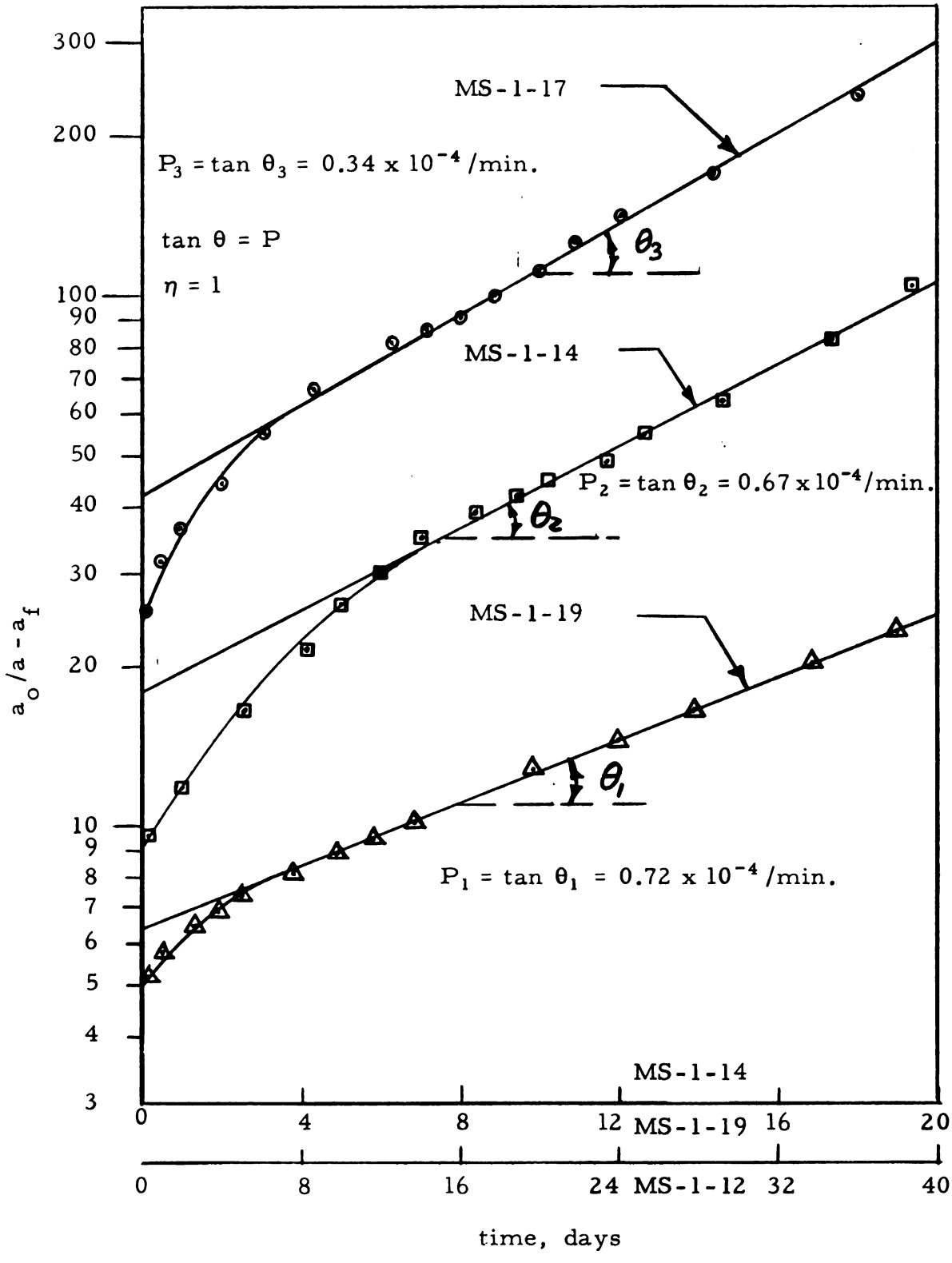

Fig. 6.17 Experimental analysis of triaxial creep in hollow cylinders illustrating determination of viscoelastic coefficients

CHAPTER VII

SUMMARY

Theories of stress, strain and boundary motion were developed to study the stress distribution in a cylindrical model cavity. Distribution of stress and strain and creep motion of the medium around the cylindrical cavity were described based on the mathematical theories of elasticity, plasticity and viscoelasticity of a continuous medium. The conditions of plane strain with $\sigma_r \geq \sigma_z \geq \sigma_\theta$ were assumed.

In this analysis six mechanical constants of the material were included, which have to be determined for the experimental verification of the theories.

A proposed mechanical model was verified by the triaxial transition test technique, which was used to determine the mechanical constants of the material. These constants are: Young's modulus, Poisson's ratio, octahedral shear strength, viscosity coefficients, and retarded shear modulus. The mechanical model consists of elastic, viscoelastic and viscoplastic elements that describe the overall behavior of rock salt with respect to time and stress conditions.

Behavior of the model cavity was described by substituting some of these constants into the theories of stress and strain and boundary motion equations. The validity of the theoretical calculations was confirmed in the laboratory by using the technique of liquid

confining medium for a model cavity. A summary of this theoretical and experimental investigation is as follows:

From experimental model cavity analysis and theoretical Eq. 2.2-9

$$E = -\frac{(1+\mu)}{\frac{\Delta u}{\Delta P_o}\left(1 - \frac{a_o^2}{b_o^2}\right)} \cdot \left[\frac{a_o^2}{r} + (1 - 2\mu)\, r\right]$$

Young's modulus was determined to be in the range of 0.7×10^6 psi to 1×10^6 psi for first cycle. Higher experimental values (4×10^6 psi) were found for second cycle and thereafter. Transition test results show that Young's modulus for second cycle and beyond range between 2.4×10^6 psi and 3×10^6 psi.

Plasticity solution for large boundary motion such as Eq. 2.2-4

where $\frac{a}{b} = e^{-\frac{3}{2\sqrt{2}} K_o \frac{1}{(P_o - P_i)}}$

were utilized to determine the octahedral shear strength of rock salt which is around 2300 psi. Experimental data from the transition test were found to agree generally with these values.

Cavity reduction as a function of elastic-plastic deformation is described by Eqs. 2.3-37, 2.3-54 and 2.4-9, such that

$$u_{r=a} = \left(\frac{1-2\mu}{G}\right)\left[\frac{3}{2\sqrt{2}}K_o\left(\frac{a}{2}\ln\frac{\rho}{a}+\frac{a}{4}\right) - \frac{\frac{3}{2\sqrt{2}}K_o}{4}\frac{\rho^2}{b_o^2} - \frac{P_o a}{2}\right]$$

$$- (1-\mu)\frac{\frac{3}{2\sqrt{2}}K_o}{2G}\frac{\rho^2}{a}$$

$$\frac{a^2}{a_o^2} = 1 - \frac{\frac{3}{2\sqrt{2}}K_o}{G}(1-\mu)\frac{\rho^2}{a_o^2}$$

based on elastic compressibility; and

$$u_{r=a} = \frac{\rho}{a}\cdot\frac{1}{2G}\left\{\frac{\frac{3}{2\sqrt{2}}K_o}{2}\left[(2\mu-1)\frac{\rho^3}{b_o^2} - \rho\right] + (2\mu-1)\rho P_o\right\}$$

based on total incompressibility in plastic region.

The radial displacement and the reduced cavity radius were expressed as functions of geometry and external pressure. Close agreement is observed between theory and experimental results, indicating rock salt may be considered as ductile, isotropic and homogeneous under triaxial compression.

From the transition test, the stress relaxation equation in the plastic and viscoelastic regions are defined respectively as:

$$\sigma_L = \left(\sigma_z \pm \frac{3}{\sqrt{2}}K_o\right) + \left[\left(\frac{\mu}{1-\mu}-1\right)\sigma_z \mp \frac{3}{\sqrt{2}}K_o\right]e^{-\frac{G_1}{\eta_1}t}$$

and

$$\sigma_L = \sigma_z \pm \frac{3}{\sqrt{2}}\left[G_1\gamma_o u(t)\, e^{-\frac{G_1+G_1}{\eta_1}t} + \left(1-e^{-\frac{G_1+G_2}{\eta_2}t}\right)\frac{G_1G_2}{G_1+G_2}\gamma_o ut\right]$$

from which the viscosity coefficients η_1 and η_2 are determined such that

$$\eta_1 = \frac{G_1}{a_1} = 5 \times 10^{14} \text{ poises}$$

and

$$\eta_2 = \frac{G_1 + G_2}{a_2} = 96 \times 10^{14} \text{ poises}$$

where a_1 and a_2 are experimental values determined from the stress relaxation figures.

The creep behavior of a model salt cavity is determined by considering the viscous behavior of rock salt beside its elastic and plastic deformations. The creep rate equations are as follows:

$$\frac{d\epsilon_r}{dt} = \frac{1}{2}\left[\frac{1}{\eta_1}\left(1 - \frac{K_o}{\tau_o}\right) + \frac{1}{\eta_2} e^{-\frac{G_2}{\eta_2}t}\right]\sigma_r'$$

$$\frac{d\epsilon_\theta}{dt} = \frac{1}{2}\left[\frac{1}{\eta_1}\left(1 - \frac{K_o}{\tau_o}\right) + \frac{1}{\eta_2} e^{-\frac{G_2}{\eta_2}t}\right]\sigma_\theta'$$

In the laboratory, an empirical creep function

$$\frac{a - a_f}{a_o} = c\, e^{-Pt}$$

that fits very closely the experimental data in the viscoelastic region, is compared with the theoretical equation developed from the above creep equations such that

$$\frac{a - a_f}{a_o} = - \frac{\sigma_\theta'}{2G_2} e^{- \frac{G_2}{\eta_2} t}$$

Both equations have exactly the same creep form. To verify the validity of this comparison the value of P and $\frac{G_2}{\eta_2}$ were calculated from experimental results of model salt cavities and those of transition tests respectively. Close agreement between these values were observed which led to the verification of the mathematical equation and the conclusions that

$$P = \frac{G_2}{\eta_2}$$

and

$$C = \frac{1}{2} \frac{\sigma_\theta'}{2G_2}$$

CHAPTER VIII

CONCLUSIONS

Based upon the theoretical and experimental analysis discussed in the previous chapters, the following conclusions have been drawn.

Mechanical Properties

The following fundamental properties of rock salt were determined by two different triaxial testing procedures.

1. Young's modulus from the first cycle of the hollow cylinder tests varied between 0.7×10^6 psi and 1.2×10^6 psi with an average of about 0.85×10^6 psi. While, from second and subsequent cycles, it was about 4×10^6 psi.
2. Value of Young's modulus from first cycles of the transition test was about 0.4×10^6 psi. From the second and subsequent cycles, it varied between 2×10^6 psi and 3×10^6 psi with an average of 2.6×10^6 psi.
3. Variations of Young's modulus within the same test technique were relatively small compared to the variation between the two different testing procedures.
4. The mean octahedral shear strength obtained from the large deformation theory of thick-walled cylinder was around 2,300 psi.
5. The octahedral shear strength of the LS-specimens ranges

from 1300 psi to 2000 psi for the first and third cycles of loading respectively as shown in Table 6.3. In comparison, the octahedral shear strength for the relatively less pure MS-specimens ranges from 1700 psi to 2100 psi for the first and fourth cycles of loading respectively.

6. Rock salt exhibits strain-hardening characteristics. The slope of work hardening part, H', decreases rapidly and approaches zero within a short range of stress.

7. Repeated cycles of loading result in a general increase in the strength of the material. The increase in strength is partially evident in the increase of octahedral shear strength value.

Structural Behavior

1. The elastic theory can be applied for analysis of the stress-strain distribution around a salt cavity so long as the octahedral shear stress is less than its maximum elastic value.

2. The elasticity theory has been used effectively to determine Young's modulus of the material as a continuous medium under triaxial compression.

3. The maximum shear theory and the energy of distortion theory are directly applicable for analyzing the strength of rock salt under multiaxial compression only if the material tested is assumed to be ductile, isotropic and homogeneous.

4. Theoretical analysis has been completed on the stress, strain and boundary motion of a cylindrical cavity. Theoretical results compared reasonably well with the experimental results. Fig. 6.6 shows the theoretical stress-displacement relation in comparison with the experimental results. The experimental behavior of the reduced cavity radius "a" as a function of applied stresses compares reasonably well with the theoretical results.

5. The volume reduction of a salt cavity is a function of the applied loads. The higher the loads, the larger the volume reduction.

6. An instantaneous stress equilibrium always exists between the advancing plastic zone and the surrounding elastic part. As the applied stresses increase the plastic radius increases and the modified inner radius decreases, resulting in a stable cavity.

7. The salt cavity is unstable and can be fractured if the internal pressure exceeds the external pressure.

8. Plastic deformation increases with the increase in applied loads. However, contrary to uniaxial tests on salts, plastic deformation rate of the cavity under constant external loads decreases rapidly with time.

9. A mechanical model describing the structural behavior of rock salt was proposed and verified in the laboratory. The model consists of elastic, viscoelastic and viscoplastic elements whose coefficients were successfully determined from laboratory tests.

10. The elasticity and plasticity constants were determined from the transition tests. The viscoplasticity coefficient, η_1, is relatively much smaller than the viscoelastic one. A simple graphical method was developed to determine these coefficients. They are calculated as follows:

$$\eta_1 = \frac{G_1}{\alpha_1}$$

and

$$\eta_2 = \frac{G_1 + G_2}{\alpha_2}$$

where

η_1 = viscosity constant in the plastic region

η_2 = viscosity constant in the viscoelastic region

α_2 = slope of the octahedral stress relaxation curve in the plastic region

α_2 = slope of the octahedral stress relaxation curve in the viscoelastic region

G_1 = octahedral shear modulus

G_2 = retarded shear modulus

11. The empirical creep equation of a hollow cylinder

$$\frac{a - a_f}{a_o} = c\, e^{-Pt}$$

established in the laboratory, agrees with the theoretical

equation derived from mathematical theory of viscoelasticity,

$$\frac{a - a_f}{a_o} = -\frac{1}{2}\frac{\sigma_\theta'}{G_2} e^{-\frac{G_2}{\eta_2} t}$$

where

a_f = modified inner radius at t equals infinity

a = modified inner radius at any time t

a_o = initial inner radius

C = constant

The P value of the empirical equation of the cavity was found to agree very closely to the value of $\frac{G_2}{\eta_2}$ obtained from transition tests.

CHAPTER IX

FUTURE RESEARCH

A phenomenological approach to rock mechanics has been studied based on simple isotropic, homogeneous and linear viscoelastic characteristics which provided a satisfactory agreement between theoretical calculations and experimental results. However, during the course of the present investigation, certain complications were encountered from which the following recommendations for future research can be made.

1. The experimental results for the determination of Young's modulus under triaxial compression, from the hollow cylinder and transition tests failed to agree. Part of this may be contributed by experimental errors in both techniques. However, a considerable amount of this error was observed to be due to the use of dial gages in measuring the axial strains. Hence, a more precise device to measure this strain would eliminate this potential error and improve the experimental results.

2. An attempt was made to determine the octahedral shear strength, K_o, from the boundary motion of a hollow thick-walled cylinder. The values obtained were based on a few readings in the completely plastic state. It is suggested to use a higher capacity pressure vessel to obtain more readings and improve the value of K_o.

3. The analytical results in the three-dimensional analysis of model cavity deformation did not show complete agreement with the experimental results at high external loads. It would be more correct to consider instantaneous cavity measurements to eliminate the plastic flow effects at such high stresses.

4. Theoretical analyses have shown that the plastic strain rate is time-dependent and a function of the deviatoric stresses. Therefore, it is inadequate from the present experimental results to determine the viscosity constant, η_1. Hence, a plastic stress-strain rates diagram might be used to evaluate η_1.

5. In the present investigation, an effort was made to determine the material properties and verify the creep equations. No effort was made to determine the creep rate equations for any particular opening such as tunnels, mines or oil wells. Such analysis might be of practical importance for different mining or drilling operations. It is suggested then, to apply the experimental and theoretical analysis of the model salt cavity developed in laboratory, to actual field measurements.

6. The theoretical analysis in this study was based on the assumption that rocks behave like a ductile material under multiaxial compression and accordingly the Maximum Shear Theory and the Energy of Distortion Theory were used. However, for a

partially confined state, where the theories for ductile material cannot be applied, Mohr's theory of rupture might be more applicable.

BIBLIOGRAPHY

1. Adams, F. D., and Nicholson, J. T., "An Experimental Investigation into the Flow of Marble," Proc. Roy. Soc. London, Ser. A, Vol. 195, PP. 363-401, 1901.

2. _____, "An Experimental Investigation into the Action of Differential Pressure on Certain Minerals and Rocks, Employing the Process Suggested by Prof. Kick," Jour. Geol., Vol. 18, PP. 485-525, 1912.

3. _____, "An Experimental Contribution to the Question of the Depth of the Zone of Flow in the Earth's Crust," Jour. Geol., Vol. 20, PP. 97-118, 1912.

4. _____, and Bancraft, J. A., "On the Amount of Internal Friaction Developed in Rocks During Deformation and on the Relative Plasticity of Different Types of Rocks," Jour. Geol., Vol. 25, PP. 597-637, 1917.

5. Allen, D. H. DEG. and Sopwith, D. G., "The Stress and Strain in a Partially Plastic Thick Tube under Internal Pressure and End Load," Proc. Roy. Soc. London, Ser. A, Vol. 205, P. 69, 1951.

6. Andrade, E. H. dac., "On the Viscous Flow of Metals and Applied Phenomena," Proc. Roy. Soc., Ser. A, Vol. 84, No. A567, P. 1, June 9, 1910.

7. Besseling, J. E., "Theory of Elastic, Plastic and Creep Deformations of an Initially Isotropic Material," AFOSR, TN60-384, Stanford Univ., Dept. Aero-Engng.

8. Bland, D. R., "Elastoplastic Thick-Walled Tubes of Work Hardening Material Subject to External and Internal Pressure," J. Mech. Phys. Solids, Vol. 4, P. 209, 1956.

9. Bridgman, P. W., The Physics of High Pressure, G. Bell and Sons, London, PP. 445, 1949a.

10. _____, Studies in Large Plastic Flow and Fracture, McGraw-Hill Book Company, New York, PP. 362, 1952.

11. Chowdiah, A. M., "Stress and Strain Distribution Around Openings in Underground Salt Formations," Ph.D. Thesis, Michigan State University, 1963.

12. Coffin, L. F., Jr., Shepler, P. R. and Cherniak, G. S., "Primary Creep in the Design of Internal Pressure Vessels," Trans. A.S.M.E., J. Appl. Mech., Vol. 16, P. 229, 1949.

13. Corneliussen, A. R. and Lee, E. H., "Basic Research in Stress Analysis in Viscoelastic Materials," Rept. No. 2, Contr. No. DA-19-020-ORD-4750, Brown University, Dec., 1958.

14. Davis, E. A., "Creep Rupture Tests for Design of High Pressure Steam Equipment," A.S.M.E. Trans. 82D, J. Basic Engng., Vol. 2, PP. 453-461, June, 1960.

15. Davis, H. E., Troxell, G. E. and Wiskocil, C. T., Testing and Inspection of Engineering Material, 2nd Ed., McGraw-Hill Book Co., New York, 1955.

16. Eringen, A. C., Nonlinear Theory of Continuous Media, McGraw-Hill Book Company, Inc., New York, 1962.

17. Findley, W. N. and Khasla, G., "Application of the Superposition Principle and Theories of Mechanical Equation of State, Strain, and Time Hardening to Creep of Plastic Under Changing Loads," J. Appl. Phys., 26, 7, pp. 821-832, July, 1955.

18. _____, and Mathur, P. N., "Modified Theories of Fatigue Failure Under Combined Stress," Proc. Soc. Exp. Stress Anal., 14, 1, PP. 35-46, 1956.

19. _____, "Fatigue of Metals Under Combinations of Stresses," A.S.M.E., Ann. Mect., Pap. 56-A-74, P. 11, New York, Nov., 1956.

20. _____, "The Effect of Temperature and Combined Stresses on Creep of Plastics," Reprint Proc. 2nd Inter. Reinforced Plastic Conf., London, Dec., 1960.

21. _____, "Prediction of Performance of Plastics Long-Term Static Loads," Proc. Conf. Test. Perf., Trans. Vol. 30, No. 87, PP. 138-151, June, 1962.

22. _____, and Onaron, K., "Combined Stress Creep Experiment on Viscoelastic Material with Abrupt Changes in State of Stress," Reprint Proc. Inter. Conf. on Creep, 1963.

23. Finnie, I., and Heller, W. R., Creep of Engineering Materials, McGraw-Hill Book Company, Inc., New York, 1959.

24. Freudenthal, A. M., The Inelastic Behavior of Engineering Materials, John Wiley and Sons, Inc., New York, 1950.

25. Gemma, A. E., "The Creep Deformation of a Symmetrically Loaded Circular Cylindrical Shells," J. Aerospace SC: 27, PP. 953-954, Reader's Forum, Dec., 1960.

26. Goodier, J. N., "Concentration of Stress Around Spherical and Cylindrical Inclusions and Flows," Trans. A.S.M.E., Vol. 55, PP. 39-44, 1933.

27. Griggs, D. T., "Deformation of Rocks under High Confining Pressure," J. Geology, Vol. 44, PP. 541-577, 1936.

28. _____, "Creep of Rocks," J. Geology, Vol. 47, P. 225, 1939.

29. Gurtin, M. E. and Sternberg, E., "On the Linear Theory of Viscoelasticity," Tech. Rep. No. 6, Office of Naval Res., Contract Nonr. 562(30), Div. Appl. Math., Brown University, June, 1962.

30. Handin, J., "An Application of High Pressure in Geophysics," Trans. A.S.M.E., Vol. 75, PP. 315-324, 1953.

31. Hondelman, G. H., Lin, C. C. and Prager, W., "On the Mechanical Behavior of Metals in the Strain-Hardening Range," Quart. Appl. Math., Vol. 4, PP. 397-407, 1947.

32. Hill, R., Lee, H. E., and Tupper, S. J., "The Theory of Combined Plastic and Elastic Deformation with Particular Reference to a Thick Tube under Internal Pressure," Proc. Roy. Soc., Ser. A, Vol. 191, PP. 278-303, 1947.

33. _____, The Mathematical Theory of Plasticity, Oxford, at the Clarendon Press, 1956.

34. Hodge, P. G. and White, G. N., Jr., "A Quantitative Comparison of Flow and Deformation Theories of Plasticity," J. Appl. Mech., Vol. 17, PP. 180-184, 1950.

35. Hoff, N. J., "Approximate Analysis of Structures in the Presence of Moderately Large Creep Deformation," Quart. Appl. Math, Vol. 12, No. 1, P. 49, April, 1954.

36. _____, "Stress Distribution in the Presence of Steady Creep," Proc. Conf. High Speed Aeronautics, Polytechnic Institute of Brooklyn, Brooklyn, N.Y., P. 271, 1955.

37. Hoffman, O. and Sacks, G., Introduction to the Theory of Plasticity for Engineers, McGraw-Hill Book Co., New York, 1953.

38. Ignaczak, J., "Plane-Strain and Generalized Plane-Stress Analysis of a Rotating Viscoelastic Cylinder," Tech. Rep. No. 4, Office of Naval Res., Contract Nonr. 562(30), Div. Appl. Math., Brown University, Feb., 1962.

39. Jastrzebski, Z. D., Nature and Properties of Engineering Materials, 2nd Ed., John Wiley and Sons, Inc., New York, March, 1961.

40. Johnson, W. and Mellor, P. B., Plasticity for Mechanical Engineers, D. Von Nostrand Company, Inc., Princeton, N.J., 1962.

41. Kamash, T. B., Murch, S. A. and Naghdi, P. M., "The Elastic-Plastic Cylinder Subjected to Radial Distributed Heat Source, Lateral Pressure and Axial Force with Application to Nuclear Reactor Fuel Elements," J. Mech. and Phys. of Solids, Vol. 8, PP. 1-25.

42. Kamb, W. B., "The Thermodynamic Theory of Nonhydrostatically Stressed Solids," J. Geophysical Research, Vol. 66, No. 1, PP. 259-264, Jan., 1961.

43. Koiter, W. T., "On Partially Plastic Thick Walled Tubes," In Anniversary Volume on Appl. Mech. Dedicated to C. B. Biezeno, N. V. DeTechnische Vitgeverij H. Stom, Haarlem, 1953.

44. Kosla, G. and Findley, W. N., "Prediction of Creep from Tension Tests at Constant Strain Rate," 9th Congre's Intern. Micon. Appl. Univ. Bruxelles, Vol. 8, PP. 275-287, 1957.

45. Lee, H. E., "Stress Analysis for Linear Viscoelastic Materials," Sonderdruch, ans., Rheological Aeta, Band 1, Nr. 416, Seite 426-430, 1961.

46. _____, and Rogers, T. G., "Solution of Viscoelastic Stress Analysis Problems Using Measured Creep or Relaxation Functions," Interim Tech. Rep. No. 1, Dept. of Army, Grant DA-ARO(D)-31-124-G54, Div. of Appl. Math., Brown University, Aug., 1961.

47. Love, A. E. H., A Treatise on the Mathematical Theory of Elasticity, 4th Ed., Dover Publications, New York, 1927.

48. Lubahn, J. D., Felgar, R. P., Plasticity and Creep of Metals, John Wiley and Sons, Inc., New York, 1961.

49. MacGregor, C. W., Coffin, L. E., and Fisher, J. C., "Partially Plastic Thick-Walled Tubes," Jr. of the Franklin Institute, Vol. 245, PP. 135-158, Feb., 1948.

50. _____, and Coffin, L. E. Jr., "Approximate Solution for Symmetrically Loaded Thick-Walled Cylinders," J. Appl. Mech., Trans. A.S.M.E., Vol. 69, PP. A301-A311, 1947.

51. Malvern, L. E., "Theory of Plastic Solids," Class Notes, Michigan State University, 1962.

52. _____, "Introduction to the Mechanics of a Continuous Medium," Unpublished Class Notes, Michigan State University, 1962.

53. Marin, J., Mechanical Behavior of Engineering Materials, Prentice-Hall, Inc., Englewood Cliffs, N.J., 1962.

54. Mendelson, A., Hirschberg, M. H. and Manson, S. S. A., "A General Approach to Practical Solution of Creep Problems," Trans. A.S.M.E., 81D, J. Basic Engng., Vol. 4, PP. 585-598, Dec., 1959.

55. Morrison, D. M., "The Transition Test as a Method for Determining the Triaxial Properties of Rocks in the Condition of Underground Formations," M.S. Thesis, Michigan State University, E. Lansing, 1962.

56. Murphy, G., "Stress-Strain-Time Characteristics of Materials," Am. Soc. Test Materials, Bull. No. 101, P. 19, Dec., 1939.

57. Nadai, A., Theory of Flow and Fracture of Solids, Vol. 1, PP. 175-228, McGraw-Hill Book Co., New York, 1950.

58. Panek, L. A., "Stress Around Mine Openings in a Homogeneous Rock Body, "Edward Bros., Inc., New York, 1951.

59. Parker, E. R., "Modern Concept of Flow and Fraction," Trans. Am. Soc. Metals, Vol. 50, P. 89, 1958.

60. Perry, C. C. and Lissner, H. R., The Strain Gage Primer, McGraw-Hill Book Company, Inc., New York, 1955.

61. Philip, A., Introduction to Plasticity, Ronald Press Co., New York, 1956.

62. Prager, W. and Hodge, P. G., Theory of Perfectly Plastic Solids, New York, 1951.

63. _____, "Recent Development in the Mathematical Theory of Plasticity," J. Appl. Phys., Vol. 20, P. 235, 1949.

64. _____, "Strain Hardening under Combined Stress," J. Appl. Phys., Vol. 16, No. 12, P. 837, Dec., 1945.

65. Raman, A. B., "Elastic Plastic Transition Tests," M.S. Thesis, Michigan State University, 1962.

66. Reiner, M., "Plastic Yielding in an Elasticity," J. Mech. Phys. Solids 8, 4, PP. 255-261, Nov., 1960.

67. Richard, C. W., Engineering Material Science, Wadworth Publishing Company, Inc., San Francisco, 1961.

68. Robertson, E. C., "Experimental Study of the Strength of Rocks," Bull. Geol. Soc. of America, Vol. 66, PP. 1275-1314, Oct., 1955.

69. Sakurai, S., Unpublished paper, Michigan State University, 1964.

70. Serata, S., "Development of Design Principle for Disposal of Reactor Fuel Waste into Underground Salt Cavities," Ph.D. Thesis, University of Texas, 1959.

71. _____, "Transition from Elastic to Plastic States of Rocks under Triaxial Compression," Proc. 4th Symposium of Rock Mechanics held at Penn. State University, University Park, Pennsylvania, April, 1961.

72. Sheild, R. T., "On Coulomb's Law of Failure in Soils," J. Mech. Phys. Solids, Vol. 4, 1955.

73. Soderberg, C. R., "Plastic Flow and Creep in Polycrystalline Materials," Wiley and Sons, PP. 238-244, 1939.

74. _____, "Interpretation of Creep Tests on Tubes," Trans. A.S.M.E., Vol. 63, PP. 737-748, 1941.

75. _____, "The Interpretation of Creep Tests for Machine Design," J. Appl. Mech., Trans. A.S.M.E., Vol. 58, PP. 733-743, 1936.

76. Steel, M. C., "Partially Plastic Thick-Walled Cylinder Theory," J. Appl. Mech., Vol. 19, P. 133, 1952.

77. Timoshenko, S. and Goodier, J. N., The Theory of Elasticity, McGraw-Hill Book Company, Inc., 1951.

78. Von Karman, T., "Festigkcites Versuche unter Allseitigem Druck," Zeits Ver Deut Ingeniure, Vol. 55, PP. 1749-1757, 1911.